Integrated Power/Signal Transmission for Smart Energy Systems

Yixuan Zhang

PhD

University of York

Electronic Engineering

January 2022

Abstract

Communication technologies, especially wired technology, have developed considerably in terms of signal stability and communication speed. Conventional renewable energy generation units in traditional energy systems require additional communication devices to manage the renewable power generation equipment, which can raise the size and expenditure of the system. Additionally, although power line communication (PLC) can simplify system wiring by eliminating the requirement for communication cables, additional signal coupling devices are still needed to combine energy and signals. Therefore, it is significant to investigate a suitable transmission approach for energy and signals in smart energy systems (SESs).

The purpose of this study is to analyse the feasibility of the integrated power/signal transmission (IPST) approach and to develop IPST-based converters for SESs. Firstly, state-of-the-art communication strategies including wireless and wired methods are reviewed and their advantages and restrictions are summarised in comparison. The review work demonstrates that it is essential to systematically analyse the possible signal modulation approaches for power converter implementations and extend IPST technology in AC power system applications. On this basis, this research then investigates the similarity between signal transmission and power conversion from a system architecture perspective and analyses the mechanisms of pulse width modulation (PWM) based signal modulation methods. Next, the integrated transmission approaches are verified through the buck converter, boost converter and cascaded H-bridge converter, and the simulation results demonstrate that the designed strategies have decent noise immunity. Finally, all the proposed IPST methods in different SESs are validated.

In summary, the main achievements of this study are the analysis of the feasibility of various converters for IPST transmission and the extension of IPST technology to different SES applications.

Key Words: Power converters; integrated power/signal transmission; signal modulation; signal demodulation; smart energy systems.

Table of Contents

List of Tables

List of Figures

Acknowledgements

First of all, I would choose to convey my heartfelt thanks to Dr. Yihua Hu, my primary supervisor, for providing me with this incredible chance to proceed my Ph.D. study. Dr. Hu's academic rigour, generosity and high level of thinking have deeply influenced me, guiding me in my academic direction as well as in my life. Every time I interacted with Dr. Hu, I gained a deeper understanding of power electronics and was inspired to think in a novel way. Once, when I was hesitant to think about how to make a technological breakthrough in the direction of signal modulation, he suggested that I use the idea of permutation to explore the feasibility of composite conventional signal modulation methods. This was like a bright light for me in the darkness of the night, illuminating the environment and warming my heart at the same time. In addition, he often urged me to maintain good research habits. I was advised to improve my sense of English by reading aloud every day and to deepen my understanding by taking notes as I read. Being his PhD student is a tremendous honour for me, and I sincerely wish that my accomplishments have conformed to his high expectations and belief in me.

Secondly, I would also like to use this chance to express my gratitude to my academic advisor, Dr. Youngwook Ko, for his unwavering support and academic advice he has offered me. At each meeting he listened carefully to my progress reports and gave critical guidance. For example, once I pointed out in a debriefing that the filtering method I was using would lead to large errors in the restored signal, he suggested that I use iterative filtering to solve the problem, which helped me a lot.

Thirdly, I would also like to thank my parents. I would not have progressed this far in my studies without their financial assistance. Especially after a series of misfortunes they still supported me without reservation. During my PhD studies, I went through study transfers, city closures due to the Covid-19 outbreak, inability to get a visa, inability to enrol, remote home study and other situations, and I even thought of termination in the middle of my studies. It was their guidance and encouragement that gave me the courage and motivation to move forward.

Fourthly, I am appreciative to my co-operators Associate Prof. Guipeng Chen (Xiamen University), Dr. Kai Ni (Huazhong University of Science and Technology), and Dr. Chao Gong, who provided me with several excellent research recommendations, such as structural planning

and presentation strategies for journal articles, as well as experimental circuit board soldering tricks and transformer winding methods. Special gratitude is expressed to my talented and wonderful colleagues and friend Guanxiong Shen, Hongzuo Liu, Yikun Huang, and Hao Feng, for many great times and excellent talks about future expectations, the nature of society, and the requirement for professionals in industrial development.

Finally, I would appreciate the Department of Electronic Engineering at the University of York for its support of various learning resources. Special thanks go to Ms. Camilla Danese who provided timely advice when I needed help and reminded me of the activities and assessments that I were obligated to attend at key research points.

Declaration

I declare that this thesis is a presentation of original work and I am the sole author. This work has not previously been presented for an award at this, or any other, University. All sources are acknowledged as References.

Major contents in Chapter 3 have been published in *Power Electronics and Drives*, vol. 5, no. 40, pp. 177-188, 2020. The title is 'Bidirectional DC–AC Converter-Based Communication Solution for Microgrid'.

Major contents in Chapter 5 have been published in *CES Transactions on Electrical Machines and Systems*, vol. 4, no. 2, pp. 123-129, June 2020. The title is 'Cascaded multilevel inverter based power and signal multiplex transmission for electric vehicles'.

Major contents in Chapter 6 have been published in *Power Electronics and Drives*, vol. 6, no. 41, pp. 260-275, 2021. The title is 'A Bidirectional Buck-Boost Converter-Based Switching Ripple Communication Strategy for Intelligent Street Lighting Systems'.

Yixuan Zhang

March. 2022

List of Publications

[1] **Y. Zhang**, G. Chen, Y. Hu, C. Gong and Y. Wang, "Cascaded multilevel inverter based power and signal multiplex transmission for electric vehicles", *CES Transactions on Electrical Machines and Systems*, vol. 4, no. 2, pp. 123-129, June 2020.

[2] **Y. Zhang** and Y. Hu, "A Review of Communication and Energy Balancing Schemes in Li-Ion Battery Management Systems", in *the 9th Renewable Power Generation Conference (RPG Dublin Online 2021)*, pp. 76-88, 2021.

[3] **Y. Zhang**, K. Ni, Y. Wang, and Y. Hu, "Bidirectional DC–AC Converter-Based Communication Solution for Microgrid", *Power Electronics and Drives*, vol. 5, no. 40, pp. 177-188, 2020.

[4] **Y. Zhang**, Y. Hu, Z. Tse, Y. Liu, J. Deng, H. Xu, Y. Wang, and W. Li, "A Bidirectional Buck-Boost Converter-Based Switching Ripple Communication Strategy for Intelligent Street Lighting Systems", *Power Electronics and Drives*, vol. 6, no. 41, pp. 260-275, 2021.

[5] **Y. Zhang**, and Y. Hu, "Integrated Power/Signal Transmission in Triple Active Bridge Converters Based on Partial Power Processing for Battery Management Systems", *IEEE Transactions on Industrial Electronics*. (Under Review)

[6] X. Ding, **Y. Zhang,** and Z. Ye, "Current Sensors Offset Fault Online Estimation in Permanent Magnet Synchronous Generator (PMSG) Drives for Offshore Wind Turbines", IEEE *Access*, vol. 9, pp. 135996-136003, 2021.

[7] H. Liu, **Y. Zhang**, Y. Hu, and Z. Tse, "Laser Power Transmission and Its Application in Laser-Powered Electrical Motor Drive: A Review", *Power Electronics and Drives*, vol. 6, no. 41, pp. 167-184, 2021.

Nomenclature

I_B	Bus current of field bus IEC61158-2
$V_{\text{CAN\_H}}$	High voltage level of CAN bus
$V_{\text{CAN\_L}}$	Low voltage level of CAN bus
V_{IDLE}	Idle voltage level of CAN bus
T_s	Switch's switching period
$C_{0,\ldots,n}$	Capacitors
$L_{0,\ldots,n}$	Inductors
$R_{0,\ldots,n}$	Resistors
$S_{1,\ldots,n}$	Switches
I_L	Inductor current
i_{out}	Output current
n_1:n_2:n_3	Transformer's turns ratio
V_{out}	Output voltage
V_{ref}	Reference voltage
K_i	Current amplified value
K_v	Voltage amplified value
φ_A, φ_B	Phase shift angle
V_{in}	Input voltage
D	Switch's duty ratio
a_n, b_n	Harmonic fractions of a PWM waveform
c_n	Amplitude of high-frequency components of a PWM waveform
ω	Angular frequency
$f_{1,2,3}$	Switching frequencies
$t_{0,\ldots,n}$	Different operation stages
φ_1, φ_2	Carriers' phase shift angle
M	Carrier's amplitude

c_{FSK}	Carrier expression of FSK method
c_{PSK}	Carrier expression of PSK method
$c_{IPSK/FSK}$	Carrier expression of integrated PSK/FSK method
e	Upper envelope expression of extracted carrier
$\hat{x}$	Hilbert transform expression
$s_{1,\ldots,n}$	Transmitted signals
$c_{1,\ldots,n}$	Carrier waveforms
$i_{1,\ldots,n}$	Current waveforms
$d_{1,\ldots,n}$	Waveforms during the demodulation process
$re_{1,\ldots,n}$	Restored signals
V_{DC}	DC voltage source
n	Motor speed
p	Pole-pair of a PMSM
P_a, P_b, P_c	Sinusoidal reference waveforms
$B_{1,2,3}$	Battery packs
$P_{12,\ 13,\ 23}$	Induced port-to-port power
$C_{12,\ 13,\ 23}$	Conducted port-to-port power
$T_{12,\ 13,\ 23}$	Total port-to-port power
$V_{1,2,3}$	Battery packs' voltage
$\Delta\varphi$	Perturbated phase shift angle
Δt	Perturbated time
R_T	Thermistor
G_c	Voltage gain of charging mode
G_d	Voltage gain of discharging mode

Chapter 1 **Introduction**

1.1 Development of Power Electronics and Communication Technologies for Energy Systems

In the last century, the development of power electronics has grown beyond leaps and bounds. This rapid development is caused by the expansion of market demand for networked and integrated power electronics-based circuits and systems in various energy conversion and processing applications [1], [2]. Furthermore, with the widespread use of renewable energy in industrial production, residents' daily life and other fields, the requirement for researchers with knowledge of energy conversion has also led more engineers to start research in the area of power electronics.

The semiconductor power devices used in the field of energy conversion and power transmission, joint with the power converter topology theory and control theory, formed the basis of power electronics technologies [2], [3], [4]. The history of power electronics can be traced back to 1900, when the vacuum tube was invented as semiconductor devices for current control [1], [2]. Then the age of vacuum tubes was ended in 1947 when the germanium transistor was created at Bell Telephone Laboratory [1]. When a commercial thyristor was introduced by General Electric Company in 1958, it signalled the beginning of the modern times of power electronics. Then silicon-controlled rectifiers (SCRs) were widely applied as substitutions of power magnetic amplifiers and mercury-arc rectifiers [1]. In the 1970s and 1980s, power electronics technology achieved leapfrog development due to the revolution of microelectronics. The utilization of integrated circuit (IC) control chips and microprocessors provided the feasibility of controlling the high-power semiconductor devices [1], [2], [3]. As the consequence of the introduced high-power, high-speed, and high temperature switching devices, as well as the employed advanced digital control mechanisms, power electronic applications have grown noticeably in recent three decades. The main functions of power electronics technology are power conversion and energy processing, including DC/AC, DC/DC, AC/DC, and AC/AC converter technology, which are widely used in various power levels of power supplies nowadays [2]. As long as humans continue to explore methods to improve

energy efficiency during power production, power transmission and power distribution, power electronics technology still has great potential for future development.

The vacuum tube was mostly used in televisions, radio and other electronic products for data transmission at early time [5]. Later with the introduction of semiconductor devices in the 1940s, it not only greatly promoted the development of electronic technology in the field of power transmission, but also expanded the scope of application of electronic technology in the field of communication [2], [4], [5]. Because the semiconductor devices are smaller, more reliable, and efficient than vacuum tubes, the vacuum tube was gradually replaced by the transistor in the mid-1960s [6]. Then the optical fibre communication was proposed by Hockman and Kao in 1966 [6]. After that, the large-scale data networks whose name were TYMNET and ARPANET were established around 1970, which first employed packet switching instead of circuit switching [6]. In the 1980s, cellular telephone switching protocol was proposed by Fluhr and Nussbaum, and cellular radio gradually became a significant part of the public switched telephone network since then [6], [7], [8].

In the 2000s, there was a tremendous breakthrough in data transmission with new techniques introduced. For instance, the maximum data rate through narrow bandwidth copper cables was increased by applying digital subscriber line technology. Additionally, other techniques such as code division multiple access and time division multiple access achieved both speech and data transmission through mobile cellular communication systems and had a profound impact on smartphones' future development [6]. After a century of development, a broad range of theories is involved in communication technology, which includes information theory, electromagnetic wave theory, stochastic process theory, signal transmission theory, and so on [5], [6], [7], [8], [9]. Nowadays, the communication technique has been widely applied in satellite communications, mobile phones, computer networks, and other areas. The communication technology will continue to evolve in the future, especially the concept of the Internet of Things (IoT) has created a new opportunity for its development [10], [11], [12], [13]. The IoT is aiming to connect various objects and devices to the Internet, thus information can be exchanged between humans and objects, objects and objects. One of the vital components of IoT technology is data communication on terminal devices. Comparing to the general Internet terminals, the communication devices of IoT technology have the characteristics of easy installation, simple peripheral circuit and low cost [10].

1.2 Applications of Smart Energy Systems

As a source of power for residents' daily production and life, energy systems have a profound impact on contemporary issues such as climate change, health and environment, sustainable development, environmental protection, global energy and food security [14]. However, traditional energy system based on fossil energy sources can no longer meet the requirements of energy development in the 21st century due to unfavourable factors such as high environmental pollution and the depletion of fossil energy sources. Therefore, it is necessary to develop smart energy systems (SESs) to replace traditional energy systems to cope with the massive demand for energy from a growing population, while mitigating environmental damage and increasing energy use efficiency. The concept of SES was first introduced in [15] and [16] as a revolutionary invention and architecture to enhance system flexibility by optimising the energy structure, particularly in the 'conversion' phase of the power system. In other words, this entails merging the electricity, transport and thermal sectors and using the flexibility of these diverse areas to complement the lack of flexibility of renewable energy sources, including hydro and tidal energy. As depicted in Fig. 1-1, the SES concept can be applied in a wide range of electrical applications such as microgrids, electric vehicles, smart cities, and energy routers. However, most of the existing research is focused on the control and management systems of microgrids to improve energy efficiency, thus there is still great potential for SES in other areas [17]. As the aim of SES is to improve energy efficiency and promote flexibility in power generation, power electronic converters are required to guarantee that the same format of power is transmitted over the power lines. Furthermore, appropriate communication strategies are needed for the system to adjust energy supply and demand in a timely manner.

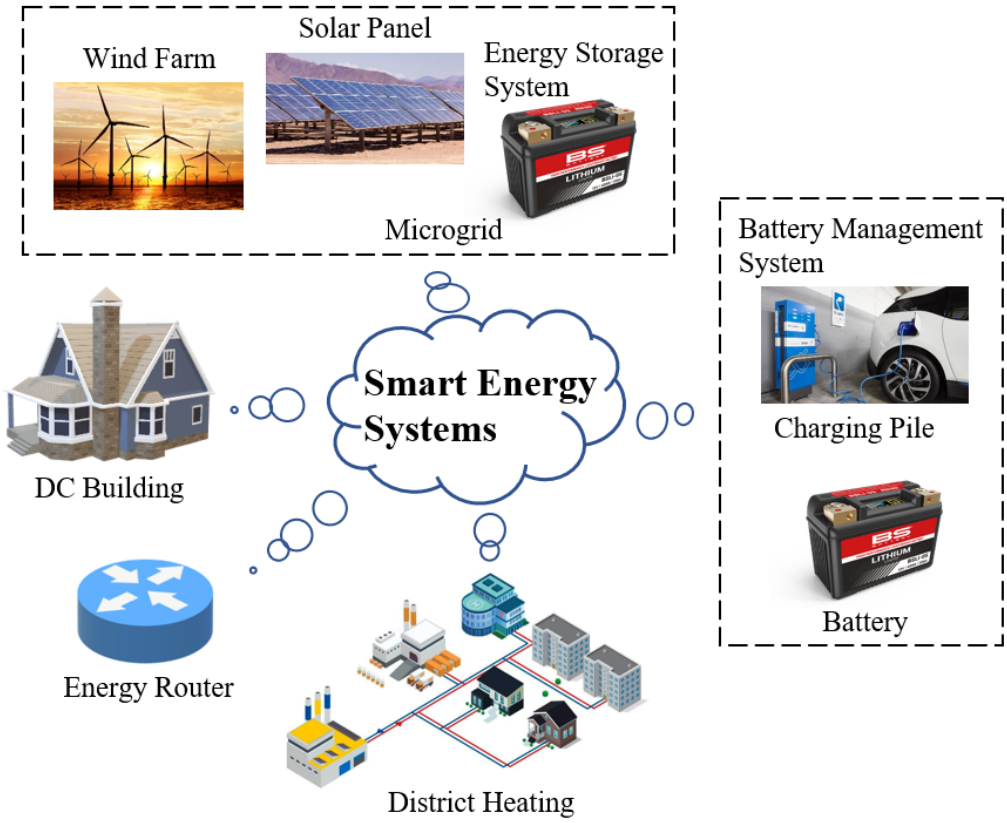

Figure. 1-1. Potential applications for smart energy systems

For example, the concept of microgrid is advocated to realise large-scale energy conversion and power transmission through resource optimization, considering the needs of high dependability and low cost in creating power grid systems [18]. Some of the microgrid system uses the two-way flow of power and information to provide consistent, secure, and efficient real-time demand–supply control [19], [20], [21], [22]. Power converters are applied in microgrids to connect various distributed power generators to the grid network. Because microgrids are expected to create and transmit a great quantity of data such as tariffs and electricity plans, an efficient information transmission technique is required not only to cope with such vast data but also to solve network security challenges such as customer information leakage and wide-scale blackouts [23], [24]. From this perspective, microgrid is consistent with SES in terms of the goal of system architecture optimisation and renewable energy integration. Moreover, the SES concept can be utilised in battery management system (BMS) of electric vehicles (EVs) to increase battery life span by managing the charging and discharging process of the battery. Power converters are employed in the powertrain of EVs to transfer energy between batteries and motors. Communication signals including battery status and motor speed signals are transmitted to enable efficient management within the EVs. Therefore, SES systems

should be developed to meet the specific requirements of these applications by considering aspects such as energy security, environmental friendliness and cost effectiveness as exhibited in Fig. 1-2. Nevertheless, power conversion and information transfer are two separate sections in conventional SES, hence this study has significant implications for reducing the size and cost of SES systems by using power converters to implement information transmission.

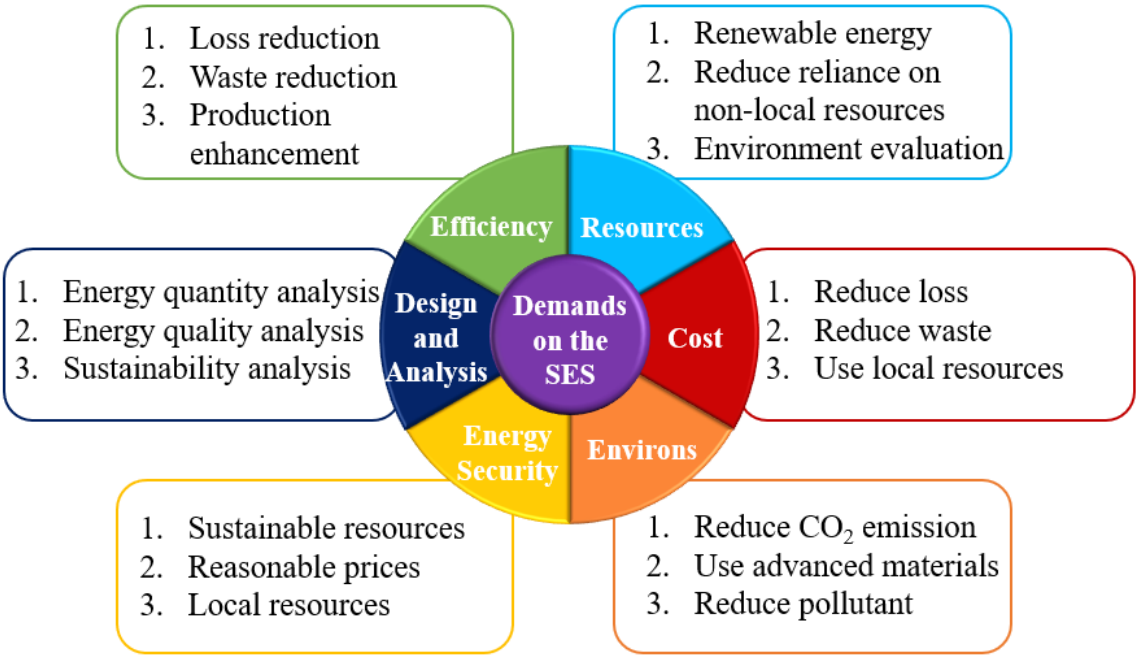

Figure. 1-2. Design considerations of a SES system [25]

1.2.1 Electric Vehicles and Battery Management Systems

Global warming is one of the major problems that the world is facing today. The challenges posed by climate change are driving sustainable energy development to reduce carbon dioxide emissions from fossil fuel combustion. However, renewable power sources like wind, hydro, and solar have a great dependence on the environment, which leads to the instability of the generated power [26]. For instance, wind turbines will not rotate if the wind speed is not within the expected speed range [26]. Additionally, the same amount of photovoltaic (PV) arrays produces much less electric power on a rainy day than on a sunny day [27]. Therefore, various solutions have been proposed in the literature to solve the variability of renewable energy sources. For example, the feasibility of demand side management for the electricity system is considered in [28]. Besides, using hybrid energy as power supply for smart grid is addressed in [29]. Moreover, employing energy storage systems such as batteries, water pumps, and oil

heaters is another possible solution to solve the unstable issue of renewable energy sources [30], [31].

Recently, the application of EV has created novel possibilities for the development of renewable energy sources. The electric power created by renewable energy sources can be stored in batteries and then consumed by EVs. Compared to the traditional internal combustion engine car, the electric vehicles not only produce fewer air pollutants such as CO and NO_2, but also generate less noise by its motor [32]. Furthermore, if the battery of EV is charged at night, it can avoid the peak of power consumption, which is beneficial to the grid to balance the load and reduce the cost [33]. There are three main types of electric vehicles: battery EV, plug-in hybrid EV, and fuel-cell EV. The technology of battery EV is relatively simple and mature comparing to hybrid EV, and its battery packs can be easily recharged from the charging station [32]. A hybrid EV obtains its power from conventional fossil fuels or rechargeable energy storage device. Because it employs hybrid power, the internal combustion engine's maximum power can be calculated using the average required power to maintain the system operates efficiently. The battery is used to complement the power of the internal combustion engine when it is insufficient. Moreover, the surplus power of the internal combustion engine can produce electricity for battery charging under low load condition [33]. Since both the energy sources are consumed reasonably during the vehicle operation, the system is energy efficient. A fuel-cell EV acquire electric power through chemical reactions in fuel cell stacks [34]. A fuel cell EV is an environmentally friendly vehicle since its chemical reaction mechanism does not generate hazardous products and its energy conversion efficiency is better than that of an internal combustion engine [34].

Electric vehicles have a broad market prospect. According to a group of data demonstrated in Fig. 1-3 [35], the number of EVs on the road maintains growing from 2010 to 2016 and reached 2 million units in 2016. One of the main challenges in increasing the market share of EV is that its price is much higher than that of the same model using an internal combustion engine [36]. Nevertheless, with the enhancement of relevant national support policies, EVs still have great potential for development in the transport market.

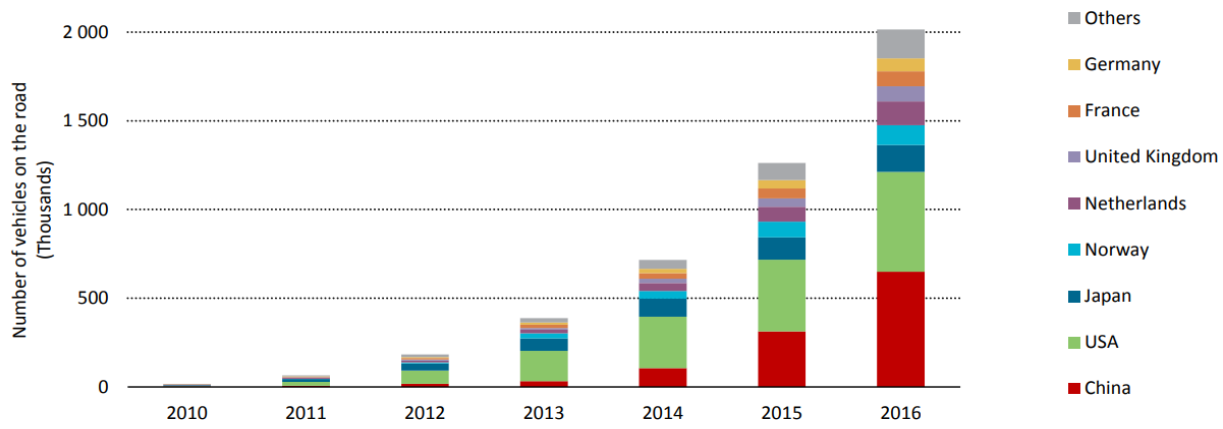

Figure. 1-3. The number of EVs on the road in different years [35]

As fossil fuel restrictions and pollution increase, electric vehicles (EVs) have become increasingly accepted as a viable alternative to regular internal combustion engine vehicles [37], [38], [39]. Lithium-ion batteries are broadly accepted in EVs due to its high energy density, high power density, low self-discharge rate, and long-life span [39], [40], [41]. However, extra care is required to ensure that the batteries operate properly. Specifically, overcharging the battery can result in overheating and even explosion. Furthermore, over-discharging the battery can hasten the ageing process and diminish the battery's capacity permanently [42], [43]. As a result, the battery management system (BMS) is designed to maintain battery packs functioning within safe limits by monitoring voltage, current, temperature, and estimated state of charge (SOC) and state of power (SOP) of battery packs [44], [45].

Battery balancing is one of the major functions of a BMS [46]. With the battery balancing function, the energy can be dispersed evenly, and the energy wasted in long battery strings that operate under frequent cycling circumstances can be reduced when the nominal voltage, current, or power is transferred among battery cells [46], [47]. According to the various energy dissipation strategies, battery balancing approaches can be classified as passive balancing and active balancing [48]. In passive balancing, the surplus energy of the overcharged battery is dissipated by the fixed shunt resistor [49] or the switching shunt resistor [50], [51]. Because of their simple structure and ease of implementation, passive balancing techniques are attractive for low-cost system applications [48]. However, because the excess battery charge is released through the heat created by the resistor, this approach is inefficient in terms of energy consumption. Active balancing approaches, as opposed to passive balancing methods where energy is dissipated through resistors, utilise inductors [52], [53], capacitors [54], [55], converters [56], [57] and transformers [58], [59] to transfer energy between independent cells.

Consequently, since power flows from higher charge batteries to lower charge batteries, there is negligible energy loss in active balancing [44]. Although active balancing is more efficient in converting energy than passive balancing, it contributes to the complexity of the circuit and switching control [48].

1.2.2 Intelligent Street Lighting Systems

Street lighting systems are critical for traffic safety, everyday life for citizens, and city beautification. As the number of streetlights utilised to satisfy the needs of urban development grows, an effective light emitting diode (LED) management method is required to decrease urban lighting system power consumption and postpone bulb ageing and failure [60], [61].

In recent years, research on Intelligent Street Lighting (ISL) systems has grown in popularity in response to the above-mentioned design criteria. ISL can facilitate the deployment of smart municipalities and improve urban and municipal service capacities as an important component of smart cities. It can perform tasks such as measuring the current, voltage, and temperature of streetlights, on-site operation monitoring of key road sections, street light-based EV charging stations, and so on [62], [63]. In such a system, the data transmission between the remote console and the LED lights, which can increase the utility of LED lights based on actual environmental situations and lower the cost of manual detection in the case of LED failure [64]. To enable communication between remote consoles and LED lights, a possible solution is to use an Internet of things (IoT) framework where embedded and wireless sensors, such as light, sound and infrared sensors, are used for status detection of the LED lights and the sampled data is transmitted to the remote console through different methods such as ZigBee [65], [66], [67], global system for mobile communication (GSM) [68] and power line communication (PLC) [69]. The inclusion of automation in the ISL control process allows for environmental protection, high system efficiency and energy savings, and provides sufficient lighting for late night travellers [70].

Various investigations have analysed the impact of utilising different communication strategies in ISL management systems. For instance, ZigBee is a short-range wireless network standard that transmits data at up to 250 kbps through the 2.4 GHz frequency spectrum [71]. Each node in the grid is linked and can operate as a transmitter and receiver at the same time [71], [72]. According to [73], a ZigBee-based wireless sensor network is proposed for an energy-conserving street lighting system. In addition, a ZigBee-based wireless streetlight control

system is studied in [74] for streetlight remote monitoring and power adjustment as well as on/off control. GSM is a long-distance communication system. The microcontroller can manage the on/off state of a streetlight by setting a time delay, and an update can be delivered to a specified phone number when GSM is used in an ISL system [75]. Furthermore, as demonstrated in [76], a GSM-based ISL system is provided for remote streetlight monitoring and control. In this system, the microcontroller processes the sampled data and sends the results to the control centre through short message service (SMS). To provide consumers with cost-effective and dependable ways to operate streetlights remotely, a command is sent to the base station for night illumination through SMS, and the user can then receive a successful initiating response [77].

Power line communication (PLC) is a technology that integrates power and signal transmission over power lines. The research of PLC-based ISL systems has attracted interest in recent years due to the benefits of cheap maintenance costs and broad coverage [78]. In a PLC-based ISL system, a signal relay strategy is applied to overcome the PLC's insufficient distance, and management and timely control functions are achieved through the efficient use of grid resources [79]. According to [80], a homemade power modem chip is developed to suppress noise in low voltage power lines, assuring the ISL remote control's efficiency and dependability. As demonstrated in [81] and [82], converter-based approaches are used to modulate and inject signals into power lines for communication between the central controller and each streetlight due to the simple signal modulation technique and high interference rejection ability. Moreover, according to [83], a baseband switching ripple communication approach for LED lighting is developed to achieve high data rates and low switching frequencies.

1.3 Motivation of Integrated Power/Signal Transmission

With the development of the smart grid and the demand for renewable energy generation systems, more and more power electronics equipment require communication. The conventional method for realizing communication is to embed optical or wireless communication modules to the original system. This does not significantly affect their size and cost for large equipment. But for terminal circuits in most distributed power systems, such as cell balancing circuits in battery management systems, and state detection and power

optimization circuits for photovoltaic modules, the volume and cost for the whole system will increase significantly [84], [85].

Although the existing wired communication approaches such as power line communication (PLC) technology, power over Ethernet (PoE) technology, and Fieldbus technology can be used for transmitting both power and communication signal simultaneously, some limitations still cannot be ignored. For instance, because the power line itself is not initially used for data transmission, the characteristics of power line impedance are different from other wired transmission media such as optical fibre. In other words, the complexity of the power line channel limits the distance and reliability of the transmitted data. Moreover, as the frequency band of carriers in broadband power line communication is from 2 MHz to 32 MHz, which is coincides with the frequency of short-wave radios, it is necessary to consider the radiation interference generated by such carrier [86]. In the IEC61158-2 Fieldbus standard, each bus typically can provide less than 10W of power, and the current-mode power supply design causes the node current cannot vary widely [87]. Moreover, since the PoE technology employs Ethernet for power transmission, its applications are limited by its low power rating restriction and are only suitable for VoIP phones, IP cameras, and other low power devices.

This research aims to analyse the approaches of signal transmission employing power converters and to investigate relevant applications of this technology. To simplify the expression, the power converter-based signal transmission method is referred to as integrated power/signal transmission (IPST) in the subsequent content. Compared to conventional wireless communication, IPST method has **higher noise immunity** and **higher data security** because its data transmission channel is a fixed power line. Due to the nature of high-power ratings of power lines, it is challenging for hackers to intercept information transmitted over power lines. Additionally, the signal couplers such as resistors, capacitors, and inductors utilised in PLC and the extra communication cables applied in wired communication system can be omitted in IPST approach, thus **reducing system volume and cost**. Although there are some related studies using converters to transmit signals, most of them are based on DC/DC converters and other topologies have rarely been studied. Therefore, it is necessary to further investigate the theoretical basis of the IPST approach and to study its potential applications. To achieve the objective of this research, it can be further divided as follows:

i. To review the state-of-the-art communication strategies. Specifically, the mechanisms of wired communication such as PLC and PoE are reviewed. Moreover, the advantages

and disadvantages of each communication approach and the areas of application are summarized. Furthermore, the up-to-date studies related to IPST technology are discussed. The limitations of these studies can be identified after the review, thus the necessity of developing IPST technology is addressed. Additionally, the potential applications of IPST technology are extended to battery management systems (BMS) for electric vehicles (EVs), microgrids, and intelligent street lighting (ISL) systems based on these studies, which are the main targets of this research.

ii. To analyse the similarities between power converters and communication technologies in terms of structures and modulation strategies and propose general ideas for data modulation and transmission using power electronic converters based on these similarities. Besides, the feasibility of baseband communication and carrier communication through power converters is proved. Moreover, the modulation and demodulation methods of IPST technology are verified by simulation with a buck converter. To promote the data rate of carrier communication, an integrated phase shift keying/frequency shift keying (IPSK/FSK) method is proposed, which is verified by a Buck converter, a Boost converter, a Buck/Boost converter, and a cascaded H-bridge converter. The results are compared with conventional carrier modulation methods, and it is demonstrated that the proposed method has a low bit error rate (BER) and excellent noise immunity.

iii. To develop an IPST-based BMS for electric vehicles for battery charge/discharge balancing. The proposed strategy employs power converters instead of a controller area network (CAN) bus for signal transmission, thus reducing the cost of EV communication system by simplifying system wiring. Besides, a partial power processing (PPP)-based triple active bridge (TAB) converter is proposed rather than isolated TAB converter to promote energy conversion efficiency. Moreover, the battery state of charge (SOC) data, motor speed control signal, vehicle light instruction signal, and other communication data can be successfully transmitted with the proposed method.

iv. To develop a bidirectional Buck/Boost converter for ISL systems to realise two-way communication. Considering that the low stability and high cost of ZigBee-based ISL systems and the complicated system wiring of a wired ISL communication system, a novel IPST-based ISL system is proposed. The remote-control centre of the designed

system can transfer control signals of light-emitting diodes (LEDs) and can receive the operating status of LEDs from each LED terminal. Moreover, the proposed system contains a 'request to send/confirm to send (RTS/CTS)' mechanism to avoid conflicts when multiple LEDs send their status at the same time. Furthermore, the streetlights in the proposed system are powered by photovoltaic (PV) panels placed on the roofs of bus station platforms, which has a great significance for the development of low-carbon-emission cities.

1.4 Dissertation Outline

The dissertation involves eight chapters. The structure of the dissertation is arranged as below:

Chapter 1 briefly introduces the background of power electronics and communication technology for SESs. In addition, the motivation of this research and the outline of this thesis are exhibited.

Chapter 2 reviews the principles of wired communication technologies for electrical energy conversion systems, and summarises their advantages, disadvantages, and applications. Besides, the latest research on converter-based signal transmission from the perspective of signal modulation and demodulation schemes are reviewed, from which the limitations of previous studies are summarized, and the feasibility of using power converters for signal transmission is concluded.

Chapter 3 compares the similarities between power converters and communication technologies and demonstrates the mechanisms of feasible IPST approaches. A comparative study of the proposed IPSK/FSK transmission method with other methods is carried out to demonstrate the higher data rate of the proposed method. Moreover, a Buck converter, a Boost converter, a Buck/Boost converter, and a cascaded H-bridge converter are employed as simulation models to present IPST results.

Chapter 4 designs a PPP-based TAB converter for BMS to achieve multi-directional energy conversion and signal transmission. The operation mechanism of the designed converter is discussed, and the signal transmission capability is verified by simulation. Besides, the extended application of the proposed converter is illustrated.

Chapter 5 designs a cascaded multi-level inverter topology for EV power system. After demonstrating the defects of CAN bus-based EV communication system, the designed system employs frequency shift keying (FSK) approach to modulate motor speed control signal and batteries SOC data. Furthermore, a batteries balance discharging strategy is presented, and the feasibility of the proposed method is examined by simulation.

Chapter 6 develops a bidirectional buck/boost converter for the ISL systems. The system configuration and on/off control mechanisms are presented. Meanwhile, the general and emergency communication strategies between the remote controller and each streetlight are discussed. In addition, the energy saved by the proposed system is estimated by placing photovoltaic panels on the roof of the bus stop platform for energy harvesting.

Chapter 7 concludes the main achievements of this research. Furthermore, future studies that related to signal transmission speed optimization and IPST application extensions are illustrated.

Chapter 2 Review of Communication Technologies for Electrical Energy Conversion Systems

To clarify the limitations of existing communication technologies and previous studies on IPST technology, this chapter reviews the mechanisms of various wired communication strategies, such as fibre-based communication, CAN bus-based communication, and PLC technologies. The merits, defects, and applications of each communication technology are concluded in this chapter. Besides, the state-of-the-art studies on IPST technology are reviewed. The signal transmission methods of IPST technology are categorised into three fractions in this research, which are baseband communication, PSK-based communication, and FSK-based communication. The author observed a valuable research direction to improve the signal transmission speed by IPSK/FSK modulation method through the review work and found that the IPST technique can be used not only for DC/DC converter-based applications but also extended to various DC/AC and AC/DC converter-based applications, such as BMS for EVs, AC microgrids, and ISL systems. Moreover, the review in this section lays the foundation for the remainder of this study.

2.1 Wired Communication

Wired communication is another communication strategy that employs wires as a communication medium. Unlike wireless communication, wired communication is more stable and relatively unaffected by adverse weather conditions because it has a fixed transmission path. This section reviews the mechanisms and limitations of commonly used wired communication strategies involving PLC, PoE, fibre optic communication, and CAN-bus based communication.

2.1.1 Power Line Communication

Power line communication (PLC) generally refers to the utilisation of power lines for data transmission, including communication for both low-voltage distribution lines and high-voltage transmission networks [88], [89], [90], [91]. The history of PLC began around 1918, and such technique has been widely applied in automatic meter reading, grid load control, and

power management since the 1950s [91]. Based on the various frequency range of the modulation wave, the PLC technique can be categorised into broadband PLC and narrowband PLC. Narrowband PLC has a lower data rate and can be applied for equipment control. On the contrary, broadband PLC was invented at around 1990, allowing up to 10 Mbps high data rate transmitted using frequencies between 2 and 30 MHz. Because of its high data transmissions rate, it can be utilized for Internet access [88], [91].

The PLC modulation techniques were evolving to increase the channel capacity. FSK method and PSK method were applied for early PLC carrier signal modulation. In binary FSK method, two discrete carrier frequencies are used to transmit binary '0' and '1'. In PSK method, by changing the phase of a carrier wave, a digital signal can be modulated using a finite number of various carriers. However, using a single frequency cannot eliminate the effects of frequency selective fading and can be easily interfered by the harmonics with the same frequency from the environment during the transmission process [88], thus spread spectrum (SS) modulations such as frequency hopping (FH) was investigated for the low-voltage PLC channel [92], [93]. In this modulation scheme, a pre-defined pseudorandom sequence is revealed to both transmitter and receiver. Such sequence is then employed for a carrier to fast switching among various frequency channels [93]. Since the transmitted data is encrypted by a pseudorandom sequence, the frequency hopping signals can effectively against deliberate interference. Nevertheless, the total bandwidth applied for frequency hopping is much larger than that used to transmit the same message with a single carrier frequency [93]. Orthogonal frequency division multiplexing (OFDM) technique is another efficient method to increase the data transmission rate in broadband PLC. The multi-carrier transmission technology OFDM realizes data transmission by converting serial data into N parallel data and then distributing it to N orthogonal subcarriers [94], [95]. Although the modulation rate of each carrier is relatively low, the overall data transmission rate can achieve 200 Mbps [96]. OFDM technique has various advantages. For example, it has high-frequency band utilization and can suppress inter-symbol interference as well as inter-carrier interference effectively by adding guard time and cyclic extension during the modulation process [95]. Moreover, as the modulation and demodulation of the sub-carriers is achieved by utilising inverse fast Fourier transform and fast Fourier transform approaches respectively, the OFDM method is highly efficient [95].

The PLC technology can be applied for distributed DC power and photovoltaic systems after optimizing line impedance and signal coupling circuits. To simplify system wiring, a PLC technique is applied to realise communication between various sensors of the robot [97]. Its

PLC signal coupling circuit adopts transmission line transformer design to increase the output current and the number of nodes. According to [98], PLC technology is used to the optimal control of photovoltaic power generation system. For the photovoltaic array consisting of multiple series-connected photovoltaic modules, the maximum output power of a partially shadowed photovoltaic array can be tracked by adding a boost circuit and PLC communication module in each photovoltaic module. The operating conditions of each PV panel can therefore be transmitted through the power cable. Additionally, this paper also verifies the feasibility of PLC applied to series DC power supply system by analysing the characteristics of transmission signals. As demonstrated in [99], the direct sequence spread spectrum signal generated by the load disturbance is directly superimposed on the output power line of the photovoltaic panel by controlling the load modulation circuit in parallel with the photovoltaic module to transmit the state information of each photovoltaic panel. This approach is cost-effective, but the communication rate is low. Although each of the above methods has its own advantages, their power supply circuit and communication circuit are completely independent.

2.1.2 Fieldbus IEC 61158-2

IEC 61158 is the international standard for Fieldbus and released the sixth version in 2014. IEC 61158-2 is the physical layer standard for Fieldbus, which specifies the implementation of bus power supply [100]. It uses Manchester encoding to transmit baseband signals. Specifically, the binary '0' is transmitted when the signal changes from 0 to 1, and the binary '1' is transmitted when the signal changes from 1 to 0. Based on this mechanism, the data is transmitted by adjusting the current +/-9 mA to the bus current I_B of the system as shown in Fig. 2-1. The bus has a large AC impedance because the bus power output and the bus node input are designed as current source types. Fig. 2-2 indicates the structure of IEC 61158-2 communication system. The transmitting terminal sends the data to the bus in the form of incremental current. Since the AC impedance of the bus is a constant value, which is determined by two 100 Ω terminal resistors, the incremental current signal can generate a voltage pulse and such pulse is then overlaid on the bus. At the receiver, the transmitted signal can be decoded by measuring the voltage variations. The system employs a twisted pair as the transmission medium and up to 32 sites can be connected to a bus segment. Unlike PLC transmitting a signal by moving its spectrum to other frequency bands, IEC 61158-2 uses power line baseband modulation approach for signal transmission. Therefore, instead of using the conventional analogue modulation and demodulation circuits, Fieldbus IEC 61158-2 only

employs a few coupling circuits, comparators, digital processing circuits, and control software to realize communication function [101].

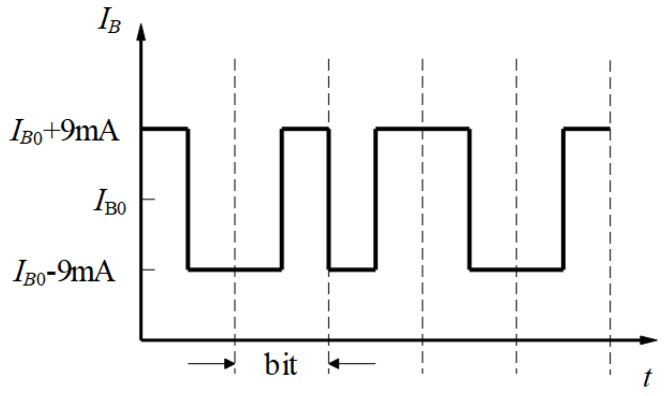

Figure. 2-1. IEC61158-2 bus communication current waveform [102]

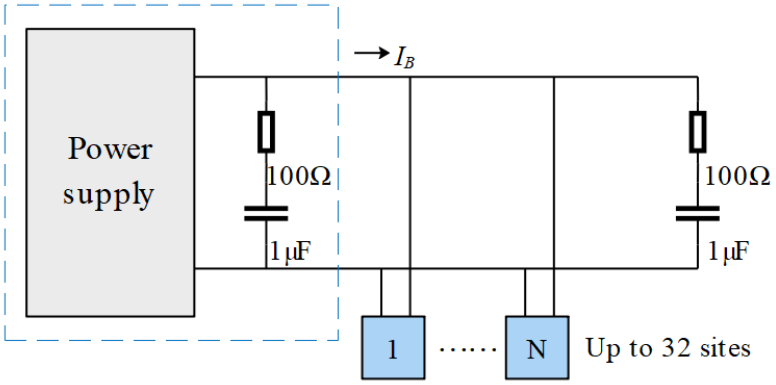

Figure. 2-2. IEC61158-2 communication system structure [102]

2.1.3 Power over Ethernet

Power over Ethernet (PoE) is a technique that employs twisted pair Ethernet cable to transmit information and power to IP-based endpoints like voice-over-Internet (VoIP) phones. [103], [104]. Conforming to the 10 Mbps 10BASE-T and 100 Mbps 100BASE-TX standards, modern Ethernet cabling consists of four twisted pairs, only two of which are used for data transmission [103]. The international standard of PoE is IEEE802.3af, which was established in 2003 [103]. This standard not only proposed a unified method to powering devices either by utilizing 24 or 48 volts to the spare pairs or by incorporating the data lines for power transmission but also enables non-PoE compatible devices that not require power to access the network [103], [104], [105]. Furthermore, power sourcing equipment (PSE) and powered device (PD) are two types

of devices identified in such standard, where the PSE offers the required power and the PD operates as the receiver of the power [104].

End-span PSE and Mid-span PSE are two different approaches for transmitting DC power through Ethernet twisted pair. In End-span PSE structure, the PSE is involved in the hub or switch. There are two different approaches for power supply connection in End-span PSE as presented in Fig. 2-3. The first approach transmit data and power through the same pairs and the power is transmitted through the spare pairs in the second method. When utilizing the spare pairs for power transmission, the cable's current carrying capacity is increased by connecting the wires inside the pairs together [104]. When employing the same pairs for data and signal transmission, there will be no DC bias occurred in the windings of the transformer if the DC currents in each of the wires in the pair are the same [104]. In Mid-span PSE structure, PSE can reside anywhere in a 100-meter Ethernet cable, connecting legacy hub or switch ports to end stations. Because the power is generated by mid-span device rather than the switch, the standard off-the-shelf Ethernet switches can be maintained in this structure [104], [105]. The power can only be carried by spare pairs for a mid-span equipment as the signals have to be transmitted without disruption. The system composition of a Mid-span PSE is displayed in Fig. 2-4. To improve power supply capacity, the maximum output power of PSE in the standard IEEE802.3af is larger than 15.4 W, the value of which is further boosted to 100 W in the standard IEEE802.3bt in 2014 [106].

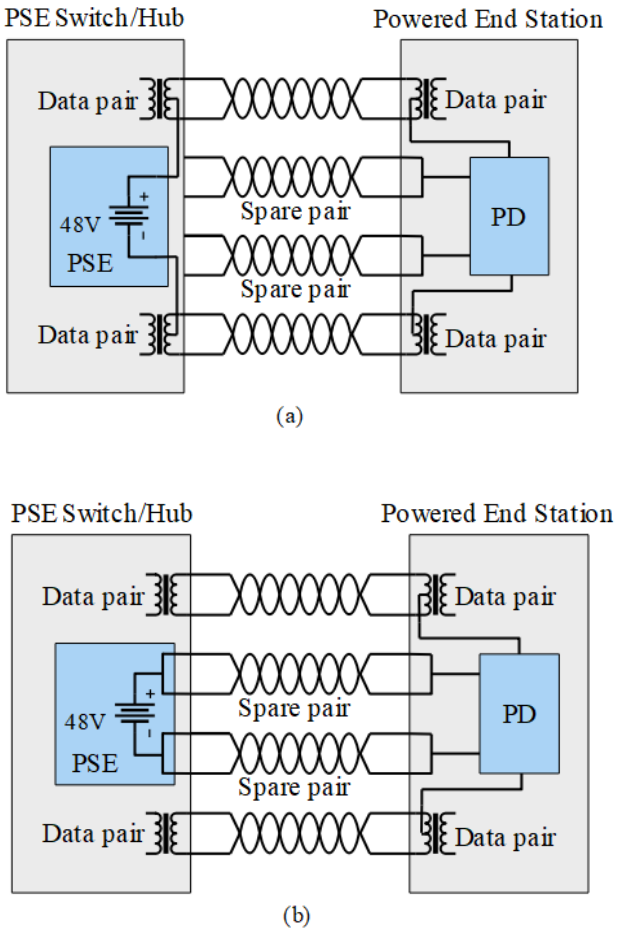

Figure. 2-3. The system structures of the End-span PSE applied in PoE, where (a) refers to the data and power transmitted through the same pairs and (b) demonstrates the power transmitted through the spare pairs [104]

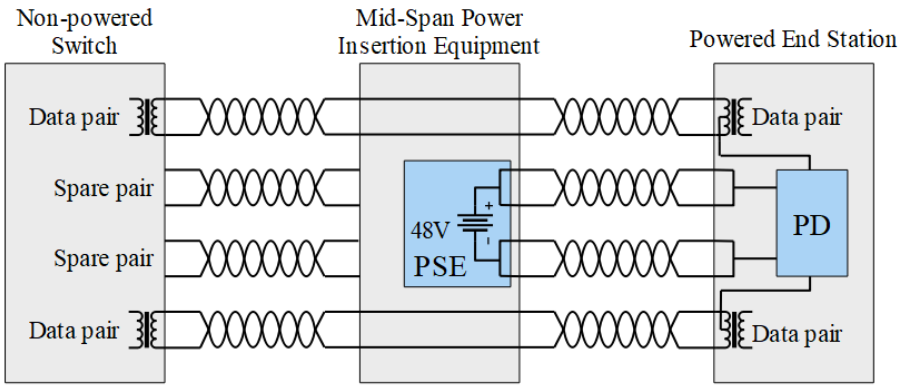

Figure. 2-4. The system structure of the Mid-span PSE applied in PoE [104]

2.1.4 Fibre Optic

A cylindrical dielectric waveguide built of low-loss materials is known as an optical fibre. It is mainly built by high-chemical-purity fused silica glass. Because the refractive index of the waveguide's core is greater than the exterior dielectric's refractive index, light is steered down the fibre axis in a fashion that guides light through total internal reflection [107]. In a fundamental fibre optic system, a transmitter firstly transforms an electrical signal into light, and then the light is transmitted through an optical fibre cable to the receiver. Finally, the light signal is received and transformed back to an electrical signal at the receiver. Fibre optic communication technology has been well developed since it was first studied around 1975 [107]. Nowadays, commercial long-haul C+L-band light wave systems can transmit up to 192 channels over a 50 GHz grid at rates up to 250 Gb/s, with a total long-haul capacity of 48 Tb/s at spectral efficiency of 5 b/s/Hz and up to 76 Tb/s at 8 b/s/Hz for short-haul applications [108]. In addition, the Pacific Cable Network can achieve 144 Tb/s bidirectional data rates in the Pacific Ocean with six fibre pairs [108].

Fibre optic communication systems have the following advantages over metal cable systems. Firstly, the potential transmission bandwidth of the optical carrier frequency is much larger than that of a metallic cable system. Besides, fibre optics are smaller in size and lighter in weight than metallic cables. Moreover, since optical fibres are composed of electrical insulators such as glass or plastic polymers, they do not cause arcs or sparks when exposed to abrasion or short circuits, making them feasible for applications where there is an electrical hazard [107]. With these merits, fibre optics is popular in computer networks and telecommunications. However, there are still drawbacks to fibre optics, including expensive installation costs, connector costs between fibres, and maintenance costs [109].

2.1.5 Controller Area Network-Based Communication

In the early 1980s, Robert Bosch GmbH invented the Controller Area Network (CAN) bus to realise robust and low-cost communication in automotive networks [110]. Then Bosch launched the CAN flexible data-rate in 2012, which has a 64-byte payload and can achieve 5 Mbps in practise [110]. A typical CAN bus structure is presented in Fig. 2-5, where it employs a twisted-wire pair as the communication medium. Besides, each node of the CAN bus contains a microcontroller unit (MCU) to connect actuators and sensors to the bus. Additionally, the transceiver at each node is used to receive and drive signals from the bus and to convert the

single-ended logic utilised by the CAN controller into differential voltage signals for transmission on the CAN bus and vice versa [111]. Therefore, each node of the CAN bus can either send or receive data, and its typical architecture supports either master-slave or point-to-point communication and determine whether to respond to the received signal [111]. Furthermore, the CAN protocol utilises differential lines to promote the noise immunity of the system and decrease electrical interference. Specifically, CAN_H and CAN_L are the two lines with different voltage level used for signal transmission. When one of the nodes transmits logic '0' to the bus, the bus signal will remain dominant logic '0' as shown in Fig. 2-6. Nowadays, CAN technology has been extended to various applications. For example, a CAN bus is applied to transmit speed and position control signals for motor drive system to avoid the defects of the RS-845 in [112]. As presented in [113], CAN bus is used in a human motion capture and analysis system for transferring human motion data among signal processing units at various locations, which is designed to assist elderly people walk properly.

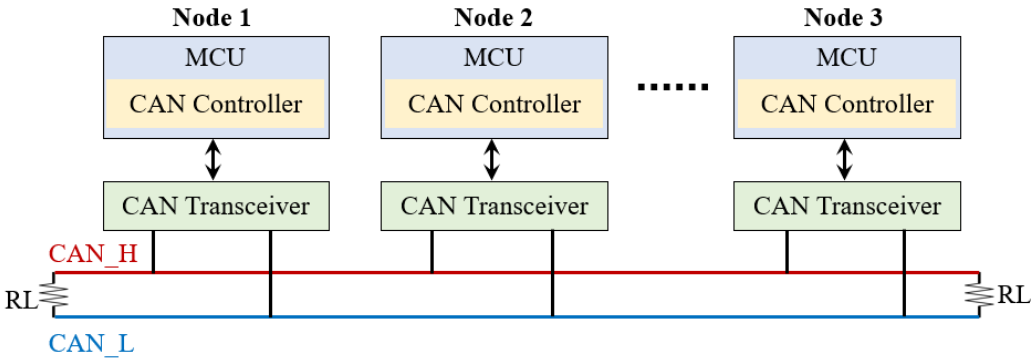

Figure. 2-5. A typical architecture of a two-wire controller area network (CAN) bus [110]

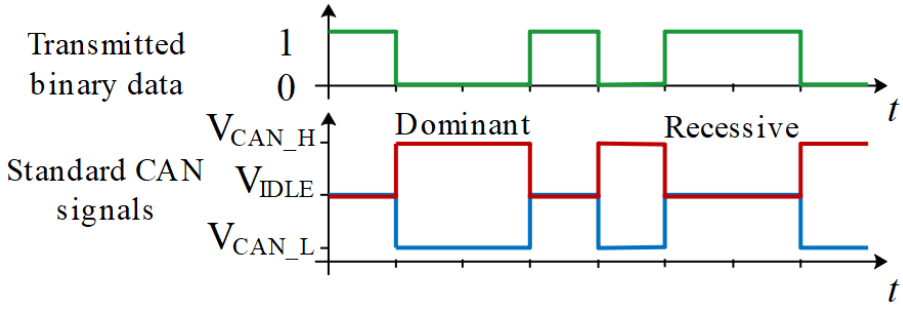

Figure. 2-6. Signalling strategies in CAN bus [114]

As CAN bus simplifies the communication system of the automotive network by reducing wires and costs, it enables efficient signal transmission through a centralised network of

electronic units [111]. In addition, because CAN features arbitration on message priority (AMP) protocols and carrier sense multiple access with collision detection (CSMA/CD), it permits nodes that have lost arbitration to deliver information while the bus is idle, without incurring any data loss or disturbance [111]. Nevertheless, only up to 64 nodes can be linked to the CAN bus, which limits the use of the CAN bus to specific areas. Moreover, although the CAN bus contains a cyclic redundancy check (CRC) algorithm for transmission faults checking, it cannot prevent adversary injection of data [110]. Therefore, the CAN protocol lacks a thorough integrity check to maintain data integrity.

2.1.6 Comparative Analysis for Wired Communication Methods

Each of the above wired communication strategies has its advantages. PLC is popular because they avoid the use of additional communication cables. Besides, the fieldbus IEC 61158-2 enables the connection of programmable logic controllers at the direct control level to plant devices at the field level through digital signals. Moreover, PoE is famous for its low installation cost, while fibre optic has the merit of high bandwidth level. Furthermore, CAN bus enables centralised control of network-connected electrical components, making it popular in automobile control systems. Table 2-1 summarises the specifications of the above wired communication technologies.

TABLE 2-1 Comparisons of Wired Communication Technologies

	Maximum speed	Distance	Standard	Application	Advantages
Power line communication [89] [90]	1-2 Mbps for broadband	100 km for low frequency	IEEE 1901	Home automation, and smart grid	Simplified wiring and low cost
Fieldbus IEC 61158-2 [100] [101]	31.25 kbps	2 km	IEC 61158-2	Power generation and distribution	Simple modulation
Power over Ethernet [103] [104]	100 Mbps	100 m	IEEE 802.3 af	IP camera and VoIP phone	Low cost
Fibre optic [107] [108]	400 Gbps	300 m	IEC 60793-2	Light guides and structural health monitoring	Wide bandwidth and light weight
CAN bus [111] [112]	1 Mbps	250 m	ISO 11898	Electric vehicle and lifts	All nodes can communicate

2.2 Integrated Power/Signal Transmission

Integrated power/signal transmission (IPST) technology is designed to transmit both power and communication signals using the same medium, thus eliminating the need for power transmission equipment or communication equipment in conventional systems to save costs. As power converters are widely utilised in power generation systems and electronic devices, it is suitable to be employed to implement IPST. Currently, some related literature has analysed the methods of implementing the communication function of power electronic systems through power converters. This section will compare these studies in two categories: baseband communication and carrier communication. Specifically, baseband communication transmits signals directly through the operating state of the switches, while carrier communication transmits modulated signals through the carrier wave. Although the application of these studies is different, the signal transmission methods introduced in the literature provide a novel direction for the implementation of IPST.

2.2.1 Baseband Communication for IPST

As demonstrated in [83], a coded pulse width modulation (PWM) approach is proposed for IPST in a LED lighting system. In this study, the 'on' and 'off' states of MOSFETs are disturbed to embed digital signals to the converter as displayed in Fig. 2-7. Besides, the number of '0' and '1' in a code string is the same to maintain the LED operates in continuous conduction state. For instance, an 8-bit code can be used to encrypt integer from 0 to 35 after arranging the combinations. After the data transmission, the received signal can be decoded at the receiving end according to its gradient. Experimental results indicate that the designed method can achieve a data transmission velocity of 1.25 Mbps using *GaN* MOSFETs with a code error rate of less than 10^{-6} [83].

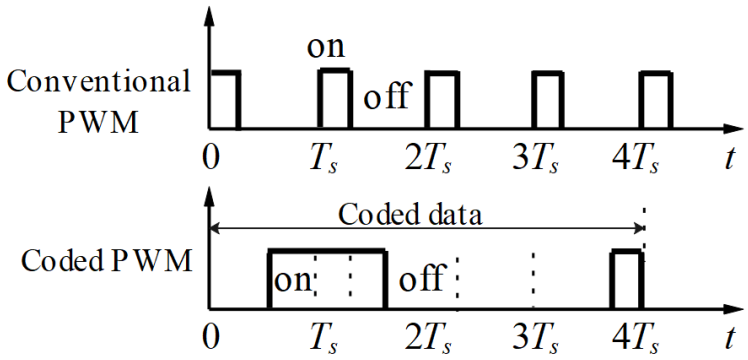

Figure. 2-7. The conventional PWM waveform and the coded PWM waveform [83]

According to [81], a bidirectional communication method for LED lighting system is proposed as presented in Fig. 2-8. In this topology, when the master node transmits data, the gate signal of MOSFET *M* consists of PWM signals of different pulse widths, representing '0' and '1'. On the contrary, when the slave node transmits data, the master node will continue to send '1' and MOSFET *Q* will turn on at the negative edge of '1' to transmit '0' on behalf of the slave node. Experimental results indicate that for a 140-meter-long wire, this method can achieve 92% LED power efficiency, and the data transfer function barely affects the output power [81].

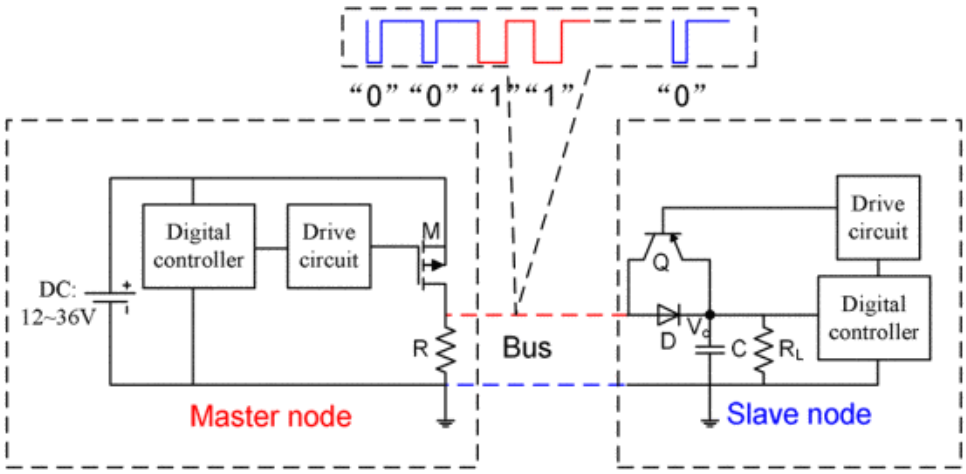

Figure. 2-8. Typical structure of a bidirectional communication topology for LED systems [81]

Similarly, according to [115] and [116], a time division multiplexing method is employed for transmitting both communication signal and power through a DC/DC topology. Because various switches operate with different duty ratio, the communication between the master module and the slave modules is realised by checking the changes of the bus voltage. Moreover, a rectifier is employed in each slave module to obtain continuous power as the electronic power transmitted from the master module is in discontinuous mode. Nevertheless, there are two limitations in the design. Firstly, only one signal can be transmitted at the same time to avoid interference. Secondly, the communication signal is not transmitted continuously, which limits the communication rate of the system.

As presented in [117], an LLC resonant DC/DC converter is proposed for smart buildings. The converter is designed to transfer sensor data and provide power to the LED arrays in this study. Specifically, the pulses at the beginning of each switching period and the pulses at the end of each switching period are utilised to represent '0' and '1', respectively, as depicted in Fig. 2-9. Moreover, the dimming level are controlled by altering the duty ratio of the switches. After the signal is transmitted through the converter, the high frequency clock of the field-programmable gate array (FPGA) can be employed to determine whether the pulse width is wide or narrow, and then the specific information transmitted can be identified at the receiver. Experimental results present that for a 4.5 m distance, this approach can achieve 47 kbps data rate with bit error rate (BER) of less than 10^{-7} [117].

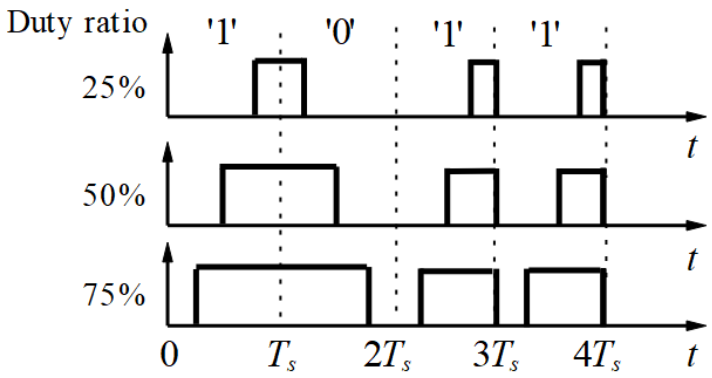

Figure. 2-9. Variable pulse position for data transmission [117]

2.2.2 Carrier Communication for IPST

According to [118], [119], and [120], a buck circuit with a multipath load structure is utilised to realise the signal transmission function and power conversion. The proposed system structure is displayed in Fig. 2-10. By adjusting the switching frequency with PWM approach, the switching ripple generated on the input bus can be modulated with the FSK method. Besides, digital ‘0’ and digital ‘1’ are modulated by carriers with various frequencies, which will be further discussed in Chapter 2.3. In their experiments, a peak detection circuit is employed to capture the switching signal, followed by band-pass filtering and signal processing to identify the transmitted ‘0’ and ‘1’. However, when there are multiple DC/DC circuits on the DC bus, the signal spectrum obtained by the peak detection circuit cannot reflect the switching frequency as the switching ripple overlap with each other, which causes the low accuracy of the received signal.

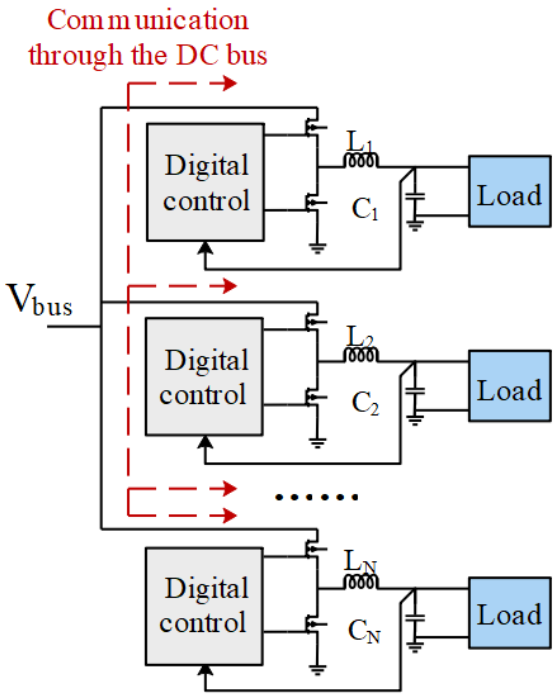

Figure. 2-10. Typical FSK-based carrier communication structure [118]

As presented in [121], a dual active bridge (DAB) converter is employed to achieve bidirectional communication in the energy router. It employs a single-phase shift PWM method for power conversion control and uses the FSK approach for signal modulation. Simulation results indicate that the designed system can realise a data rate of 100 kbps with a time delay less than 10 ms [121]. Additionally, according to [122], FSK method is employed to modulate communication signals by adjusting the turn-off angle of the switched reluctance machine for voltage ripple generation on power line and uses autoregressive power spectrum density approach for signal demodulation. Moreover, As presented in [123] and [124], the feasibility of employing FSK-based IPST technique in microgrid and wireless power transfer systems are verified, respectively.

The PSK method can also be applied for signals transmission in converters. In this approach, digital ‘0’ and digital ‘1’ are modulated by carriers with various phase angle, which will be further discussed in Chapter 3. Some relevant studies are listed below. For example, the multi-carrier communication approach to visible light communication system is introduced in [125], where the transmitted signals are modulated by the envelopes and the instantaneous phases of the carriers. The experimental results show that the proposed pulse width and pulse phase modulation scheme can be successfully implemented in a six-carrier controlled buck converter to achieve 96% power conversion efficiency [125]. Moreover, the feasibility of combing the

PSK and PWM methods for signals and power transmission is theoretically analysed in [126]. It proves that triangular carriers are more suitable for IPST than sawtooth carriers, which cause more interference to the circuit. Nevertheless, the research also observed some limitations of the IPST technology. For instance, it is inappropriate to realise IPST in a communication-based control system. In addition, crosstalk between signal transmission and power control signals can increase the data error rate. In addition, the proposed system in [126] should comply with the harmonic frequencies and amplitudes of electromagnetic interference (EMI) standards, as it uses voltage ripple for signal transmission [126]. According to [127], a full bridge converter is proposed to achieve dual power/signal transmission, where its conversion power is modulated by a phase shifted PWM method and its transmission signal is modulated by a PSK method. Its system topology is depicted in Fig. 2-11. The designed system uses digital signal processor (DSP) to produce control signals for the four switches. Besides, digital '1' is modulated by shifting carrier phase while digital '0' is modulated by the normal carrier. It is worth mentioning that the carrier of the digital '1' is alternately leading or lagging the normal carrier phase to maintain the average current constant [127]. Moreover, it verifies that the amplitude of the data carrier is proportional to the output power and that the proposed method can achieve 5 kbps data rate in a 2-kW system. However, current ripple generated by other converters on the DC bus at the same frequency as the data carrier can affect the quality of the transmitted signal by this approach.

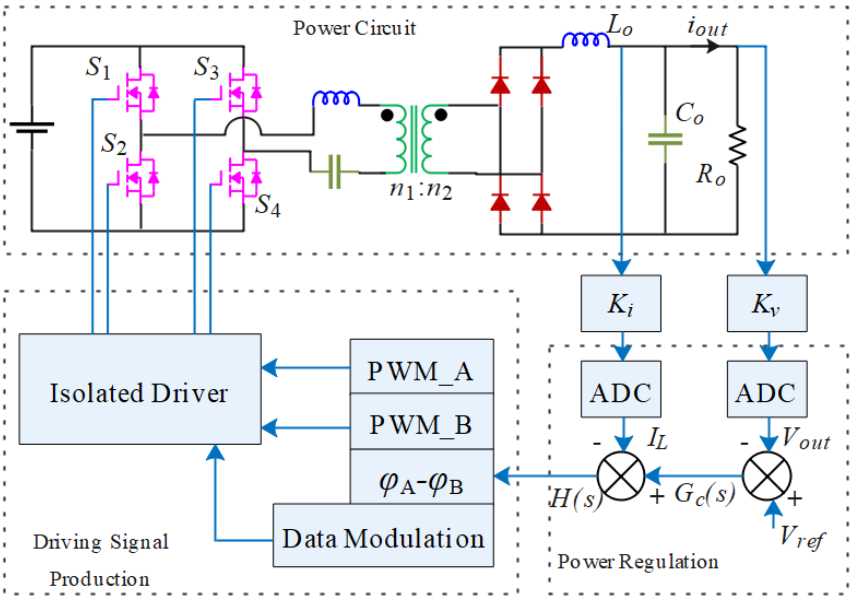

Figure. 2-11. Topology of a full-bridge converter and its power/signal regulation mechanisms [127]

A combination of direct sequence spread spectrum (DSSS) and PWM is proposed in the [128] for energy and data transfer. The signal transmission mechanisms demonstrated in this study is exhibited in Fig. 2-12. The transmitted data is first spread to a broad spectrum and then modulated with phase shifted PWM carriers. Next, the modulated carrier is further processed with the output voltage reference signal for gate signals generation. After applying the gate signals to the DC/DC converter, the transmitted signal can be demodulated from the receiver voltage ripple using the discrete Fourier transform (DFT) method. Additionally, the predominant harmonics of the DC/DC converter voltage ripple are extended to nearby frequencies because of the use of the DSSS technique in the data modulation process [128]. Experimental results indicate that this method is suitable for IoT applications and microgrid. Nevertheless, the signal transmission rate is restricted by the switching frequency, thus it can only be employed in low-bandwidth communications [128].

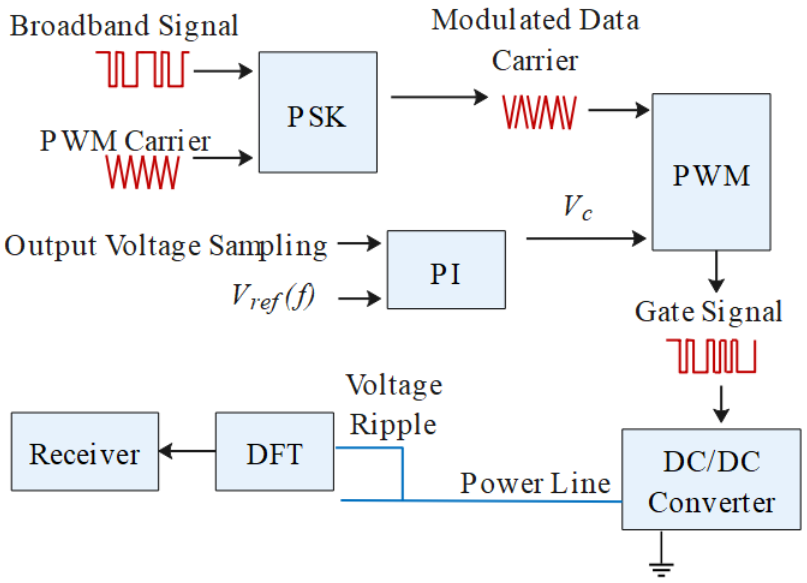

Figure. 2-12. Signal and power transmission schemes of a DSSS method [128]

2.2.3 Comparative Analysis for IPST

Each of the above baseband and carrier IPST strategies has its advantages and disadvantages. For example, the baseband IPST method has the advantage of a relatively simple signal transmission scheme and fast data rates, while it is subject to more environmental interference. Because the baseband IPST method transmits signals without carriers, its data rate is equal to its switching frequency. As the carrier IPST method employs carriers for signal modulation, its data rate is less than the switching frequency. Furthermore, the carrier IPST method has

relatively decent noise immunity, but sacrifices high data rates due to the complex modulation and demodulation processes used. Table 2-2 summarises the comparisons of the above baseband and carrier IPST technologies.

TABLE 2-2 Comparisons of the Baseband and Carrier IPST Technologies

	Data Rate	Advantages	Disadvantages
Baseband IPST [83] [115] [116]	Up to 1.25 Mbps	1. High data rate 2. Simple control scheme 3. Low cost	1. Low communication security 2. Weak anti-interference capability
Carrier IPST [120] [124] [127]	Up to 10 kbps	1. High communication security 2. Decent noise immune capability 3. Long transmission distance	1. Low bit rate due to low bandwidth utilisation 2. Complex modulation and demodulation 3. High maintenance cost

2.3 Comparison of Various Communication Approaches

The various communication approaches mentioned above are compared in this section to have an intuitive impression of their merits and limitations. Wireless networks are popular in the daily life of residents because of their low maintenance cost, mobility, and ease of installation. However, interference and data security are the main drawbacks of wireless communication and therefore require further investigation. Moreover, wired networks offer the benefits of high bandwidth and good data security, but have limited mobility. In addition, the IPST method can greatly reduce cost and system size by using power lines for data transmission and has a good level of data security because the transmitted data can hardly be hijacked directly from the power lines. Nevertheless, the data transmission rate of this method is low, and the communication signal is subject to interference from other electronic devices connected to the same power line. Table 2-3 summarises the advantages and disadvantages of wired, wireless, and IPST communication technologies.

TABLE 2-3 Comparisons of Wired, Wireless, and IPST Technologies

	Advantages	Disadvantages
Wired Communication	1. High data rate 2. High reliability 3. Low installation cost as cables is cheap 4. Good security 5. Less interference	1. Difficult for wiring 2. Limited mobility 3. High maintenance cost
Wireless Communication	1. Easy installation 2. High mobility 3. Low maintenance cost 4. High reliability	1. High interference 2. Small signal coverage area 3. Poor service quality
IPST Approach	1. Simplified system wiring 2. Reduced system volume 3. High data security 4. Low cost	1. Low bit rate 2. Interference from other electronic devices 3. Applications limited by power electronics

The IPST method is worth further study because of its good data security and its ability to save system size and cost. The previous research has the following limitations. Firstly, most studies use voltage ripple for data transmission, which can cause data errors when there are large fluctuations in the output voltage waveform. Secondly, most studies use DC/DC converters for signal transmission, and there is still a gap in the feasibility study of IPST in DC/AC converters and AC/DC converters. Thirdly, previous studies have combined existing signal modulation techniques including FSK and PSK with PWM for integrated transmission, thus other modulation methods can be tested for signal rate breakthroughs. Fourthly, existing research provides theoretical support for IPST technology, but further research is needed to promote this approach in various applications and to address potential technology integration challenges. Based on these limitations, this study systematically analyses the mechanism of the IPST technique and proposes an IPSK/FSK modulation method. Besides, the transmitted signals are demodulated according to the waveforms of the current at the receivers. Moreover, some potential applications of this technology are explored, including battery power balancing for BMS and motor speed control for electric vehicles.

2.4 Analysing Power Electronic Converters from a Communications Perspective

Power electronics and information electronics are two major branches of electronics. The two disciplines have the same origin, similar nature, and operating principles, but they have developed into different directions. Information electronics focuses on the information loaded on the electrical signals, while power electronics focuses on the transformation and processing of electrical energy itself [129]. Based on the similarity between power electronics and information electronics, an intensive analysis of the content of power electronic converters, revealing the fundamental property that power electronic converters themselves can exchange information when converting and controlling electrical energy is presented. On this basis, the concept, principle, and method of integrated power/signal transmission (IPST) approach through power electronic converters are introduced. The integrated approaches including FSK/PWM and PSK/PWM are analysed in this chapter in terms of their modulation and demodulation mechanisms.

2.4.1 Communication Systems Overview

The purpose of communication is to transfer information between two points in physical space. A typical communication system consists of three main components: a transmitter, a communication channel, and a receiver, as shown in Fig. 2-13. Firstly, the signal source containing various types of messages is converted into their original electrical signals. Specifically, analogue and digital sources are two types of signal sources, where analogue sources output continuous analogue signals such as audio and video signals, and digital sources output discrete digital signals such as keyboard characters. Besides, the signals from the analogue sources can be converted into digital signals after digitisation. Digital signals are more widely used than analogue signals because they are less prone to distortion during transmission and have a high degree of fidelity [130]. Then the transmitter is used to modulate and amplify the source signal to enable it to be suitable for transmission in the communication channel. In this process, baseband data is typically modulated to a higher frequency band to satisfy the sufficient power and immunity required for long-distance transmission. Communication channels are intended to connect transmitting and receiving devices at different locations in physical space and can be further divided into wired and wireless channels. Nevertheless, the channel provides a transmission path for the signal and at the same time

causes noise interference to the signal due to the exposure of the channel to the physical space. After the signal has been transmitted through the communication channel, it finally reaches its destination: the receiver. The receiver's function is the opposite of that of the source. It demodulates the transmitted signal and restores it to the corresponding original source signal.

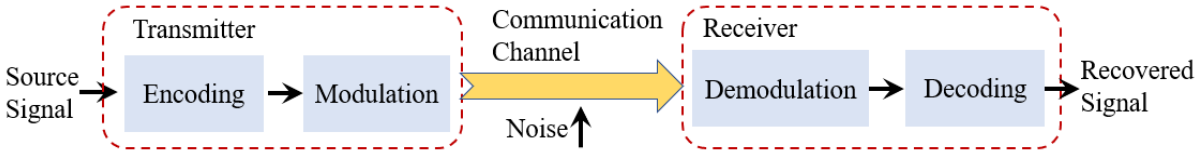

Figure. 2-13. Block diagram of a typical communication system

Communication systems can be categorised into analogue and digital systems. In an analogue system, the analogue source is modulated directly into the frequency band by a modulator and then demodulated at the receiver to obtain an analogue signal in the baseband. Digital communication involves more technical approaches, including encoding, decoding, channel coding, channel decoding and synchronisation of the original digital signal [129]. In addition to the processing of the digital sequences, the main technologies involved in a digital communications system include the modulation process of moving the baseband digital signals to the frequency band and the reverse process (demodulation) at the receiver. Therefore, modulation and demodulation are the core elements of both analogue and digital communications systems.

2.4.2 Feasibility Analysis of Using Power Electronic Converters for Signal Modulation

Power electronic converters have been widely applied in energy devices for power conversion and energy processing. Specifically, the form and level of electrical energy is controlled by the high frequency operation of switches, combined with passive devices such as capacitors, inductors, and diodes [131]. The buck converter presented in Fig. 2-14 is used as an example to explain the energy conversion process. A voltage reference signal V_{ref} is used to generate the gate signal of the MOSFET S thus the voltage source V_{in} transfers the desired output voltage V_{out} to the output via the controller. Therefore, power conversion process of the converter can be simplified as depicted in Fig. 2-15.

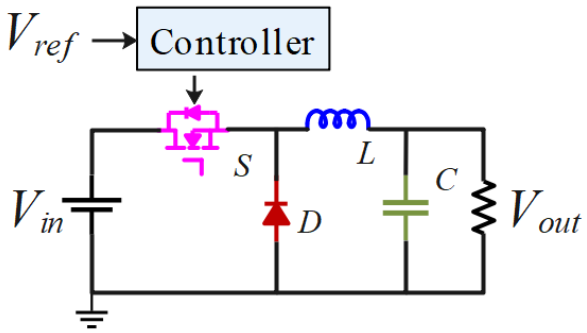

Figure. 2-14. Structure of a typical buck converter

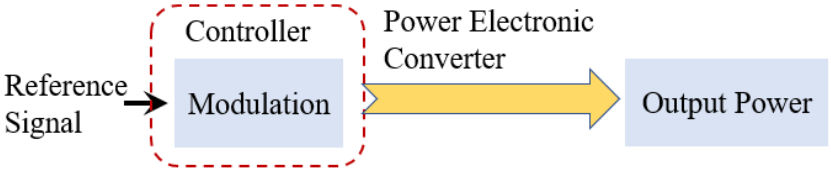

Figure. 2-15. Block diagram of a typical power conversion system

Fig. 2-13 and 2-15 demonstrate that both the communication and energy conversion systems contain transmission processes, with the difference that the former transmits electrical signals through a physical medium, and the latter transmits energy through converters. Because the modulated gate signals are applied to manipulate the output power in the power conversion system, it is possible to utilise the gate signals for data transmission.

PWM modulation is a commonly used power control method in DC converters where the modulated pulse width is applied to control the output voltage level. A typical PWM waveform is exhibited in Fig. 2-16, and its Fourier expression is as follows:

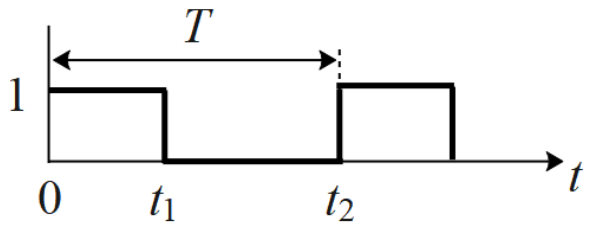

Figure. 2-16. A typical PWM waveform

$$f(x) = a_0 + \sum_{n=1}^{\infty} (a_n \cos n\omega t + b_n \sin n\omega t) \qquad (2-1)$$

$$\begin{cases} a_0 = D \\ a_n = \dfrac{2}{\pi n}\sin(\pi D n)\cos(\pi D n) \\ b_n = \dfrac{2}{\pi n}\sin^2(\pi D n) \\ c_n = \sqrt{a_n^2 + b_n^2} = \dfrac{2}{\pi n}\left|\sin(\pi D n)\right| \end{cases} \quad (2-2)$$

In Fig. 2-16, *T* represent the amplitude and the period of the PWM waveform, respectively. In its Fourier expression, ω and *D* represent the angular frequency of the typical waveform and the duty ratio associated with the period *T*, respectively. Besides, c_n is the amplitude of high-frequency components of the PWM waveform, which demonstrates that these components exist during the power conversion process and thus can be further used as carriers for signals transmission. Specifically, since the Fourier expression of the PWM waveform involves three coefficients: a_0, a_n, and b_n, where a_0 can be considered as DC component of the output waveform and a_n and b_n as the harmonic fractions of the waveform, the frequencies, phase angles, and amplitudes involved in a_n and b_n can be utilised for data modulation without affecting the value of a_0. For instance, when the buck converter mentioned earlier operates in continuous conduction mode, the initial value of the inductor will be equal to its final value at each cycle and the relationship between the input voltage V_{in} and the output voltage V_{out} is derived as:

$$V_{out} = D \cdot V_{in} \quad (2-3)$$

Therefore, the output voltage of the Buck converter is only affected by the duty ratio. Additionally, other parameters such as the frequency and phase angle involved in the PWM waveform are not participating in the energy conversion process, which proves that they can be used for signal modulation.

2.5 Signal Modulation for Converters Based IPST

2.5.1 Frequency Shift Keying

The frequency shift keying (FSK) method employs carriers of different frequencies for signal modulation. As the communication signal is modulated by the fast switching of the converter switches in the IPST system, square waves are used as the carrier. A typical FSK modulated waveform is exhibited in Fig. 2-17, where the digital '1' is modulated by the carrier of

frequency f_1 and the digital '0' is modulated by the carrier of frequency f_2. If the carriers are represented by the sinusoidal waveforms with the fundamental frequencies of the impulse carriers for simplicity of analysis, their expressions can be acquired as below, where M is the amplitude of the carriers.

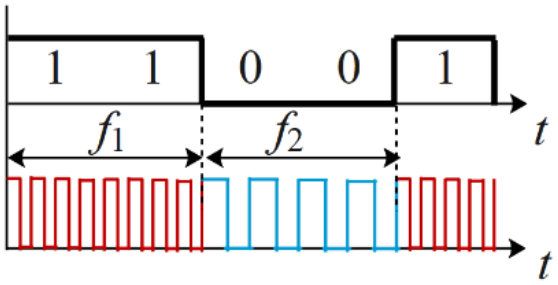

Figure. 2-17. A typical FSK modulated waveform

$$c_{FSK}(t) = \begin{cases} M\cos(2\pi f_1 t), \text{when transmit digital '1'} \\ M\cos(2\pi f_2 t), \text{when transmit digital '0'} \end{cases} \quad (2-4)$$

As the pulse widths of the carriers are not involved in the signal modulation process, they can be further modulated by PWM methods for power conversion. Fig. 2-18 depicts the integrated modulation approach in an intuitive way. Similarly, the phase shift keying (PSK) and integrated PSK/FSK modulation processes discussed later can be represented by this block diagram.

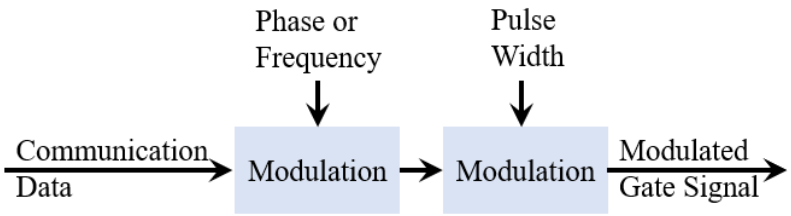

Figure. 2-18. Integrated power and signal modulation approach

2.5.2 Phase Shift Keying

The phase shift keying (PSK) method employs carriers of different frequencies for signal modulation. A typical PSK modulated waveform is exhibited in Fig. 2-19, where the digital '1' is modulated by the carrier of phase angle φ_1 and the digital '0' is modulated by the carrier of phase angle φ_2. If the carriers are represented by the sinusoidal waveforms with the fundamental frequencies of the impulse carriers for simplicity of analysis, then their expressions can be acquired as below. Next, the pulse widths of the carriers can be further modulated by PWM method.

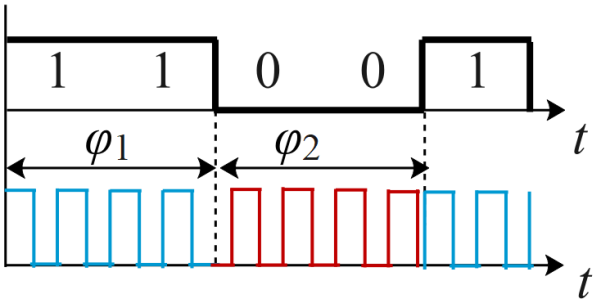

Figure. 2-19. A typical PSK modulated waveform

$$c_{PSK}(t) = \begin{cases} M\cos(2\pi f t + \varphi_1), \text{when transmit digital '1'} \\ M\cos(2\pi f t + \varphi_2), \text{when transmit digital '0'} \end{cases} \quad (2-5)$$

2.6 Signal Demodulation for Converters Based IPST

The demodulation process is aiming to detect the original data from the modulated signal from the receiver. Envelope detection, over-zero detection and coherent demodulation are the three commonly used demodulation algorithms. This thesis focuses on envelope detection and coherent demodulation, because the over-zero detection method may be affected by the noise interference of the switch harmonics and lead to false codes.

According to communication theories, if the two frequencies used for signal modulation are orthogonal to each other within a coding period, one frequency used for coherent demodulation will not interfere with the other. In other words, if a modulated signal containing two carriers expressed as

$$s(t) = A_1\cos(2\pi f_1 t + \varphi_1) + A_2\cos(2\pi f_2 t + \varphi_2) \quad (2-6)$$

then the carrier orthogonality indicates that

$$\int_0^{T_s} \cos(2\pi f_1 t + \varphi_1)\cos(2\pi f_2 t + \varphi_2) = 0 \quad (2-7)$$

where T_s is a random code period. The expression in (2-7) can be further derived as

$$\frac{\sin[2\pi(f_1+f_2)T_s + \varphi_1 + \varphi_2] - \sin(\varphi_1+\varphi_2)}{2\pi(f_1+f_2)} + \frac{\sin[2\pi(f_1-f_2)T_s + \varphi_1 - \varphi_2] - \sin(\varphi_1-\varphi_2)}{2\pi(f_1-f_2)} = 0 \quad (2-8)$$

If the above equation valid, then the carriers' frequencies should satisfy the following condition

$$\begin{cases}(f_1 + f_2)T_s = p \\ (f_1 - f_2)T_s = q\end{cases} \quad (2-9)$$

where p and q are integers. If p equals to q, then the relationship between the carrier frequency and the coding period is derived as

$$f_1 \text{or} f_2 = \frac{p}{2T_s} \quad (2-10)$$

The two frequencies are spaced

$$f_1 - f_2 = \frac{p}{T_s} \quad (2-11)$$

This expression provides the frequency relationship between the two carriers, thus ensuring orthogonality between the carriers. In other words, this is the fundamental requirement of the frequency that the carrier should meet when modulating the signal.

2.6.1 Envelope Detection

The envelope detection method is an approach that uses a high frequency amplitude modulated signal as input and provides a demodulated envelope of the original signal as output [132]. The envelope detection is mainly used for demodulating FSK modulated signals and its process is exhibited in Fig. 2-20. Firstly, the modulated signal is extracted from the current waveform and processed by a bandpass filter. Because digital '1' and digital '0' are modulated by carriers with different frequencies, the bandpass filter suppresses the amplitude of harmonics beyond the passband frequency in the time domain. Next, the upper envelope representing the position of the initial data in the time domain can be obtained by envelope detection. Finally, the original digital data is recovered by judging the envelope amplitude followed by down sampling. The downs sampling process resamples the judged waveform using the original data rate to obtain the original data string. If the digital '1' is restored using this demodulation process, the digital '0' will be transmitted in the complementary time slot of the digital '1' by default. This method can greatly reduce the calculation burden on demodulating two digital numbers respectively.

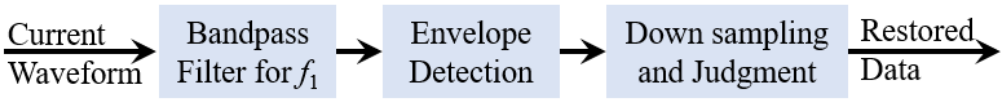

Figure. 2-20. Block diagram of envelope detection

Specifically, if the envelope detection process is applied to demodulate the digital '1' from the FSK modulated signal, the demodulated carrier after bandpass filtering can be assumed as

$$x(t) = M_1 \cos(2\pi f_1 t + \theta_1)[1 - y(t)] + M_n \cos(2\pi f_n t + \theta_n) \qquad (2-12)$$

where

$$y(t) = \begin{cases} 1, \text{ if digital '0' is sent or the channel is idle} \\ 0, \text{ if digital '1' is sent} \end{cases} \qquad (2-13)$$

In (2-12), the waveform after bandpass filtering is simplified as the sum of the demodulated carrier and noise, where M_1 is the amplitude of the extracted carrier, and M_n is the superimposed amplitude of the other harmonics and noise in the bandpass region. The envelope $e(t)$ of $x(t)$ can then be extracted through the Hilbert transform approach.

$$\begin{cases} e(t) = \sqrt{x(t)^2 + \hat{x}(t)^2} \\ \hat{x}(t) = \dfrac{1}{\pi}\displaystyle\int_{-\infty}^{\infty} \frac{x(\tau)}{t-\tau} d\tau \end{cases} \qquad (2-14)$$

Since the amplitude of other order harmonics is decreased after filtering, a threshold value V_{th} is utilised to further isolate the carrier-envelope from the noise envelope, with the range of V_{th} is set between $M_n < V_{th} < M_1$. The selection of V_{th} will be further discussed in Section 2.7 with specific examples. Fig. 2-21 presents the typical waveforms of envelope detection method, where $s(t)$, $x(t)$, and $r(t)$ refer to the transmitted signal, bandpass filtered waveform, and recovered signal, respectively.

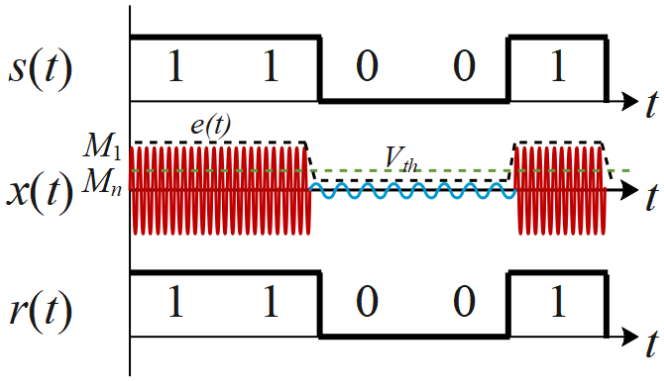

Figure. 2-21. Typical waveforms for envelope detection approach

2.6.2 Coherent Demodulation

The core of coherent demodulation lies in the multiplication of a coherent carrier wave that has the same frequency and phase as the transmitted data carrier at the receiving end with a bandpass filtered carrier wave through a multiplier. In contrast to envelope detection methods that use the carrier frequency difference for signal recovery, coherent methods demodulate the signal by the product of carrier and low pass filtering and therefore have a wider range of applications than envelope detection that is only applicable to frequency modulated signals. As the modulation process shifts the original signal to a higher frequency band (carrier frequency), the demodulation process can be seen as the reverse method of modulation, i.e., recovering the signal from a higher frequency band. The coherent demodulation process for a FSK modulated signal is exhibited in Fig. 2-22. Moreover, the coherent demodulation is applicable for PSK modulated signals. After coherent demodulation, the initial information transmitted can be recovered by comparing the filtered result with the threshold amplitude after lowpass filtering. The lowpass filter used in this process will be introduced in Section 2.7 with specific examples. Furthermore, the demodulation process can be implemented by the sliding discrete Fourier transform (SDFT), where the computation time of the discrete Fourier transform (DFT) can be significantly reduced by shifting the phase window. The mechanisms of SDFT will be further discussed in Chapter 4.

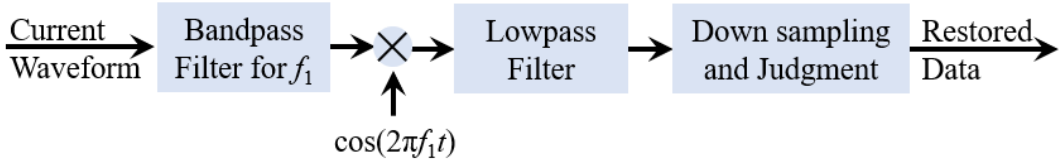

Figure. 2-22. Block diagram of coherent demodulation

For a modulated signal $s(t)\cdot\cos\omega_c t$ with the initial signal of $s(t)$ and the carrier angular frequency of ω_c, the coherent demodulation result is

$$s(t)\cdot\cos\omega_c t\cdot\cos\omega_c t=\frac{1}{2}s(t)[1+\cos 2\omega_c t] \qquad (2-15)$$

which indicate that the high frequency components can be further removed by a low pass filter. If the coherent demodulation is applied for another modulated signal $s(t)\cdot\cos(\omega_c+\varphi)t$, the result is

$$\begin{aligned} s(t)\cos(\omega_c+\varphi)\,t\cdot\cos\omega_c t &= s(t)\cos\omega_c t\cdot[\cos\omega_c t\cos\varphi t-\sin\omega_c t\sin\varphi t] \\ &=\frac{1}{2}s(t)[\cos\varphi t+\cos\varphi t\cos 2\omega_c t-\sin\varphi t\sin 2\omega_c t] \end{aligned} \qquad (2-16)$$

Assuming $cos(\omega_c t)$ is the carrier used for demodulation and $cos(\omega_c t+\varphi)$ is another carrier, then the results in (2-16) indicate that a cosine component $\cos\varphi t$ can still exist after lowpass filtering. As the amplitude of $\frac{1}{2}s(t)$ and $\frac{1}{2}s(t)cos\varphi t$ is different, a threshold value can then be set between these values for signal restoration.

Because in a real communication system, either the frequency divider or the phase-locked loop may shift state, the reference phase may change phase angle by 180 degrees. Thus, a coded invertor or differential coherent modulation is applied in practice to avoid phase ambiguity [133].

In addition to PSK and FSK, the amplitude of the carrier can also be modulated using the amplitude shift keying (ASK) method. For example, the digital ‘1’ and the digital ‘0’ can be modulated by carriers with amplitudes of M and 0 respectively. However, as ASK modulation relies on amplitude level, which is subject to amplitude degradation and noise interference during transmission, the transmitted signal is vulnerable to be falsely restored at the receiver. Therefore, ASK modulation is less immune to interference than FSK and PSK and is rarely used in practice. The detailed modulation and demodulation of the ASK method will not be discussed in this thesis.

2.7 Summary

This chapter reviews the standards and applications of wired communication technologies such as PLC, PoE, and fibre optic. After summarising other studies in the literature on IPST in terms

of baseband and carrier communication methods, this chapter introduces the mechanisms of the commonly used modulation approach such as FSK and PSK, as well as demodulation methods including envelope detection and coherent demodulation. Three significant targets of this review work can be achieved. Firstly, a valuable subject that promotes the existing IPST methods regarding data rate and error rate is observed, which provides a feasible direction for the subsequent research. Secondly, researchers can acquire a thorough understanding of the advantages and disadvantages of various communication approaches. Thirdly, the review work discovers a signal demodulation method for extracting data from current ripple, which provides an innovation point for future research.

Chapter 3 Converters Based Integrated Phase Shift Keying/Frequency Shift Keying Approach

In this chapter, the proposed integrated phase shift keying/frequency shift keying (IPSK/FSK) method will be presented, and the proposed method will be verified by simulation results in buck converters, buck/boost converters and cascaded full bridge converters. Furthermore, the noise immunity of the proposed method will be compared with other modulation methods such as FSK and PSK in the Buck converter.

3.1 Mechanisms of Integrated Phase Shift Keying/Frequency Shift Keying

The IPSK/FSK approach combines the conventional PSK and FSK methods for signal modulation. Because of the simultaneous use of the carrier's frequency and phase angle for data modulation, it offers greater data rates than conventional single modulation methods. A typical IPSK/FSK modulated waveform is exhibited in Fig. 3-1, where two signals can be simultaneously transmitted through the converter. Specifically, digital '1' and '0' of signal S_1 are modulated by carriers with frequencies φ_1 and φ_2 respectively. Besides, digital '1' and '0' of signal S_2 are modulated by carriers with phase angle f_1 and f_2 respectively. If the carriers are represented by their first order harmonics, their expressions can be derived as below. Then the pulse widths of the carriers can be further modulated by PWM method. Although this modulation scheme has a greater data rate, it requires a more complex demodulation strategy, which will be discussed later.

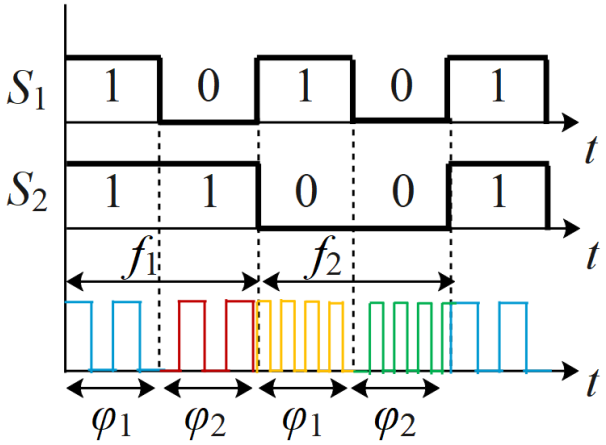

Figure. 3-1. A typical IPSK/FSK modulated waveform

$$c_{IPSK/FSK}(t) =$$

$$\begin{cases} M\cos(2\pi f_1 t + \varphi_1), \text{when } S_1 \text{transmit digital '1' and } S_2 \text{ transmit digital '1'} \\ M\cos(2\pi f_1 t + \varphi_2), \text{when } S_1 \text{transmit digital '0' and } S_2 \text{ transmit digital '1'} \\ M\cos(2\pi f_2 t + \varphi_1), \text{when } S_1 \text{transmit digital '1' and } S_2 \text{ transmit digital '0'} \\ M\cos(2\pi f_2 t + \varphi_2), \text{when } S_1 \text{transmit digital '0' and } S_2 \text{ transmit digital '0'} \end{cases} \quad (3-1)$$

When the converter operates without signal transmission, it only requires a single PWM waveform for power conversion control. In addition, a preamble can be inserted before each frame of data to alert the receiving device to prepare for data reception.

For signal demodulation, a combination of envelope detection and coherent demodulation is used. Specifically, the envelope detection approach is applied to restore the frequency modulated digital numbers and the coherent method is employed to recover the phase modulated digital numbers. As four different carriers are applied in the proposed method and the envelope detection only considers the carrier frequency during signal recovery, the method is used only once to separate two frequencies of carriers. Besides, since the coherent demodulation considers both the carrier frequency and phase during signal recovery, the method is used twice to distinguish two phases of carriers.

3.2 Simulation Results and Analysis for Different Converters

3.2.1 Simulation Results of the IPST Integrated Buck Converter

The feasibility of the IPST is verified by simulation in MATLAB/Simulink with a buck converter. The simulation model is presented in Fig. 3-2 and the simulation parameters are listed in Table 3-1. Typical waveforms for FSK and PSK approaches are presented in (a) and (b) of Fig. 3-3 respectively. In Fig. 3-3(a), from top to bottom, these curves refer to the initial transmitted signal, the load current waveform, the extracted carrier, the upper envelope of the carrier, and the restored signal, respectively. In Fig. 3-3(b), from top to bottom, these curves refer to the initial transmitted signal, the load current waveform, the extracted carrier, the waveform after coherent demodulation, the waveform after lowpass filtering, and the restored signal, respectively. In this simulation, a Gaussian bandpass filter of order 80 with a passband between 9.9 kHz and 10.1 kHz is used to extract a 10 kHz carrier. In addition, a Gaussian low-pass filter of order 20 with a cut-off frequency of 1080 Hz is used to recover the 1 kHz signal.

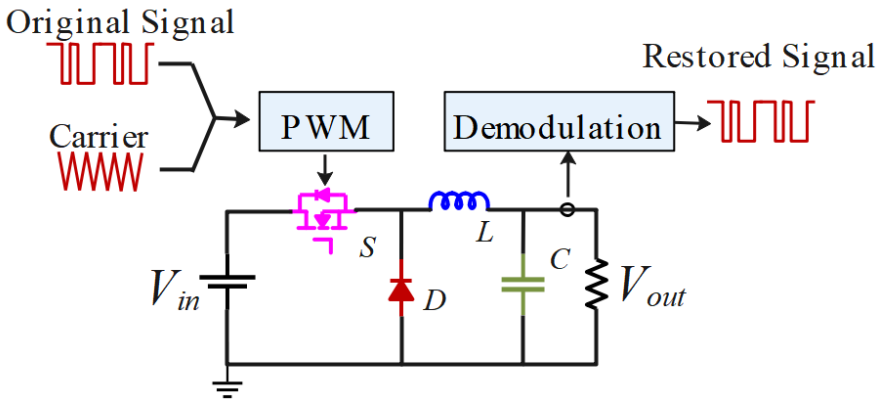

Figure. 3-2. The simulation model of the Buck converter

TABLE 3-1 Simulation Parameters of the Buck converter

Parameter Name	Value
Input Voltage	200 V
Inductor	0.3 mH
Capacitor	3 μF
Load Resistor	10 Ω
Carrier phase of digital '1' in s_2 (IPSK/FSK)	0
Carrier phase of digital '0' in s_2 (IPSK/FSK)	π/3
Carrier frequency of digital '1' in s_1 (IPSK/FSK)	10 kHz
Carrier frequency of digital '0' in s_1 (IPSK/FSK)	20 kHz
Duty ratio of the switch	0.5

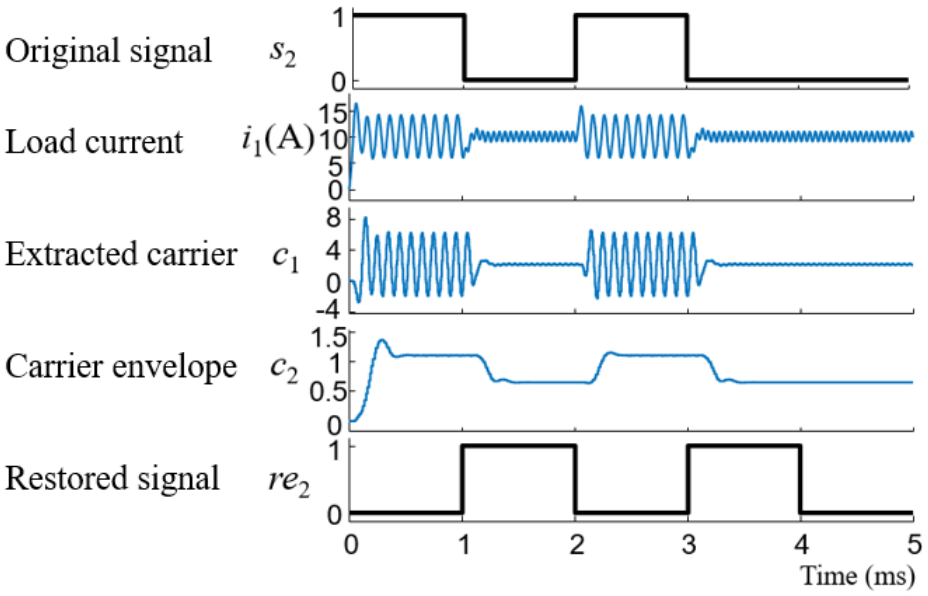

(a)

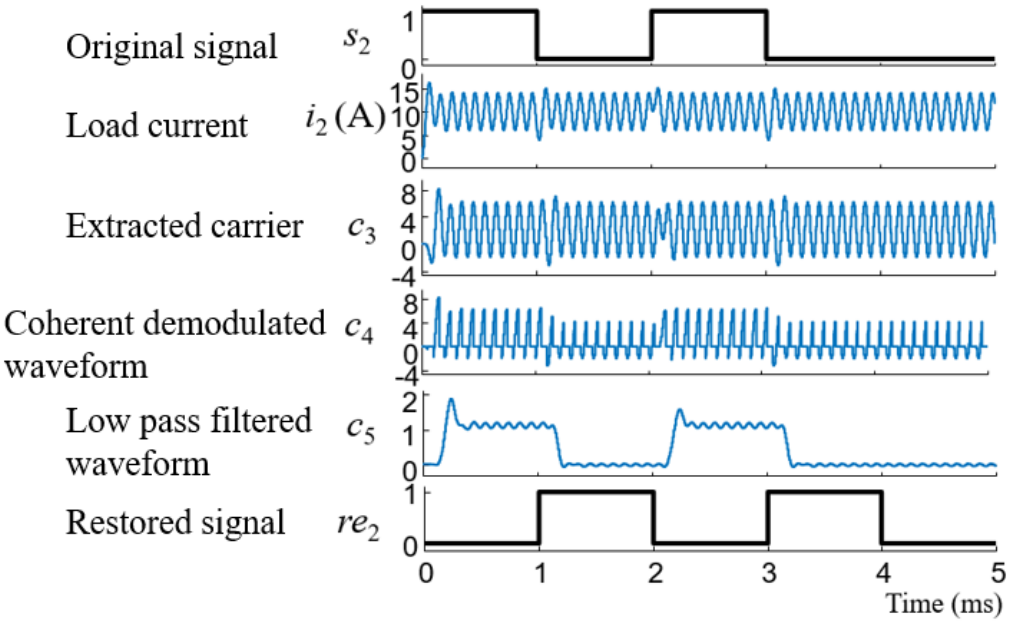

(b)

Figure. 3-3. Typical simulation waveforms of FSK and PSK of the Buck converter

It can be observed from Fig. 3-3(a) that the fluctuation of c_1 decrease dramatically at 1ms and 3ms, which indicates the bandpass filter successfully inhibit the amplitude of 20 kHz carrier. Besides, a minor delay can be investigated from c_1, and this is caused by the filtering process. Since the attenuation at cut-off frequencies is set at 6 dB in the bandpass filter, the attenuation ratio R can be obtained as 0.5 from (3-2). In other words, the amplitude of waveform c_2 in cut-off frequencies region (0.6) is half of its amplitude in the passband frequencies region (1.2). Therefore, digital value '1' is selected as threshold to separate the cut-off frequencies region and passband frequencies region of the filtered wave. As the transmitted signal is recovered by resampling the threshold waveform at the initial data rate as the sampling frequency, the received signal is eventually delayed by one bit as presented in re_2 of Fig. 3-3(a).

$$20 \log R = -6 \qquad (3-2)$$

From Fig. 3-3(b), it can be investigated that the waveform of extracted carrier c_3 fluctuates at 1ms, 2ms, and 3ms, which is caused by the carrier phase variation. Like the results in Fig. 3-3(a), a minor delay can be found in c_3, and this is caused by the filtering process. As the carriers used in the PSK method have the same frequency and different phases, the band-pass filter cannot suppress the amplitude of the carriers with the same frequency, which results in PSK having more ripples than FSK.

Similarly, the simulation results of the combined FSK/PSK modulation approach are presented in Fig. 3-4, where the transmitted signal s_2 is demodulated by envelope detection method and signal s_1 is restored by coherently demodulating the two carriers separately. In Fig. 3-4, i_3, c_6, c_7, and c_8 respectively represent the output current, the upper envelope of the extracted carrier, lowpass filtered carrier containing f_1, φ_1, and lowpass filtered carrier containing f_2, φ_1. Besides, the restored signals of s_1 and s_2 are exhibited as re_1 and re_2, respectively.

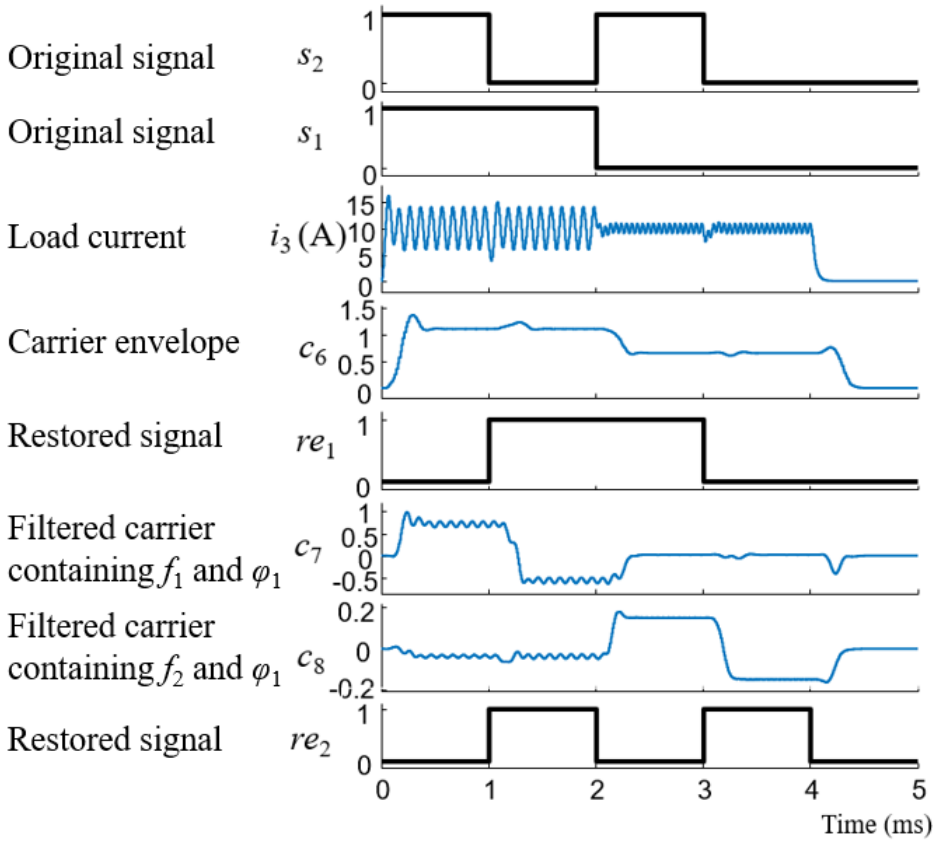

Figure. 3-4. Typical simulation waveforms of FSK/PSK modulation of a Buck converter

The amplitude of i_3 changes at 2ms because of the alteration of carrier frequency. Besides, i_3 fluctuates at 1ms and 3ms because of the alteration of carrier phase. The simulation results indicate that the modulated power contains the harmonics of the converter switch and that first order harmonics can be used for signal modulation. Moreover, the proposed IPSK/FSK method can have higher data compared to the single FSK or PSK methods described previously, as it can transmit two signals simultaneously while maintaining the same carrier frequency and phase as the FSK and PSK methods.

The bit error rate (BER) of the IPST approach is then obtained by comparing the original data with the recovered data. The BER is defined by the number of bit errors per unit time. As

shown in Fig. 3-5, simulation results for FSK and differential binary phase shift keying (DBPSK) methods are compared with PSK and quadrature phase shift keying (QPSK) methods for conventional communication systems with respect to BER, where FSK is demodulated by envelope detection and DBPSK is demodulated by differential coherent modulation [134]. DBPSK is a method of encoding symbols with phase differences between consecutive samples and QPSK uses four phases to encode two bits per symbol. In this simulation model, the data rate is 1 kbps and the probability of both the digital '1' and the digital '0' is set to 50% for a random data string. Simulation results demonstrate that the IPST approach has decent noise immunity and its BER is close to 0 when the signal-to-noise ratio (SNR) is greater than 5 dB.

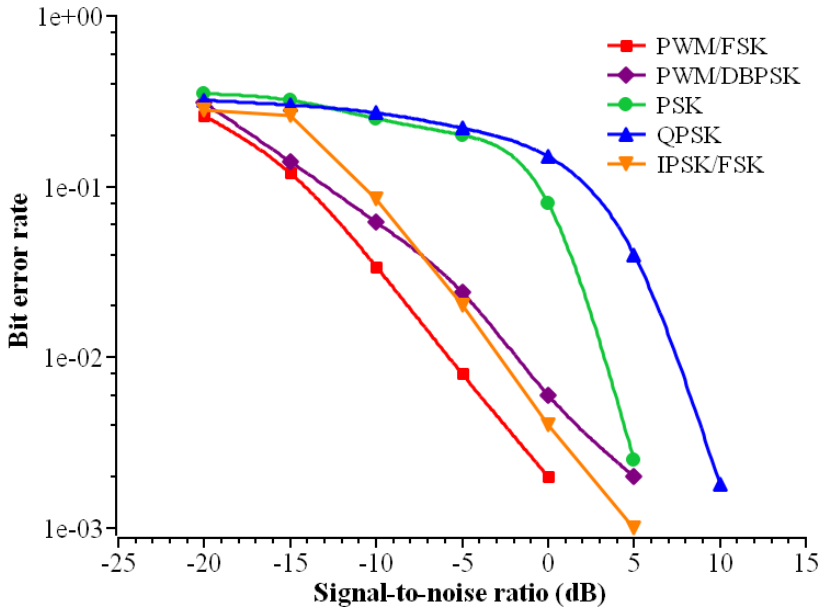

Figure. 3-5. Simulated results of BER vs SNR for PWM/FSK, PWM/DBPSK, PSK, QPSK, and IPSK/FSK

The comparison among PWM/FSK, PWM/PSK, PWM/DBPSK, and the proposed IPSK/FSK approach is listed in Table 3-2. PWM/FSK is more susceptible to noise interference than other methods because it uses the carrier frequency for signal modulation and the high frequency noise can be attenuated by a bandpass filter. Besides, PWM/PSK is subject to phase blurring during demodulation and therefore has a high BER. In addition, the proposed IPSK/FSK method can achieve higher data rates than PWM/PSK and PWM/FSK by fully utilising the carrier phase and frequency for signal modulation, but it introduces a more complex modulation and demodulation scheme. Therefore, the appropriate IPST method requires consideration of the actual requirements in specific applications.

TABLE 3-2 Comparison Among Different IPST Methods

	Bit error rate	Band utilisation	Noise immunity	Data rate	Complexity
PWM/FSK	Moderate	Low	Low	Low	Simple
PWM/PSK	Moderate	High	High	Low	Moderate
PWM/DBPSK	Low	High	High	Moderate	Complex
IPSK/FSK	Low	High	Moderate	High	Complex

3.2.2 Simulation Results of the IPST Integrated Boost Converter

The topology of the Boost converter using the IPST method is presented in Fig. 3-6. After modulating the transmitted signals s_1 and s_2 by means of the converter switch S, the output current and voltage waveforms of the proposed IPSK/FSK method are depicted in Fig. 3-7. Unlike the previous Buck converter, this simulation model employs a closed loop to simulate the dynamic performance of load variation. In this figure, R_L, i_O, V_{in}, and V_o respectively represent the load resistance, output current, input voltage, and output voltage. The simulation parameters applied in this model are listed in Table 3-3.

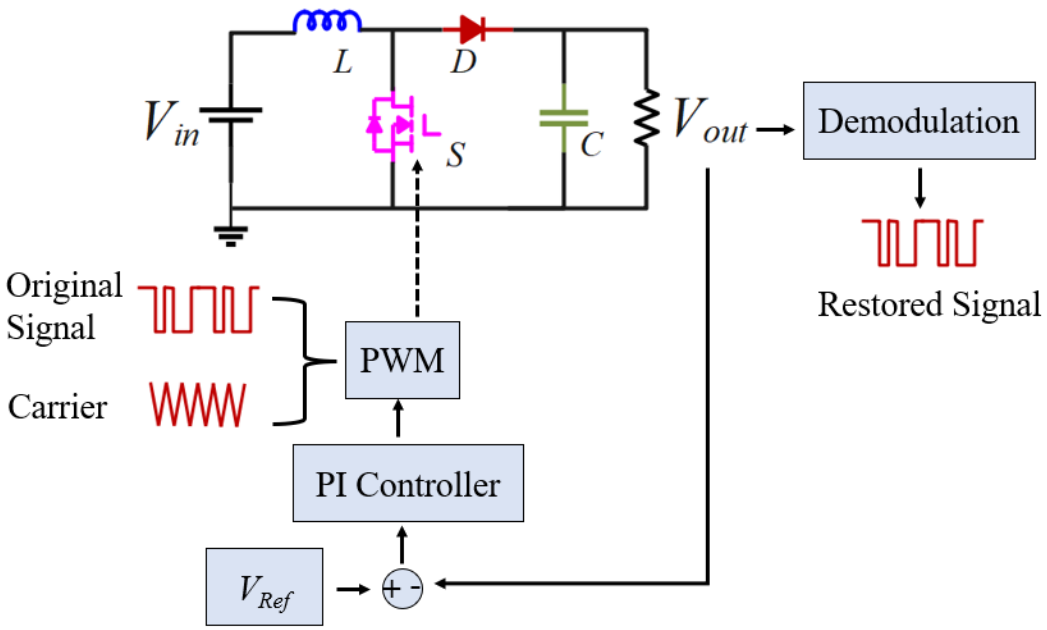

Figure. 3-6. The simulation model of the Boost converter

TABLE 3-3 The Simulation Parameters of the Boost Converter

Parameter Name	Value
Input Voltage	220 V
Inductor	0.3 mH
Capacitor	0.3 mF
Load Resistor	30-40 Ω
Carrier phase of digital '1' in s_2	0
Carrier phase of digital '0' in s_2	π/3
Carrier frequency of digital '1' in s_1	10 kHz
Carrier frequency of digital '0' in s_1	28 kHz
Proportional of PI controller	0.03
Integral of PI controller	200
Output voltage and V_{Ref}	300 V

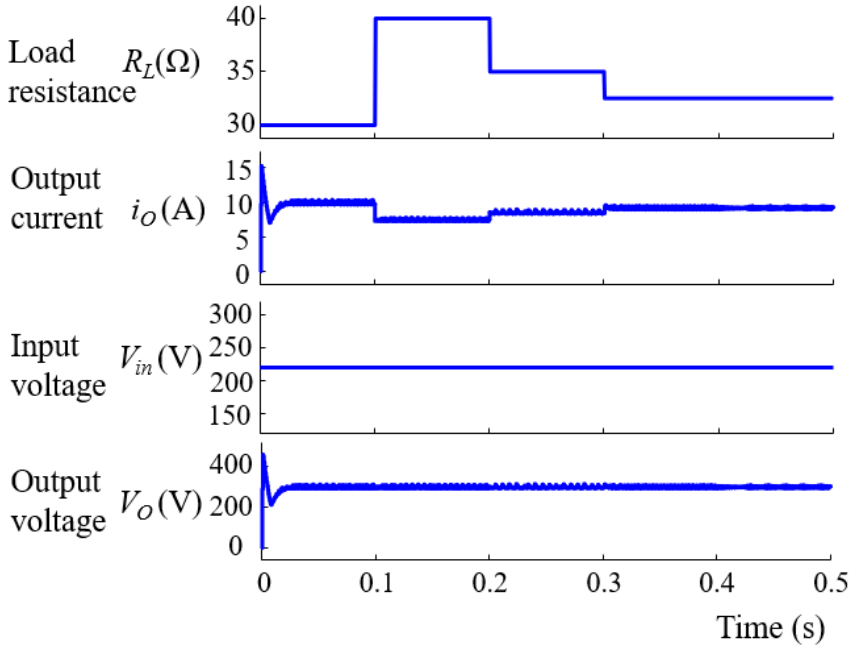

Figure. 3-7. Typical waveforms of the Boost converter

The load resistance changes at 0.1, 0.2 and 0.3 seconds and a corresponding change in output current can be observed. Besides, the 220 V input voltage is successfully boosted to 300 V as

expected. The output voltage waveform achieves its steady state at about 0.02s. As the designed model transmits signals with different carriers, it can be investigated from the output voltage waveforms that fluctuations in different time ranges (e.g., 0.1-0.2s and 0.2-0.3s) can have different amplitudes. The signal transmission results are presented in Fig. 3-8. In Fig. 3-8, c_1, c_2, and c_3 respectively represent the upper envelope of the extracted carrier, lowpass filtered carrier containing f_2, φ_1, and lowpass filtered carrier containing f_1, φ_1. Besides, the restored signals of s_1 and s_2 are exhibited as re_1 and re_2, respectively.

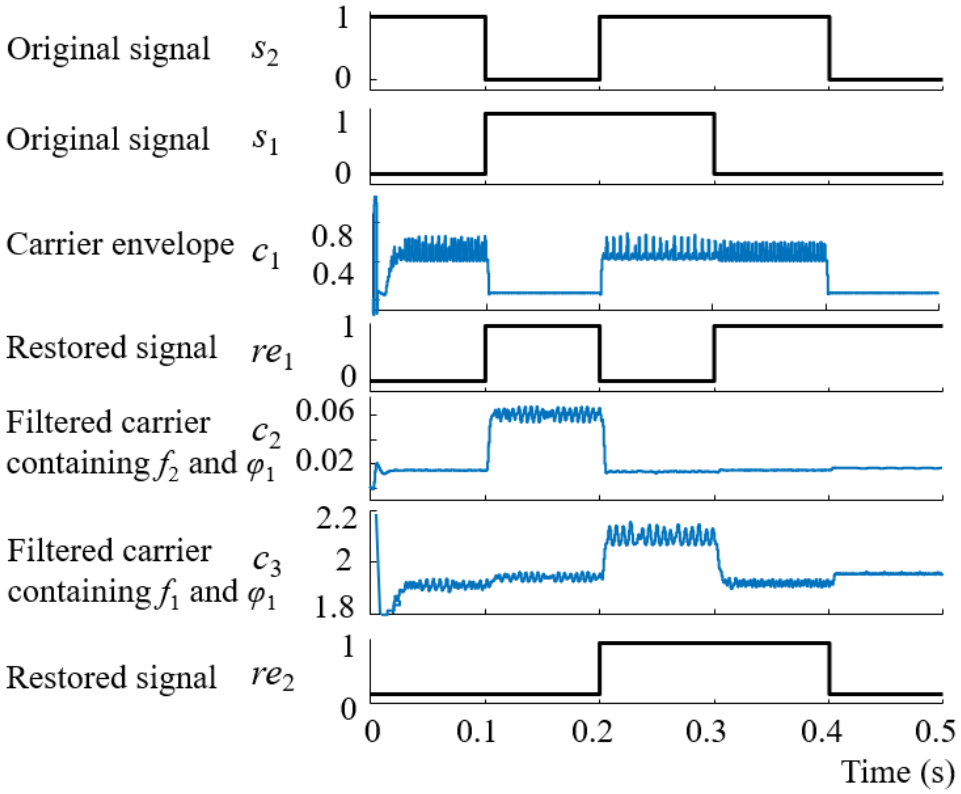

Figure. 3-8. Typical simulation waveforms of IPSK/FSK modulation of a Boost converter

The signal rate is set as 10 bps in this model. Besides, s_1 is '0110', and s_2 is '1011'. As the order of the bandpass filter is increased to 120, the waveforms of c_1, c_2, and c_3 in Fig. 3-8 have sharper rising and falling edges than that in Fig. 3-4. Moreover, unlike the previous Buck model which used the output current waveform for signal demodulation, this model uses the output voltage waveform for carrier extraction as the amplitude variation of the current waveform can lead to misinterpretation of the transmitted data. After the demodulation process, the transmitted two signals are successfully recovered with a time delay of one bit. The reasons for the delay have already been mentioned in the previous paragraphs. The simulation results

indicate that the proposed method can be applied in both open-loop and closed-loop controlled converters.

3.2.3 Simulation Results of the IPST Integrated Cascaded Full-Bridge Converter

The proposed IPSK/FSK method can be applied to DC/AC converters. Fig. 3-9 presents a cascaded full-bridge topology for integrated power/signal transmission. The topology contains two series-connected full-bridge converters, where the upper full-bridge cell is used for signal modulation and the lower full-bridge cell is applied for power modulation. The intrinsic inductance of the transmission line is represented by L. When the converter is operating, the transmitted power will eventually be conducted to the load R. Specifically, the AC output power is obtained using a sinusoidal pulse width modulation (SPWM) method that compares a reference sine wave to the triangle carrier and utilises the comparison outcomes to drive the four IGBT switches. For signals modulation using the four fast-switching switches of the top full-bridge converter, switches Q_1 and Q_2 operate simultaneously using four different carriers for the modulation of two signals. Meanwhile, switches Q_3 and Q_4 turn on and turn off at the opposite conditions of Q_1 and Q_2 to avoid short circuit. The modulated signal is overlaid on the modulated current waveform because the two full-bridge converters for signal transmission and energy conversion are connected in series. Because the amplitude of power source V_1 is substantially lower than that of power source V_2, the modulated signal is overlaid on the current as a minor amplitude fluctuation, causing no significant distortion to the current waveform.

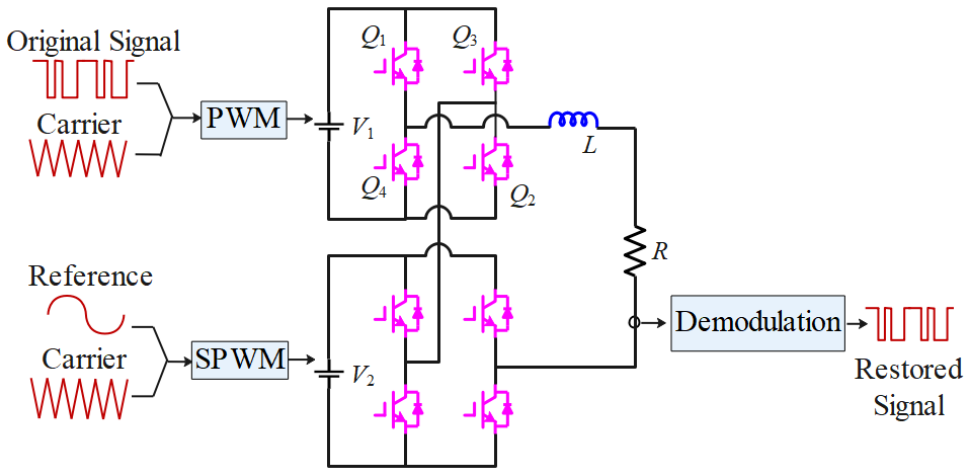

Figure. 3-9. The simulation model of the cascaded full-bridge converter

Table 3-4 lists the parameters that used in this model. A 200 V DC voltage source is used for AC power generation. An extra 10 V DC voltage source is used to create the modulated signals on the current waveform. It is appropriate to use a 10 V voltage source for carrier generation because the amplitude of the carrier produced by the 10 V power supply will not significantly distort the current waveform of the power conversion, and the carrier energy is large enough to be detected in the demodulation process. The transmission line's intrinsic inductance is adjusted to 200 μH. Moreover, two 4-bit signals are transmitted along with energy conversion. In the designed simulation model, s_1 is '1100', and s_2 is '1010', and both signals have the data rate of 5 bps. The simulation results are exhibited in Fig. 3-10, where c_1, c_2, and c_3 respectively represent the upper envelope of demodulated carrier of s_1, and two demodulated carriers with the same phases and various frequencies. Besides, re_1 and re_2 in Fig. 3-10 refer to the recovery signals of s_1 and s_2, respectively. These signals are demodulated from the current waveform and the successful recovered signals verify the feasibility of the proposed method in a DC/AC converter.

TABLE 3-4 Simulation Parameters of the Cascaded DC/AC Converter

Parameter Name	Value
AC reference frequency	50 Hz
DC voltage source for power conversion	200 V
DC side carrier voltage	10 V
Carrier frequency of digital '1' in s_1	1 kHz
Carrier frequency of digital '0' in s_1	2 kHz
Carrier phase of digital '1' in s_2	0
Carrier phase of digital '0' in s_2	π/3
Power line inductance	200 μH
Load resistance	2 Ω
DC side carrier frequency for AC current modulation	20 kHz

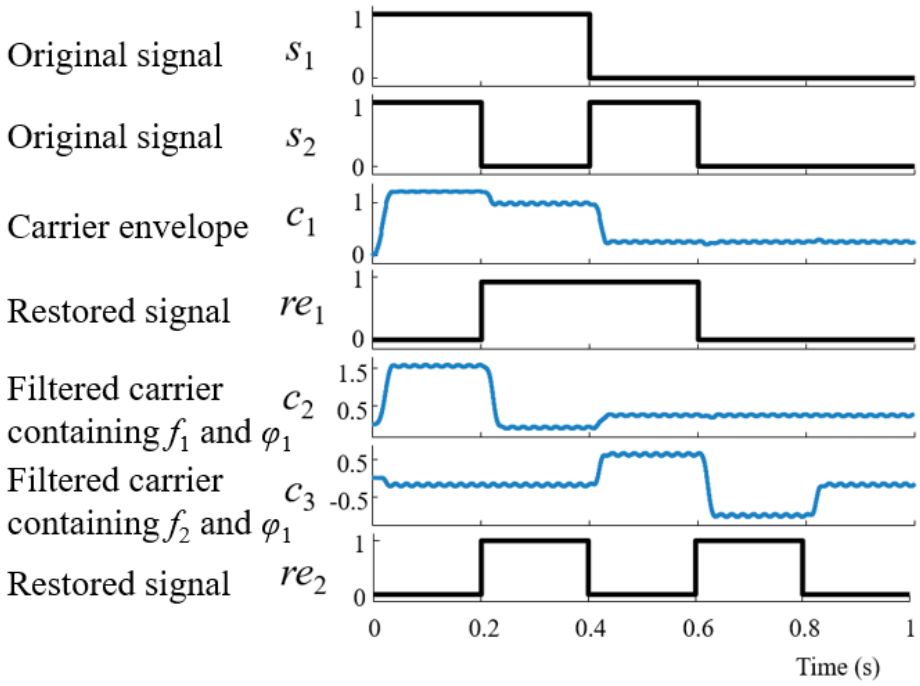

Figure. 3-10. Typical simulation waveforms of IPSK/FSK modulation of a cascaded full-bridge converter

3.3 Summary

This chapter summarises the similarities between communication and power conversion systems, both of which require the transfer of data or energy between different areas. Based on this commonality, the feasibility of the IPST approach is analysed. In addition, the mechanisms of FSK and PSK data modulation methods combined with PWM power modulation methods are investigated. Besides, methods for demodulating data from current waveforms including coherent demodulation and envelope detection are studied. This chapter then proposes the IPSK/FSK method to facilitate data rates by making full use of the carrier phase and frequency for data modulation and analyses its feasibility through simulation. The simulation results of the buck converter proves that the IPST approach can simultaneously transmit data and energy. Furthermore, the proposed IPST method has acceptable noise immunity compared to the PSK and FSK methods applied in conventional SESs.

Chapter 4 Integrated Power/Signal Transmission in a Triple Active Bridge Converter Based on Partial Power Processing for Battery Management Systems

4.1 Introduction

Partial power processing (PPP) is a technology that employs converters to process part of the total power while most of the unprocessed system energy transfers directly through power cables [135]. Power losses can be decreased since the PPP converter processes less power, resulting in enhanced system efficiency and power density [136]. The concept has been successfully implemented in a variety of applications, including fast charging stations for EVs [137], mismatch effects mitigation in photovoltaic system [138], battery balancing in energy storage systems [139], and maximum power point tracking operation in offshore wind farms [140]. Furthermore, previous research has developed other PPP converters incorporating flyback converters [139], dual-active bridge converters [141], and quasi-Z-source converters [142] based on their equivalent full-power isolated converters. Nevertheless, because these studies are mainly focused on PPP in two-port converters, PPP in multi-port converters requires further investigation. A family of PPP multi-port converters is presented in [143] to implement the bidirectional energy flow of each port, which is critical for multi-port applications in practice. Nonetheless, to establish a theoretical basis for the bidirectional flow of energy, it is important to understand the energy flow at each port. With the merits of high energy conversion efficiency, PPP multi-port converters have a promising future and deserve further research in topology design and application.

A PPP-based triple active bridge (TAB) converter is proposed in this chapter to facilitate data communication among several BMS battery packs. The proposed converter has three ports, and power is exchanged among them using a phase-shift PWM mechanism. Furthermore, each battery pack's communication signals, such as temperature, voltage, current, and SOC, are superimposed into power conversion process using phase perturbation modulation (PPM) [127]. This method enables charging and discharging between battery packs while inheriting the high

efficiency merits of the PPP converter. Through simulations, this chapter demonstrates the practicality of the integrated transmission method in battery balancing applications.

This chapter is arranged as below. Firstly, the power flow control methods and the configuration of the proposed TAB converter are briefly described. Secondly, the signal transmission strategies are demonstrated. Thirdly, a simulation model that contains a TAB converter is implemented in MATLAB/Simulink and a brief conclusion is provided at the end of this chapter.

4.2 Topology Configuration

Fig. 4-1 presents the traditional TAB converter topology [144] and the proposed PPP-based TAB converter structure. The proposed topology has three ports, each of which involves an active bridge with four switches, an inductor L_i (i=1, 2, 3), and a transformer with winding N_i at each port. Moreover, capacitors C_2 and C_3 are connected in parallel with the H-bridge cells at Ports 2 and 3, respectively, and operate as energy buffers among the three ports. Furthermore, a battery pack B_i are connected at the terminal of each port. The positive electrodes of these three battery packs are connected through the active bridges and the negative electrodes of the battery packs are linked by wires, thus forming a charge/discharge circuit. In this design, the partial power transferred among three ports by magnetic coupling of the three windings, while the rest of the power flows directly from the discharging battery packs to the charging battery packs. In contrast to conventional DC/DC converters such as buck/boost converters and flyback converters, the design contains multiple ports and can therefore cater for multi-directional power flow requirements. In addition, the designed system uses a distributed battery pack rather than the entire battery module in a conventional BMS system and can therefore be flexibly placed in different parts of the electric vehicle to save space.

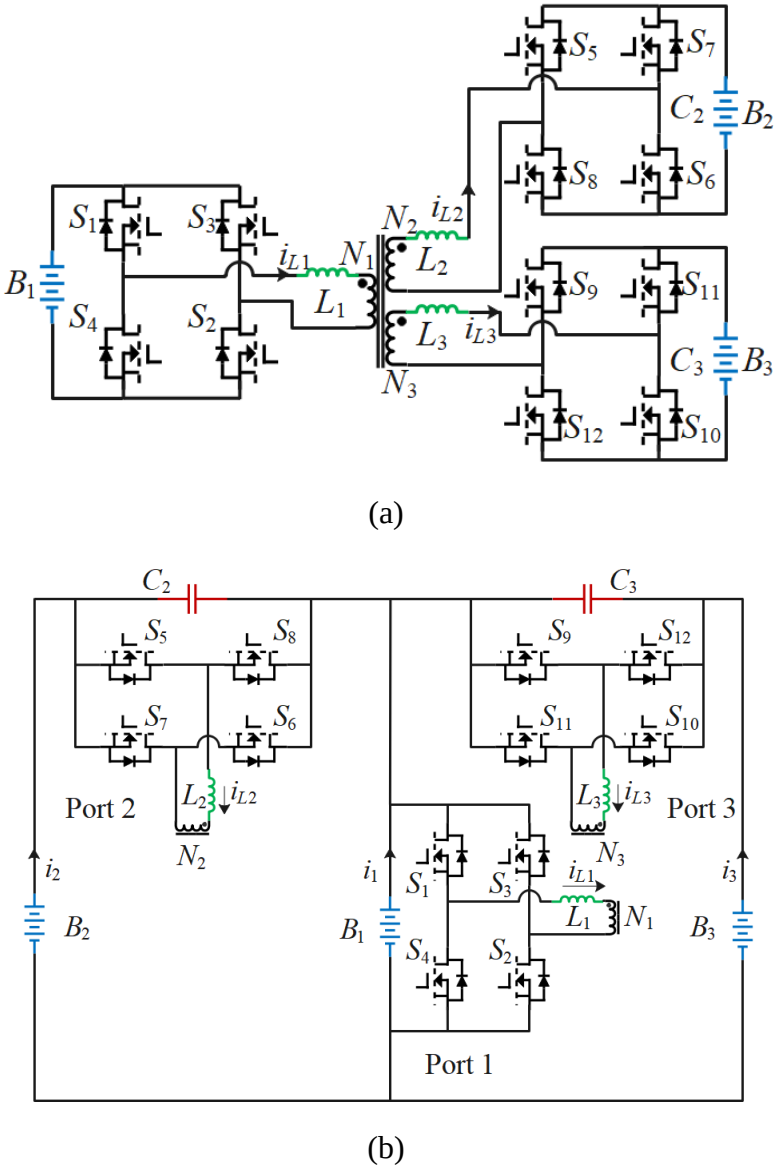

Figure. 4-1. Topology of (a) the traditional TAB converter [144]**; and (b) the proposed PPP-based TAB converter**

4.3Energy Flow Analysis

4.3.1 Dual Active Bridge Converter

To derive the energy flow expression of a PPP-based TAB converter, the characteristics of an isolated dual active bridge converter (DAB) are first analysed. Assuming all the converter switches are instantaneous, the phase shift-controlled waveforms can be acquired as shown in Fig. 4-2, where S_1, S_2 respectively refer to the gate signal of the switches at different positions

in the two branches of a full-bridge converter at Port 1. Besides, S_7 and S_8 are the gate signals of the switches of the other full-bridge converter at Port 2, which lag S_1 and S_2 for φ_1 radian. As an inductor L is connected between the two full bridge converters, its inductance current i_L can be used to represent the total current. Therefore, there are four different states of inductor current in a switching cycle T_s, and the current states can be derived from the following equation.

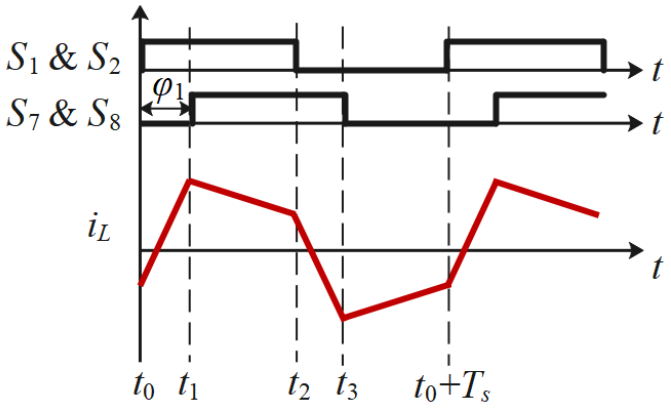

Figure. 4-2. Typical waveforms of a DAB converter

When $t_0 \leq t \leq t_1$,

$$i_L(t) = \frac{V_1 + V_2}{L}(t - t_0) + i_L(t_0) \qquad (4-1)$$

where $t_1 = t_0 + (\varphi_1 T_s)/2\pi$ and V_1, V_2 are the equivalent voltages of the two H-bridge cells at the primary side of the transformer.

When $t_1 \leq t \leq t_2$,

$$i_L(t) = \frac{V_1 - V_2}{L}(t - t_1) + i_L(t_1) \qquad (4-2)$$

where $t_2 = t_0 + T_s/2$.

When $t_2 \leq t \leq t_3$,

$$i_L(t) = \frac{-V_1 - V_2}{L}(t - t_2) + i_L(t_2) \qquad (4-3)$$

where $t_3 = t_2 + (\varphi_1 T_s)/2\pi$.

When $t_3 \leq t \leq t_0 + T_s$,

$$i_L(t) = \frac{-V_1 + V_2}{L}(t - t_3) + i_L(t_3) \tag{4-4}$$

Because the converter operates in continuous conduction mode, the inductor current at the beginning and end of each cycle are equal. Therefore, the inductor current can be further derived as

$$\begin{cases} i_L(t_0) = -i_L(t_2) = -i_L\left(t_0 + \dfrac{T_s}{2}\right) = -\dfrac{(V_1 - V_2)\pi + 2V_2\varphi_1}{4\pi f_s L} \\ i_L(t_1) = -i_L(t_3) = -i_L\left(t_1 + \dfrac{T_s}{2}\right) = \dfrac{(V_2 - V_1)\pi + 2V_1\varphi_1}{4\pi f_s L} \end{cases} \tag{4-5}$$

where f_s=1/T_s represents the switching frequency. Then the expression for the power P_{ab} transmitted from Port 1 to Port 2 in a switching period can be acquired as

$$\begin{aligned} P_{ab} &= V_1 I_1 = V_1\left(\frac{1}{T_s}\int_{t_0}^{t_0+T_s} i_L(t)dt\right) \\ &= V_1\left[\frac{2}{T_s}\left(\int_{t_0}^{t_1} i_L(t)\,dt + \int_{t_1}^{t_2} i_L(t)\,dt\right)\right] \\ &= \frac{\varphi_1(\pi - \varphi_1)V_1V_2}{2\pi^2 f_s L} \end{aligned} \tag{4-6}$$

where I_1 denotes the equivalent current of Port 1 on the primary side of the transformer. Similarly, the power migration of the converter can be obtained in the same approach when the switches S_7 and S_8 lead the switches S_1 and S_2. Finally, the expression of the power P_{ab} for these two scenarios can be derived as

$$P_{ab} = \frac{\varphi_1(\pi - |\varphi_1|)V_1V_2}{2\pi^2 f_s L} \tag{4-7}$$

from which it can be observed that when the phase shifted PWM method is utilised, the power flow direction is related to the leading/lagging conditions of the switches (φ_1) and independent to the port voltages.

4.3.2 Partial Power Processing Based Triple Active Bridge Converter

The phase-shift PWM method is applied to control the power flow direction in the proposed converter. Specifically, the switches of the various ports are managed by shifted signals, and

the two switches in the same bridge arm are designed to operate conversely. Taking the control signals of switches S_1 and S_2 as references, the control signals of switches S_7 and S_8 and switches S_{11} and S_{12} are lagged by φ_2 and φ_3 radians, respectively, as exhibited in Fig. 4-3, where $-\pi<\varphi_2<\pi$, $-\pi<\varphi_3<\pi$, and the duty ratio of each switch is half of the switching cycle. Additionally, the current waveforms of L_1, L_2, and L_3 of a traditional phase-shift isolated TAB converter are depicted in Fig. 4-3 for i_{L1}, i_{L2}, and i_{L3}, respectively. The voltages of the three battery packs are arranged to the same initial SOC value and the turns ratio N_1: N_2: N_3 of the transformer is set to 1:1:1 for a simplified analysis.

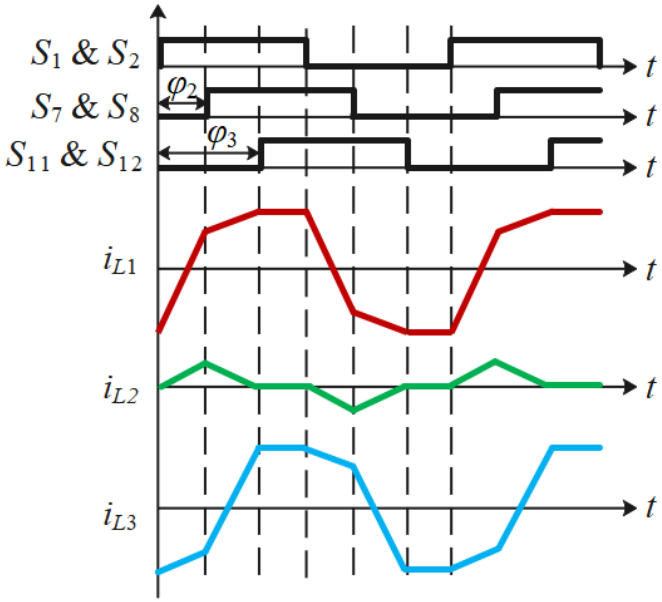

Figure. 4-3. Typical waveforms of an isolated phase-shift TAB converter

The power flow characteristics of a phase-shift isolated TAB converter can be derived from the DAB converter and the expression in (4-7) can be extended to (4-8) by analysing various operating states of the TAB converter.

$$\begin{cases} P_{12} = \dfrac{\varphi_2(\pi - |\varphi_2|)V_1V_2}{2\pi^2 f_s(L_1 + L_2)} \\ P_{13} = \dfrac{\varphi_3(\pi - |\varphi_3|)V_1V_3}{2\pi^2 f_s(L_1 + L_3)} \\ P_{23} = \dfrac{(\varphi_3 - \varphi_2)(\pi - |\varphi_3 - \varphi_2|)V_2V_3}{2\pi^2 f_s(L_2 + L_3)} \end{cases} \quad (4-8)$$

In this expression, V_1, V_2, and V_3 refer to the voltages of batteries B_1, B_2, and B_3, respectively, and P_{12}, P_{13}, and P_{23} are the power flow from Port 1 to Port 2, from Port 1 to Port 3, and from Port 2 to Port 3, respectively. Furthermore, f_s is the switching frequency. In the proposed

topology, since the rest unprocessed energy transfers directly through inductors, the conducted energy in one operation cycle can be obtained in (4-9), where C_{12}, C_{13}, and C_{23} are the conducted power flow from Port 1 to Port 2, from Port 1 to Port 3, and from Port 2 to Port 3, respectively.

$$\begin{cases} C_{12} = \dfrac{(V_1 - V_2)}{(L_1 + L_2)f_s} \\ C_{13} = \dfrac{(V_1 - V_3)}{(L_1 + L_3)f_s} \\ C_{23} = \dfrac{(V_2 - V_3)}{(L_2 + L_3)f_s} \end{cases} \tag{4-9}$$

Next, the total power transferred among these three ports in one switching period can be acquired from (4-8) and (4-9) by adding together the processed power and conducted power. The equation of the total power converted among various ports is presented in (4-10), where T_{12}, T_{13}, and T_{23} are the total power flow from Port 1 to Port 2, from Port 1 to Port 3, and from Port 2 to Port 3, respectively.

$$\begin{cases} T_{12} = \dfrac{\varphi_2(\pi - |\varphi_2|)V_1V_2 + 2\pi^2(V_1 - V_2)}{2\pi^2 f_s(L_1 + L_2)} \\ T_{13} = \dfrac{\varphi_3(\pi - |\varphi_3|)V_1V_3 + 2\pi^2(V_1 - V_3)}{2\pi^2 f_s(L_1 + L_3)} \\ T_{23} = \dfrac{(\varphi_3 - \varphi_2)(\pi - |\varphi_3 - \varphi_2|)V_2V_3 + 2\pi^2(V_2 - V_3)}{2\pi^2 f_s(L_2 + L_3)} \end{cases} \tag{4-10}$$

Suppose each inductor has the same inductance and the sum of each two inductors is L_e, the port power can be derived from

$$\begin{cases} T_1 = T_{12} + T_{13} = \dfrac{\varphi_2(\pi - |\varphi_2|)V_1V_2 + \varphi_3(\pi - |\varphi_3|)V_1V_3 + 4\pi^2V_1 - 2\pi^2(V_2 + V_3)}{2\pi^2 f_s L_e} \\ T_2 = -T_{12} + T_{23} = \dfrac{-\varphi_2(\pi - |\varphi_2|)V_1V_2 + (\varphi_3 - \varphi_2)(\pi - |\varphi_3 - \varphi_2|)V_2V_3 + 4\pi^2V_2 - 2\pi^2(V_1 + V_3)}{2\pi^2 f_s L_e} \\ T_3 = -T_{13} - T_{23} = \dfrac{-\varphi_3(\pi - |\varphi_3|)V_1V_3 - (\varphi_3 - \varphi_2)(\pi - |\varphi_3 - \varphi_2|)V_2V_3 + 4\pi^2V_3 - 2\pi^2(V_1 + V_2)}{2\pi^2 f_s L_e} \end{cases} \tag{4-11}$$

where T_1, T_2, and T_3 represent the total power of Port 1, Port 2, and Port 3, respectively. Therefore, the direction of power transmission is determined by both the port voltages and phase shift angles of the switching gate signals. For instance, Fig. 4-4 displays five typical

energy flow scenarios. When $T_1>0$, $T_2<0$ and $T_3<0$, the total power flows from Port 1 to Port 2 and Port 3 as presented in Fig. 4-4 (a). In this case, the relationship among φ_2, φ_3, V_1, V_2, and V_3 can be acquired from (4-11) and exhibited in (4-12), where $\varphi_2=\varphi_3$ and $\delta=\varphi_2(\pi-|\varphi_2|)=\varphi_3(\pi-|\varphi_3|)$ are assumed in this formula. Therefore, the multi-directional power flow can be realised by alternating the phase shift angle of the converter switches within a certain variation of the port voltages. When there is neither energy flowing in nor out of one port during a switching cycle, the proposed topology will operate as a DAB converter with energy flowing between the remaining two ports, as depicted in Fig. 4-4(e).

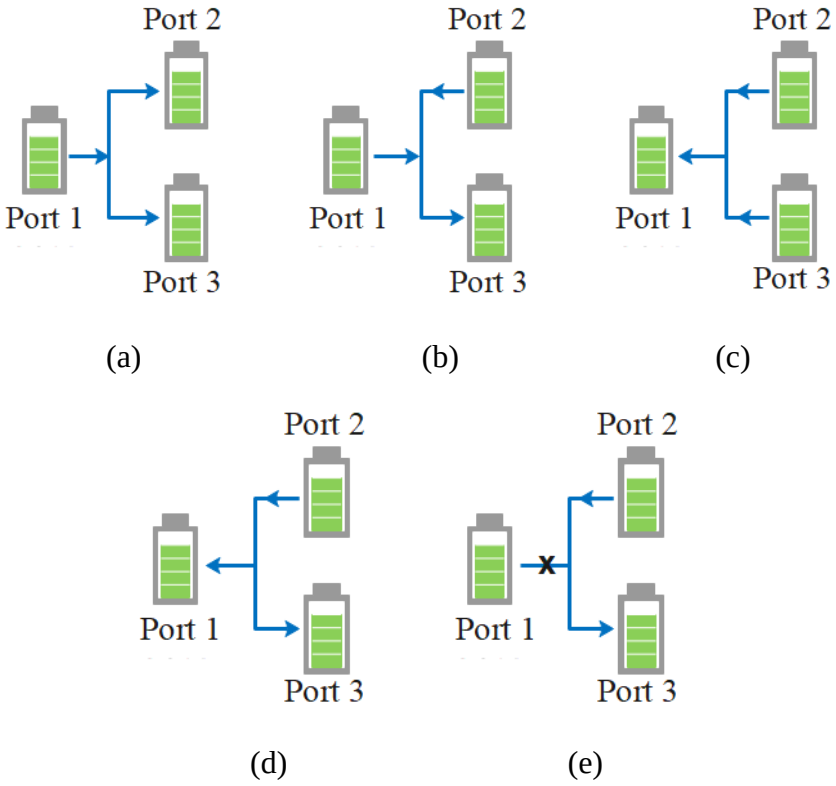

Figure. 4-4. Typical power flow directions of the proposed topology, where (a) $T_1>0$, $T_2<0$ and $T_3<0$; (b) $T_1>0$, $T_2>0$ and $T_3<0$; (c)$T_1<0$, $T_2>0$ and $T_3>0$; (d) $T_1<0$, $T_2>0$ and $T_3<0$; (e) $T_1=0$, $T_2>0$ and $T_3<0$

$$\delta > \begin{cases} \dfrac{2\pi^2(V_2+V_3-2V_1)}{V_1(V_2+V_3)} \\ \dfrac{-2\pi^2(V_1+V_3-2V_2)}{V_1V_2} \\ \dfrac{-2\pi^2(V_1+V_2-2V_3)}{V_1V_3} \end{cases} \qquad (4-12)$$

4.3.3 Efficiency Analysis

The total losses (P_t) of the designed topology can be seen as the composition of semiconductor components loss (P_s), high-frequency transformer loss (P_{tr}), and heat loss on passive devices (P_{pa}), which is presented in (5-13).

$$P_t = P_s + P_{tr} + P_{pa} \quad (4-13)$$

Specifically, conduction loss and switching loss are two types of semiconductor losses. In addition, high-frequency transformer losses can be categorised into copper loss and iron loss. As only a partial of power is processed by the transformer in the proposed topology, the transformer loss is less than that of the traditional isolated TAB converter. Nevertheless, the conduction loss of the designed topology is higher as the results of the introduced power lines. If the conduction loss is omitted in low-resistivity and short-distance power lines, the designed topology can have lower total losses and thus realise higher efficiency than the conventional isolated TAB converter.

4.4 IPST Integrating in Triple Active Bridge Converters

The phase perturbation approach is employed in the proposed converter for signal modulation and the typical modulation waveforms are exhibited in Fig. 4-5, where *S(t)* is the original signal, and Car_1, Car_2, and Car_3 denote the triangle carriers utilised in port 1, port 2, and port 3, respectively. To be more specific, the carrier used for modulating digital '1' of the transmitted will be shifted for $+\Delta t$ and $-\Delta t$ when the corresponding port requires communication. Meanwhile, the carrier used for modulating digital '0' and the carriers utilized in other ports will remain unchanged. Since the energy flow is controlled by the phase shift of the carrier, the signal transmission method is achieved by further perturbing the carrier phase shift angle on the basis of the power conversion. As shown in Car_1 of Fig. 4-5, the triangular carrier is shifted left and right by the same time Δt when modulating the digit '1'. This method allows the same power to be processed by keeping the resulting duty cycle constant when transmitting '1' and '0'.

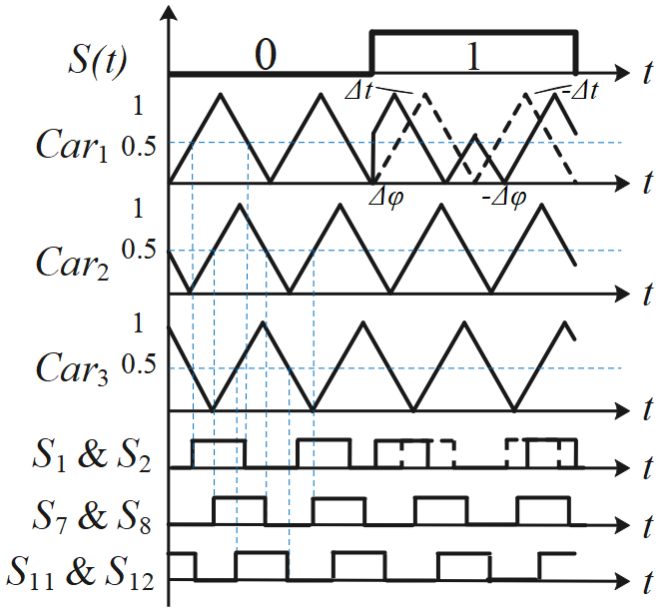

Figure. 4-5. Typical waveforms of phase perturbation modulation

The relationship between Δt and $\Delta\varphi$ is

$$\Delta t = \frac{\Delta\varphi}{2\pi f_s} \tag{4-14}$$

Taking a conventional isolated DAB converter for instance, the output power with and without phase perturbation for transmitting a digital '1' are derived as P_n and P_m in (4-15), respectively.

$$\begin{cases} P_n = \dfrac{[\varphi(\pi-\varphi)-\Delta\varphi^2]V_1V_2}{\pi^2 f_s L_e} \\ P_m = \dfrac{\varphi(\pi-\varphi)V_1V_2}{\pi^2 f_s L_e} \end{cases} \tag{4-15}$$

In this equation, φ and $\Delta\varphi$ respectively represent the initial phase shift angle and perturbated phase shift angle. Besides, the carrier frequency is supposed to be two times the signal frequency. The difference between P_n and P_m is

$$P_n - P_m = \frac{\Delta\varphi^2 V_1V_2}{\pi^2 f_s L_e} \tag{4-16}$$

which indicate that the perturbated phase shift angle has little effect on the average output power when $\Delta\varphi$ is small. Therefore, the phase perturbation method can be used for signal modulation in the proposed TAB converter.

After the communication data is transmitted through the proposed converter, the carrier for digital '1' is then demodulated from the current waveform using the sliding discrete Fourier transform (SDFT). If the switches in port 1 are employed for data modulation, the data can be demodulated from the current at port 2 or port 3 because of the multi-directional power flow capability of the proposed converter. For a discrete-time series *x(n)*, its DFT expression is

$$X(k) = \sum_{n=0}^{N-1} x(n) e^{\frac{-j2\pi nk}{N}}, k = 0, 1, \dots, N-1 \quad (4-17)$$

where *k* is the frequency index and *n* is the time index within the sequence length *N* of each frame for DFT transformation. Besides, *X(k)* denotes the DFT output result at the k^{th} frequency point. In two adjacent and non-significantly overlapping time series with each other, the DFT expressions are

$$\begin{cases} X_n(k) = \sum_{n=0}^{N-1} x(n) e^{\frac{-j2\pi nk}{N}} \\ X_{n+1}(k) = \sum_{n=0}^{N-1} x(n+1) e^{\frac{-j2\pi nk}{N}} = \sum_{m=1}^{N} x(m) e^{\frac{-j2\pi (m-1)k}{N}} \end{cases} \quad (4-18)$$

where $m=n+1$. Using the iteration method, the DFT expression of the next time sequence is derived in [145] and can be expressed as

$$X_{n+1}(k) = e^{\frac{j2\pi k}{N}} [X_n(k) - x(n+1-N) + x(n+1)] \quad (4-19)$$

Therefore, the result of the DFT calculation at $X_{n+1}(k)$ is equal to the result of the previous DFT calculation $X_n(k)$ plus the difference between the current sampled signal value $x(n+1)$ and the value of the sampled signal $x(n+1-N)$ before the window length, which is then phase-shifted. With the SDFT method, the time spent on DFT calculation is greatly reduced, thus decreasing the system computational burden. Moreover, the magnitude and phase variations in time domain and frequency domain are derived in [146] and presented below

$$\begin{cases} Mag\ x_n(k) = \frac{2}{N} \cdot Mag\ X_n(k) \\ Phase\ x_n(k) = Phase\ X_n(k) + \frac{2\pi k}{N} \end{cases} \quad (4-20)$$

from which the amplitude of the carrier used for modulating digital '0' can be suppressed in time domain after the SDFT processing. Next, coherent demodulation and a low-pass filter are

applied to recover the digital '1'. Finally, the restored digital '1' waveform is compared to a threshold value and resampled using the initial data rate.

4.5 Simulation Results

A simulation model containing three battery packs is designed in MATLAB/Simulink to examine the feasibility of the proposed transmission method. The designed model is the same as depicted in Fig. 4-1 (b), with three battery packs connected with each other in parallel through full-bridge converters. The system configurations are exhibited in Table 4-1, where the voltages of the three battery packs are set to 180 V, 200 V, and 210 V, respectively, with an initial SOC of 50%. Moreover, the converter switching frequency is chosen as f_s=10 kHz and the transformer turns ratio is N_1:N_2:N_3=1:1:1.

TABLE 4-1 Parameters of the TAB Simulation Model

Parameter name	Value
$V_1/V_2/V_3$ (Battery pack voltages)	180/200/210 V
$SOC_1/SOC_2/SOC_3$ (Initial state of charge)	50%
N_1:N_2:N_3 (Transformer turns ratio)	1:1:1
f_s (Converter switching frequency)	10 kHz
f_d (Transmitted data frequency)	1 kHz
$L_1/L_2/L_3$ (Series inductance)	300 μH
C_2/C_3 (Series capacitance)	100 μF
$\Delta\varphi$ (Perturbated phase shift angle)	π/2

4.5.1 Energy Conversion

1) φ_2=π/3, φ_3=2π/3: In this scenario, phase-shift angle φ_2 and φ_3 are lagging the port 1 bridge waveform and φ_2 is leading φ_3 as shown in Fig. 4-6. Therefore, power from B_1 is transferred to B_2 and B_3. Additionally, the inductor current waveforms in steady state are exhibited in Fig. 4-6. Fig. 4-7 presents the variation of SOC for the three battery packs, from which it can be investigated that B_1 is discharging while B_2 and B_3 are

charging. The slope of B_2 is smaller than that of B_3 as $\varphi_2<\varphi_3$, which is consistent with the analysis in the previous sections.

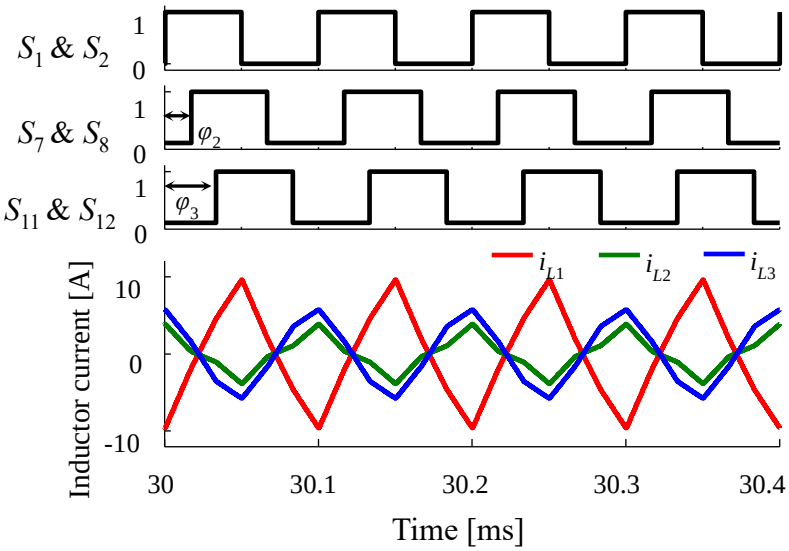

Figure. 4-6. Typical simulation results when $\varphi_2=\pi/3$, $\varphi_3=2\pi/3$

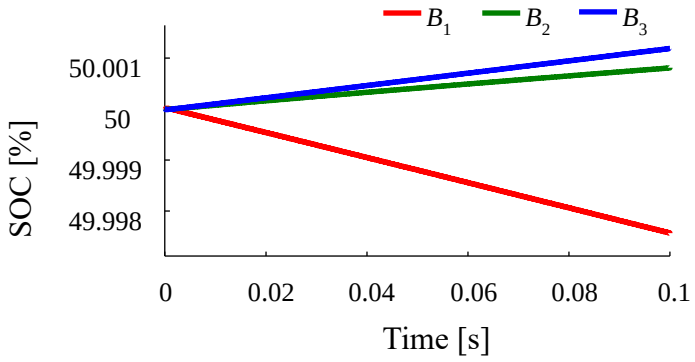

Figure. 4-7. SOC values of the three battery packs when $\varphi_2=\pi/3$, $\varphi_3=2\pi/3$

2) $\varphi_2=-\pi/4$, $\varphi_3=5\pi/12$: In this scenario, phase-shift angle φ_2 is leading φ_3 and the port 1 bridge waveform as depicted in Fig. 4-8. Because the charge of battery pack B_1 is less than its discharge with $|\varphi_2|<|\varphi_3|$ in this scenario, B_1 and B_2 supply power to B_3 together. Furthermore, the discharge rate of B_1 is smaller than that of B_2 as φ_2 is leading the port 1 bridge waveform. Fig. 4-9 presents the variation of SOC for the three battery packs, which is consistent with expectations.

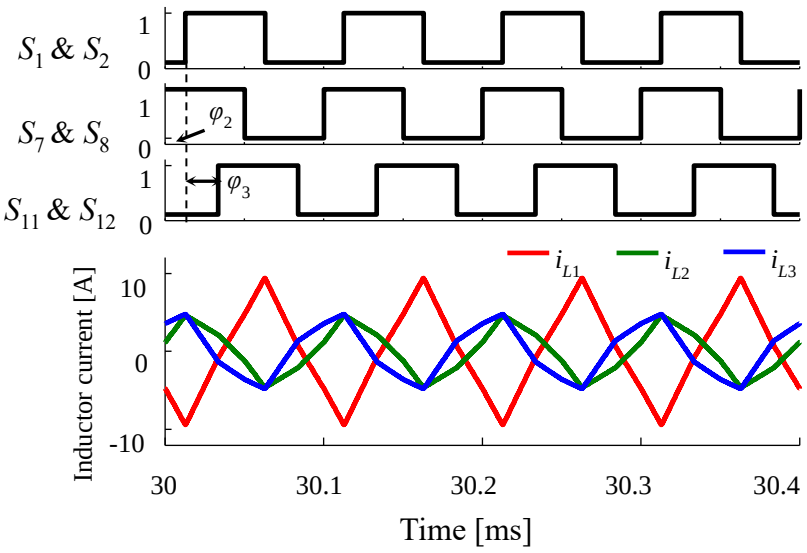

Figure. 4-8. Typical simulation results when φ_2=-π/4, φ_3=5π/12

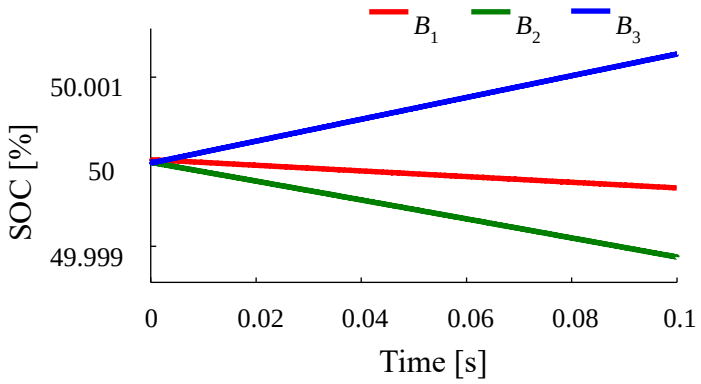

Figure. 4-9. SOC values of the three battery packs when φ_2=-π/4, φ_3=5π/12

3) φ_2=-2π/3, φ_3=-4π/15: In this situation, phase-shift angle φ_2 and φ_3 are leading the port 1 bridge waveform and φ_2 is leading φ_3 as shown in Fig. 4-10. Therefore, power from B_2 and B_3 is transferred to B_1. Additionally, the inductor current waveforms in steady state are exhibited in Fig. 4-10. Fig. 4-11 presents the variation of SOC for the three battery packs, from which it can be investigated that B_1 is charging while B_2 and B_3 are discharging. The discharge rate of B_2 is larger than that of B_3 as $|\varphi_2|>|\varphi_3|$, which is consistent with the analysis in the previous sections.

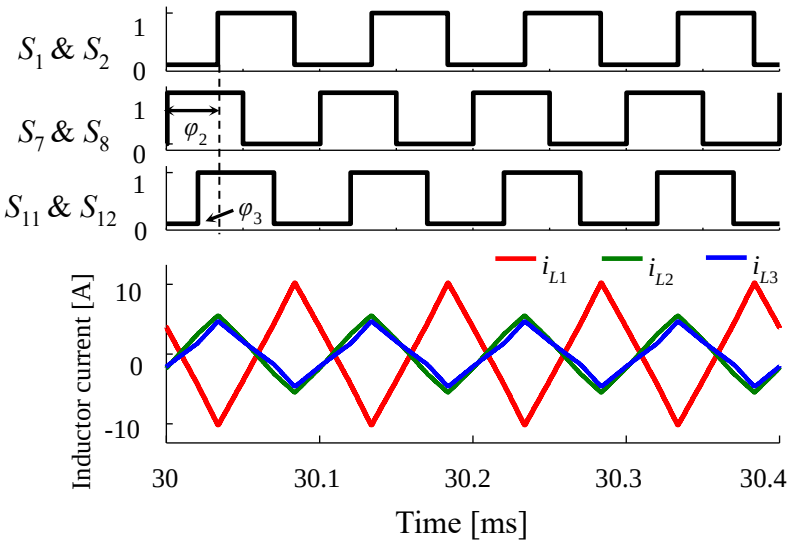

Figure. 4-10. Typical simulation results when φ_2=-2π/3, φ_3=-4π/15

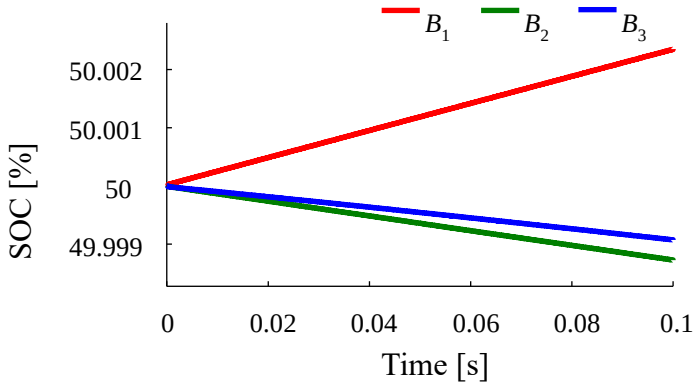

Figure. 4-11. SOC values of the three battery packs when φ_2=-2π/3, φ_3=-4π/15

4) φ_2=-π/3, φ_3=π/15: In this scenario, phase-shift angle φ_2 is leading φ_3 and the port 1 bridge waveform as depicted in Fig. 4-12. The inductor current waveforms in steady state are exhibited in this figure. Fig. 4-13 presents the variation of SOC for the three battery packs, from which it can be investigated that B_1 and B_3 are charging while B_2 is discharging. The charge rate of B_1 is larger than that of B_3 as B_3 has a larger voltage value, and B_1 is charging because $|\varphi_2|>|\varphi_3|$.

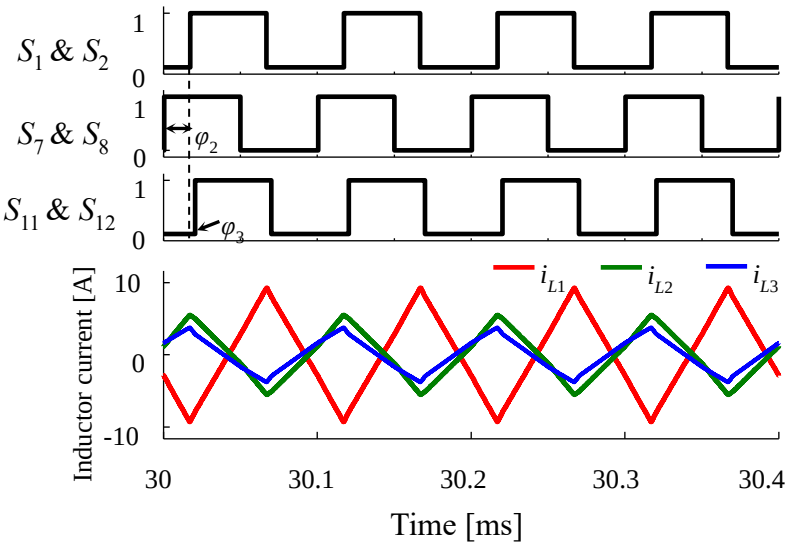

Figure. 4-12. Typical simulation results when φ_2=-π/3, φ_3=π/15

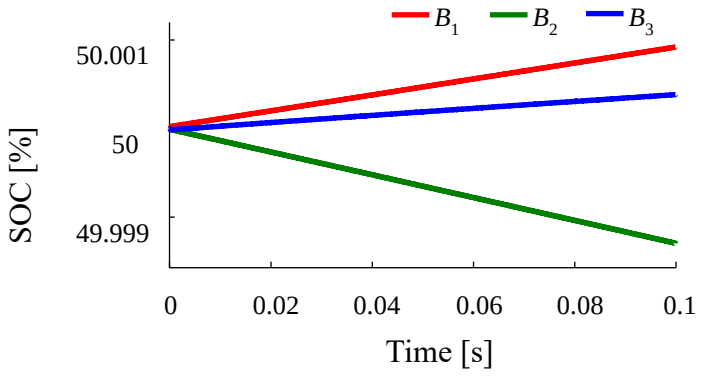

Figure. 4-13. SOC values of the three battery packs when φ_2=-π/3, φ_3=π/15

5) φ_2=-π/3, φ_3=π/3: In this scenario, phase-shift angle φ_2 is leading φ_3 and the port 1 bridge waveform as depicted in Fig. 4-14. The inductor current waveforms in steady state are exhibited in this figure. Fig. 4-15 presents the variation of SOC for the three battery packs, from which it can be investigated that B_3 is charging while B_2 is discharging. Moreover, the amount of charge of B_1 remains unchanged as $|\varphi_2|=|\varphi_3|$. In other words, the total power flows directly from B_2 to B_3 in this case.

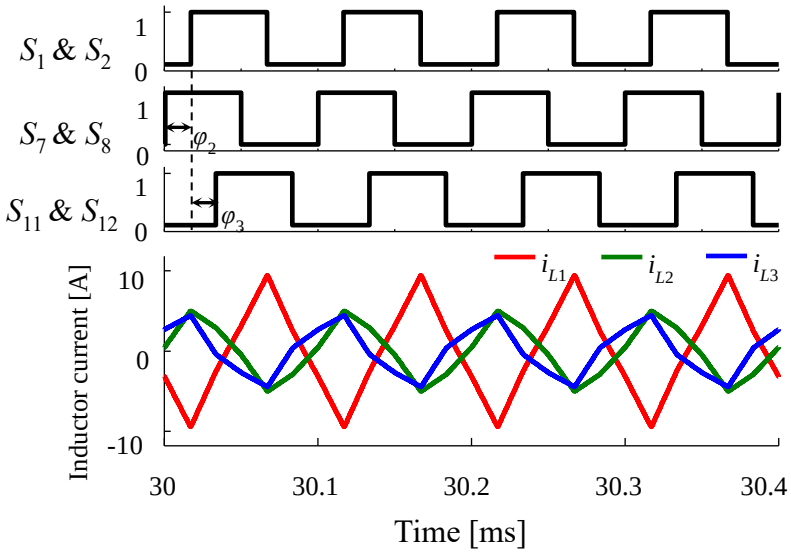

Figure. 4-14. Typical simulation results when φ_2=-π/3, φ_3=π/3

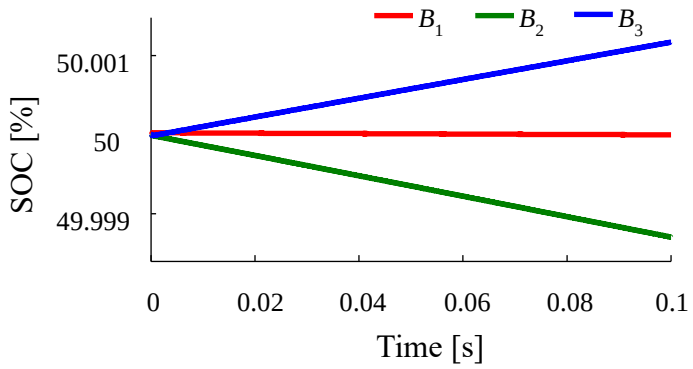

Figure. 4-15. SOC values of the three battery packs when φ_2=-π/3, φ_3=π/3

When comparing Fig. 4-8, Fig. 4-12, and Fig. 4-14, and comparing Fig. 4-9, Fig. 4-13, and Fig. 4-15, it can be observed that the state (charging/discharging) of the battery packs can be changed when φ_2 and φ_3 are altered slightly without changing their leading/lagging conditions. However, since the voltage differences among the three battery packs can affect the power flow directions, the proposed PPP-based topology can balance the battery packs with small voltage differences by changing the phase-shift angles.

4.5.2 Signal Transmission

The signal transmission capability of the designed converter is examined by transmitting an 8-bit frame '11010010'. The simulation results when the circuit is operating for φ_2=π/3, φ_3=2π/3 are exhibited as an example. Fig. 4-16 presents the key waveforms when the switches in port

1 are employed for signal modulation, where Sig_1, i_1, i_2, Sig_2, Sig_3, and Sig_4 refer to the original signal, the current waveform of port 1, the current waveform of port 2, the curve after SDFT processing, the curve after coherent demodulation and the restored signal, respectively. In this simulation, the speed of the transmitted data is 1 kbit/s. Besides, the value of k in (4-17) is 2, which indicates that each DFT sliding window contains two carrier periods. As can be seen from i_1 in Fig. 4-16, the waveform fluctuates differently when transmitting different digital numbers, which is caused by changes in the carrier phases. Because the total energy flows from port 1 to port 2 and port 3 in this case, the simulation results indicate that the communication signal can be transmitted in the same direction as the power flow.

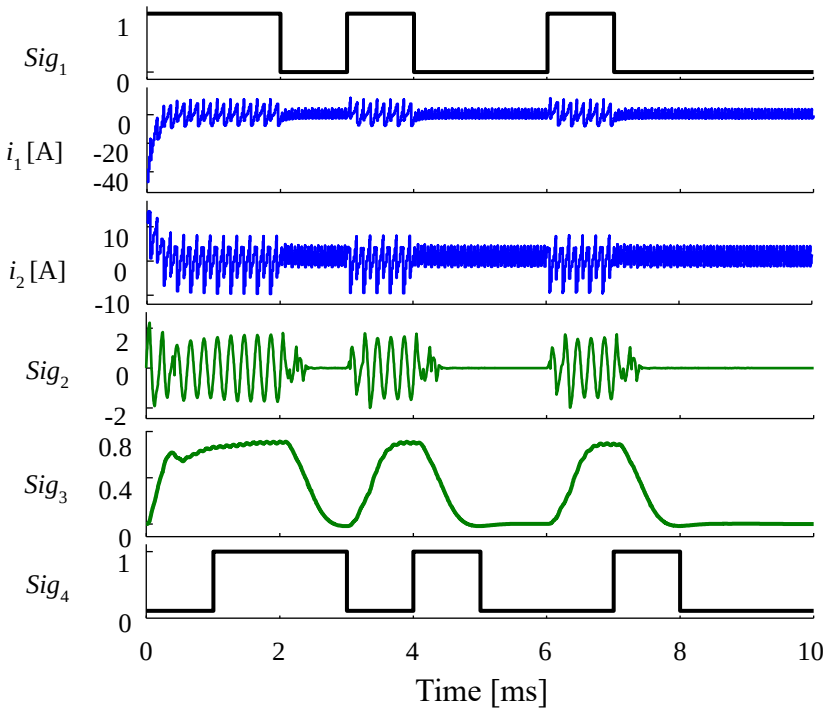

Figure. 4-16. Key waveforms when port 1 is transmitting signal

Similarly, the key waveforms when the switches in port 3 are employed for signal modulation are shown in Fig. 4-17, where i_3 represents the current waveform of port 3. With the rest of the parameters set to the same values as those used to obtain the results in Fig. 4-16, the simulation results indicate that the communication signal can be transmitted in the opposite direction to the power flow. Therefore, the energy and communication signals can be transmitted independently through the phase-shift PWM approach in the proposed converter.

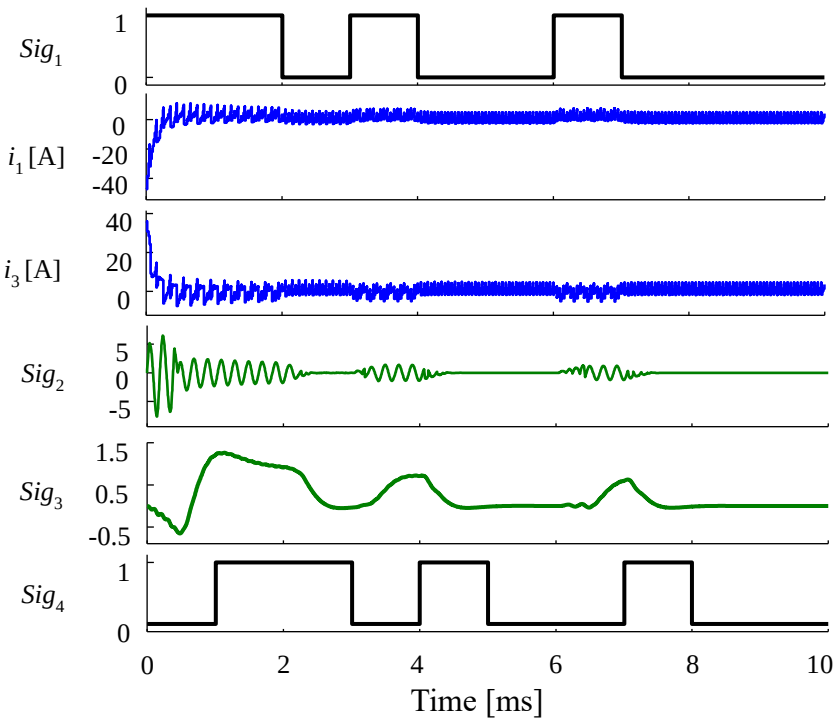

Figure. 4-17. Key waveforms when port 3 is transmitting signal

4.6 Summary

A PPP-based TAB converter is exhibited for realising battery balancing and signal transmission functions in this chapter. The energy conversion is achieved by the phase-shift PWM method, and the transmitted data is modulated by the PPM approach. The energy flow direction in the three ports is controlled by the leading/lagging condition of the converter switches. Because only a fraction of the power is processed while the rest flows directly among the three ports, the proposed converter topology has a higher energy conversion efficiency compared to a conventional isolated TAB converter. Moreover, since the transmission signals are integrated into the current waveform by perturbating carrier phase-shift angle, the cost and volume for system wiring can be reduced. With a simulation model implemented in MATLAB/Simulink, the feasibility of the IPST method in the proposed converter is verified. Furthermore, the direction of signal transmission is independent of the direction of power conversion, which means that any of the three ports can operate as either a transmitter or a receiver.

This chapter exhibits a three-port topology for charging/discharging battery packs, which can be extended to more than three ports for specific applications. Besides, the proposed PPP-based

TAB converter can be employed in the energy management system of the microgrid energy router.

Chapter 5 **Integrated Power/Signal Transmission of Distributed Battery Management Systems for Electric Vehicles**

5.1 Introduction

Although electric vehicles have many advantages as described in Chapter 1, the limitations of the EV battery are still an important barrier to large-scale adoption of EVs [147]. Specifically, the battery maximum capacity decreases with its operating time and the battery life span are influenced by several factors including overcharging, operating temperature, depth of discharge in each charge/discharge cycles, and rate of charge/discharge [148], [149]. Therefore, the batteries state of charge (SOC) will unbalance after using an EV for a period. It is essential to design a battery management system (BMS) to extend the life span of an EV by controlling its batteries discharging process. Besides, it is essential to develop an effective signals transmission approach for EV since the various subsystems such as the motor control unit (MCU) and the BMS in an EV require communication with the transmission control unit (TCU) [150], [151]. One of the generally accepted methods of signal transmission in EVs is through the CAN bus thanks to its high baud rate and high reliability [152], [153].

Fig. 5-1 exhibits the powertrain architecture of an EV. Usually, the battery voltage is boosted by a DC/DC converter and then processed by a 2-level inverter [154], [155]. Nevertheless, large voltage change rates (*dV/dt*) can be generated with this method, resulting in high switching losses [154]. Furthermore, Because the large number of inductors applied in the DC/DC boost converter, the system is costly and has a low power density [155]. Because classic EVs employ the CAN bus for internal communication, the communication function and the power transmission function are still two separate parts that can be combined into one.

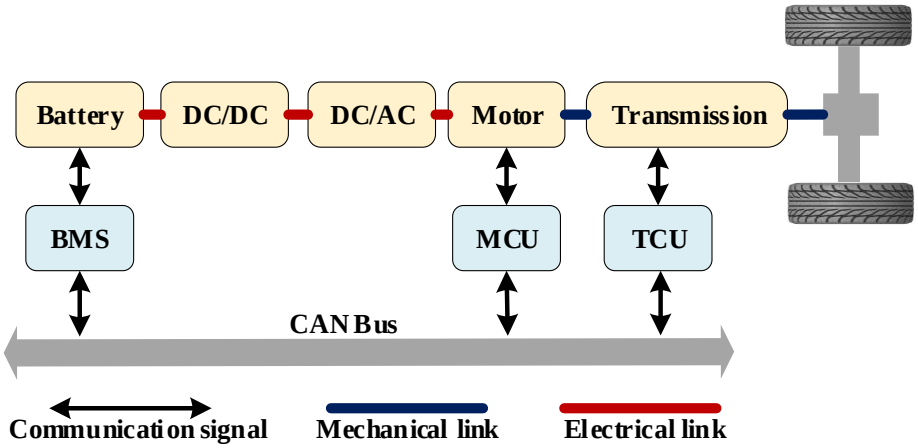

Figure. 5-1. The general powertrain structure of an EV

This chapter presents an IPST approach for EVs that uses a three-phase multilevel inverter topology to transfer both communication data and energy. The proposed topology has lower switching losses than a 2-level inverter, and a DC/DC converter is not compulsory because the battery voltage can be boosted by the inverter itself. The power conversion in the proposed topology is accomplished using the PWM method, and the transmitted signals are modulated using the FSK method. Rather than using a CAN bus as a communication channel in modern EVs, the suggested solution can significantly lower communication system costs by transmitting power and signals simultaneously over the same power line.

This chapter is arranged as below. Firstly, the structure and the IPST mechanisms of the proposed system is introduced. Secondly, the battery balance strategy is analysed. Thirdly, a simulation model incorporating a multilevel inverter and a permanent magnet synchronous motor (PMSM) is designed in MATLAB/Simulink and simulation results are provided as a proof of feasibility. Finally, a brief conclusion is drawn at the end of this chapter.

5.2 System Structure and Battery Balance Function

5.2.1 System Structure

Fig. 5-2 presents the suggested system structure for an EV utilising the IPST approach. Signals are sent between the battery and the BMS, as well as between the MCU and the motor, using a three-phase multilevel inverter circuit. Compared to the conventional powertrain depicted in Fig. 5-1, DC/DC converters and CAN bus are omitted to save cost and size. Fig. 5-3 depicts

the suggested structure of a three-phase IPST system. Each phase of the inverter architecture has four series linked H-bridge cells, where the first cell is used for signal transmission and the other three cells are applied for energy transfer. As the overall output voltage of a cascaded multilevel inverter is equal to the sum of the voltages of each cell, this design is suitable for distributed battery systems where the voltage boost function of a conventional DC/DC converter can be replaced by applying more cells in series. The phase *A* branch is designed to send the SOC signal. Besides, the *B*-phase and *C*-phase branches do not transmit signals under normal operation and future research will employ them to transmit motor speed control signals, vehicle light control signals and other signals. A PMSM is utilised as the inverter load in this model.

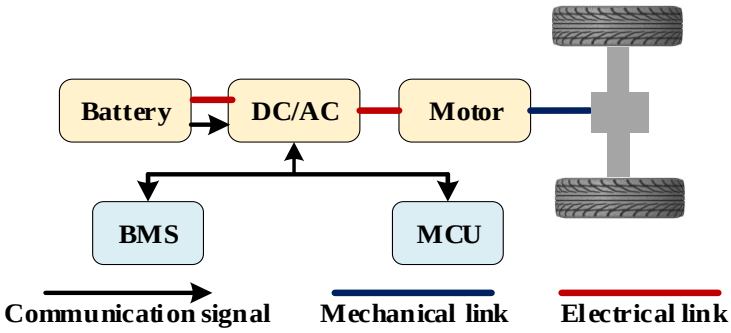

Figure. 5-2. The designed system structure of an EV with the IPST approach

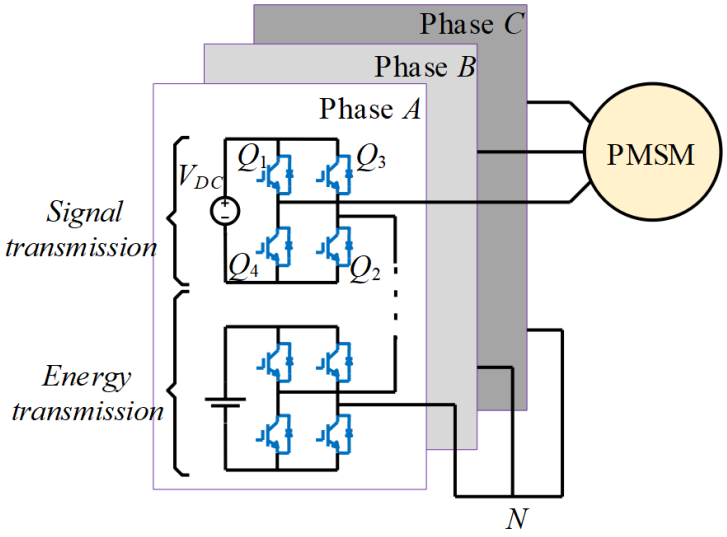

Figure. 5-3. Topology of the proposed IPST system for EVs

Because the proposed system employs SPWM approach to modulate output power for the PMSM, the three-phase reference sinusoidal waves can be expressed as

$$\begin{cases} P_a = M\sin(2\pi f) \\ P_b = M\sin(2\pi f - \frac{2}{3}\pi) \\ P_c = M\sin(2\pi f - \frac{4}{3}\pi) \end{cases} \quad (5-1)$$

The reference sinusoidal waves are employed for power modulation and P_a, P_b, and P_c from the equation are the reference wave in phase *A*, phase *B*, and phase *C* respectively. Besides, constant *M* and *f* are the amplitude and power frequency of the reference wave, respectively. The phase *B* and phase *C* reference waves lag the phase A reference wave by 2π/3 and 4π/3 radians respectively. Finally, the PMSM motor are finally powered by the modulated sine waves.

The block diagram in Fig. 5-4 presents the integrated power/signal transmission path in an intuitive method. The battery SOC signals are transmitted through the phase *A* current waveform. As phase *B* and phase *C* is not currently designed for signal transmission, an FSK modulated H-bridge cell is required to balance the phase voltage with the other two phases. Therefore, two random data strings are transmitted through phase *B* and phase *C* in this model and these data strings can be replaced with specific data in future studies.

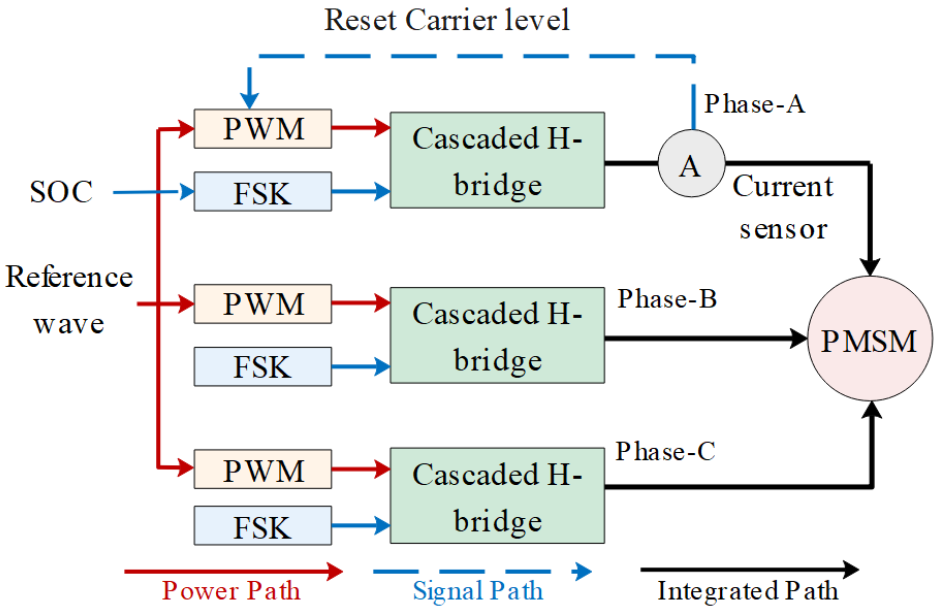

Figure. 5-4. Signal and power transmission path of the proposed EV powertrain

5.2.2 Battery Balance Discharging

The designed battery balancing algorithm is for the batteries within one phase and this section focuses on the batteries balancing in phase *A*. In the traditional SPWM method, the gating signal of a switch is created by comparing the reference wave with a triangular carrier. Since various carriers and the reference wave overlap at different points, each switch's duty cycle varies. For example, in a single period from 0 to *T* as exhibited in Fig. 5-5, a switch controlled by a 'Level 3' carrier has a lower duty cycle than a switch modulated by a 'Level 1' carrier ($t_1 < t_2$). In other words, the duty ratio of s_1 is less than that of s_2 in a switching period *T*. Because the input power is supplied by batteries, a switch with a low duty cycle consumes less energy than a switch with a high duty cycle. After a period of system operation, the remaining capacity of the battery becomes unbalanced. Balanced battery discharge can therefore be achieved by periodically rescheduling the carrier level during the PWM process.

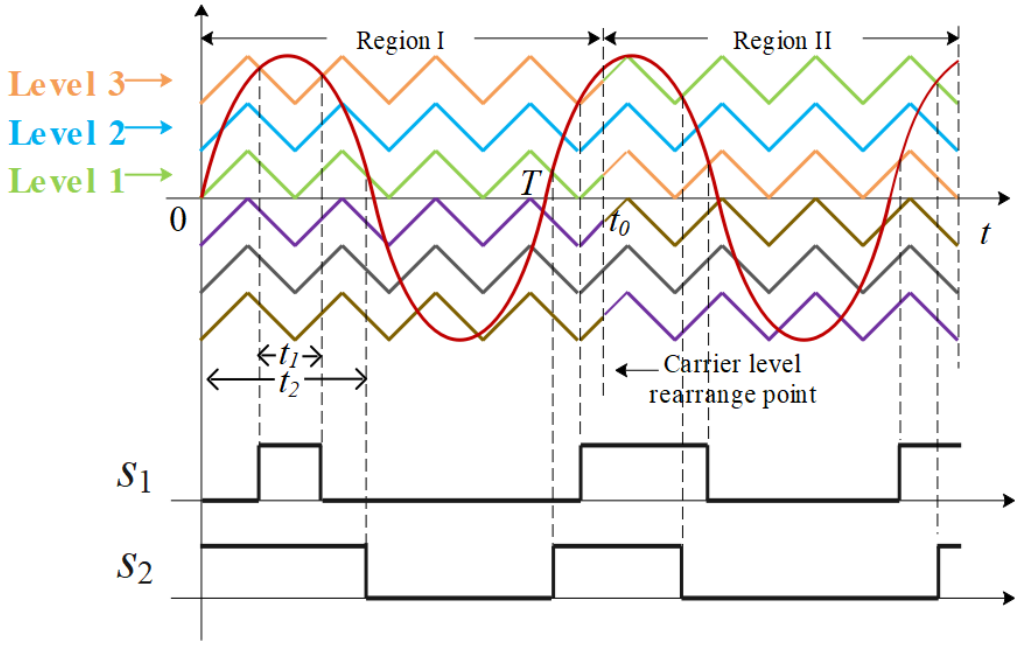

Figure. 5-5. Carrier level reset in the SPWM process

To achieve this goal, the battery balancing process can be summarised as demonstrated in Fig. 5-6. The SOC can be defined as the ratio of the remaining capacity of the battery to the current maximum available capacity. Firstly, the battery SOC values at the periodic sample points are aggregated into a data stream and then transferred using the FSK technique with a full-bridge converter through the Phase *A* current. After demodulating the signal from the phase current, the SOC values are recovered into different decimal numbers. Finally, the carrier levels are

reorganised based on the communicated SOC numerical values, as depicted in Fig. 5-5 at point t_0, with the carriers for greater battery charges restored to lower levels and those for smaller battery charges restored to higher levels. The carriers of the SPWM can be periodically reset according to the SOC numerical values and the batteries balance discharging function can be achieved using this method. The proposed method has the advantages of internal energy self-regulation and no additional electronics compared to conventional battery balancing methods such as the application of shunt inductors or capacitors [156], and vehicle-to-grid methods [157].

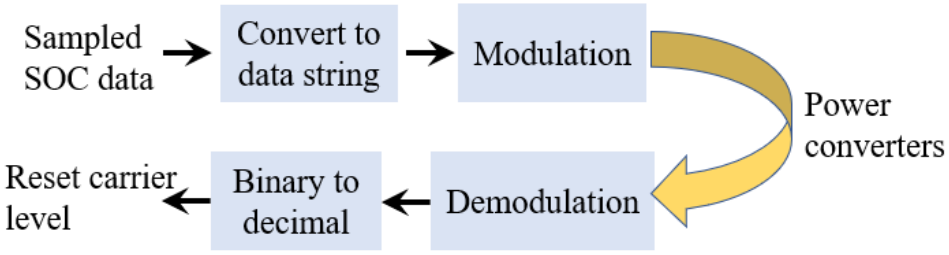

Figure. 5-6. The block diagram of battery balancing scheme

5.3 Simulation Results and Analysis

5.3.1 Feasibility Analysis of a Single-Phase Topology

The output waveforms of a single-phase cascaded full-bridge converter using the proposed IPST modulation schemes is exhibited in Fig. 5-7. In this simulation, four full-bridge converters are series connected with each cell contains a 30 V battery as power supply. The sinusoidal reference waveform has a frequency of 40 Hz, so the output current and voltage waveforms have the same power frequency of 40 Hz. The load impedance and inductance are set to 10Ω and 1mH respectively. Therefore, it can be observed from Fig. 5-7 that the maximum output voltage is approximately 120 V. Three full-bridge units employ a 10 kHz carrier for power modulation, and another unit uses 15 kHz and 20 kHz carriers to modulate the digits ‘1’ and ‘0’ respectively. The output current and voltage waveforms demonstrate the proposed method can be applied in a single-phase topology successfully.

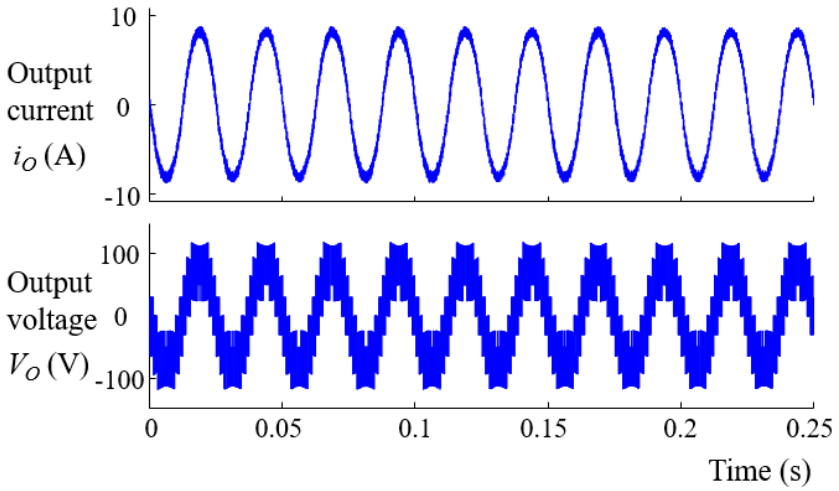

Figure. 5-7. Output current and voltage waveforms of a single-phase topology

The simulation results of signal transmission are presented in Fig. 5-8. The transmitted 6-bit signal is '101101' and the signal is demodulated from the output current waveform. In this simulation, a Gaussian bandpass filter of order of 80 with passband between 14.9 kHz and 15.1 kHz is applied to extract the 15 kHz carrier to further recover digital '1'. As the transmitted signal is recovered by resampling the threshold waveform at the initial data rate as the sampling frequency, the received signal is eventually delayed by one bit. The successfully implemented simulation results indicate that the proposed IPST method can be applied in a DC/AC converter for both signal and power transmission.

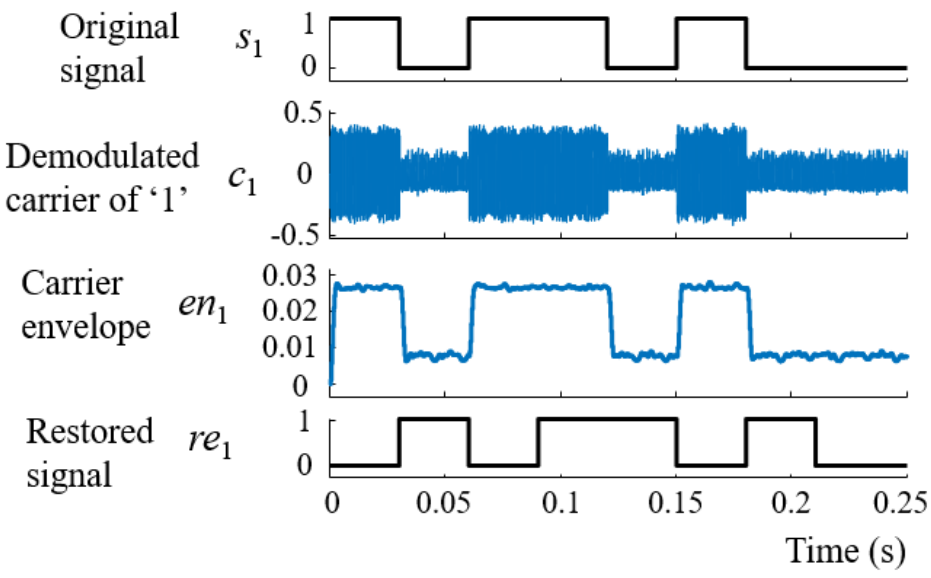

Figure. 5-8. The signal transmission results of a single-phase topology

5.3.2 Parameters of the BMS Simulation Model

The single-phase model is then extended to a three-phase structure for the transfer of battery charging information in the BMS. A simulation model is developed in MATLAB/Simulink based on the mechanisms presented in the previous section. Table 5-1 summarises the parameter values of the simulation model. Three 48 V batteries for power transmission and a 30 V DC voltage source for signal modulation are employed in each phase of the topology. As a result, the amplitude of the transmitted signal is neither too small to be recovered nor too large to have a significant effect on the output sine wave. Furthermore, as the system uses a carrier wave with a frequency distribution in the range of 2 to 10 kHz, the silicon IGBT devices can operate in this frequency range [158].

TABLE 5-1 Simulation Parameters of the Proposed Topology for EV

Parameter Name	Value
DC voltage source	30 V
Battery voltage	48 V
SPWM carrier frequency	2 kHz
SPWM referenced sine wave frequency	60Hz
Signal speed	240 bps
Carrier frequency of SOC signal	6 kHz for ‘1’ and 10 kHz for ‘0’

5.3.3 SOC Signals Transmission for Batteries Balancing

In this simulation, the SOC values of the three phase-*A* batteries are transferred by the phase current. Firstly, the three batteries’ initial SOC values are set to 100%, 40%, and 35%, respectively, resulting in the transmitted three frames being ‘01100100’, ‘00101000’, and ‘00100011’ in binary format. As displayed in Fig. 5-9, the three binary strings are then merged to generate a new code string s_{cb}. Because each battery’s SOC value is sampled every 0.1s, the produced code string’s period is likewise set to 0.1s to maintain these two times consistent. As a result, the system is managed to send 24 bits of data every 0.1 second at a signal rate of 240 bps. Nevertheless, since in practice the SOC of the battery does not alter much in a short period

of time, the SOC value is the same as the value of the first cycle in the subsequent sampling time.

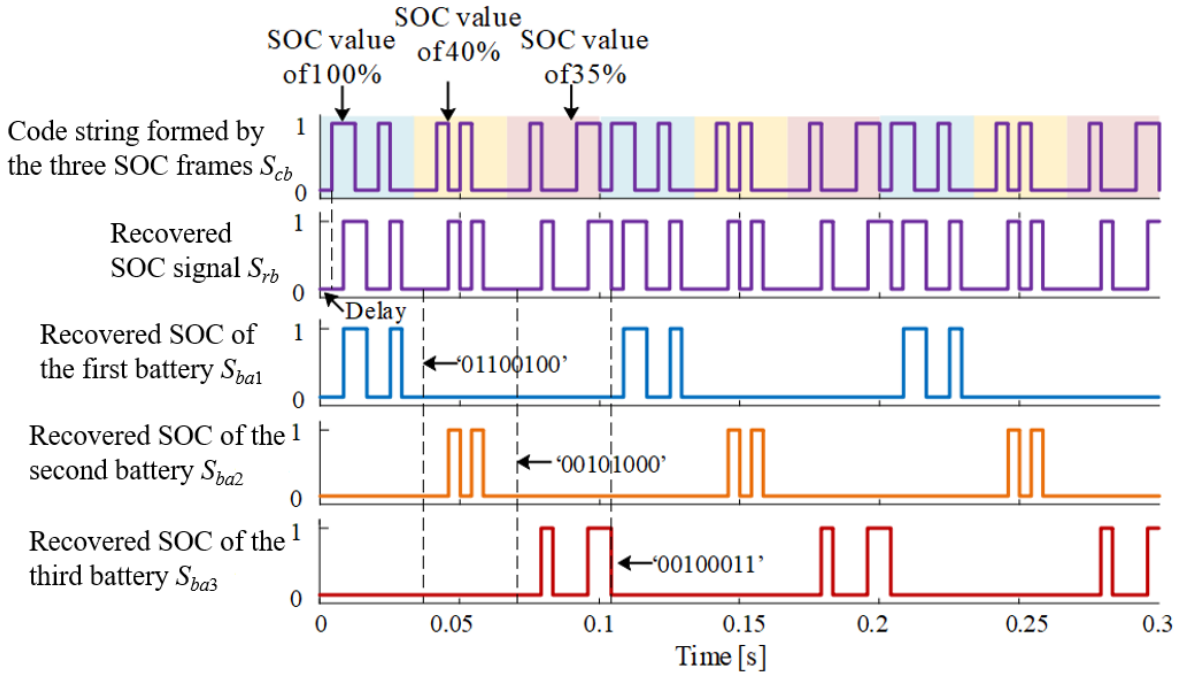

Figure. 5-9. The transmitted SOC signals

The recovered SOC signal s_{rb} in Fig. 5-9 is produced by demodulating the SOC signal from the phase current waveform. The filtering operation causes s_{rb} to delay the original sent signal s_{cb} by 1-bit time (0.1/24s). The separated three SOC values from the code string s_{rb} are displayed in Fig. 5-9 as s_{ba1}, s_{ba2}, and s_{ba3}.

After comparing the three SOC values, the carrier levels in the SPWM process are reordered for the upcoming cycle. The results of the carrier level rearranging procedure are exhibited in Fig. 5-10, where the carrier levels are reorganised at 0.4/3s. In particular, the initial carrier levels for H-bridge cells with SOC values of 100%, 40%, and 35% are set to level 3, level 1, and level 2, respectively, and they are moved to level 1, level 2, and level 3 based on the numerical sizes of the three SOC values. After the initial rearrangement point, the carrier levels are rearranged every 0.1s. Nevertheless, the carrier levels are not modified at the subsequent level reset point in Fig. 5-10, which is due to the batteries' SOC not varying much over a short period of time.

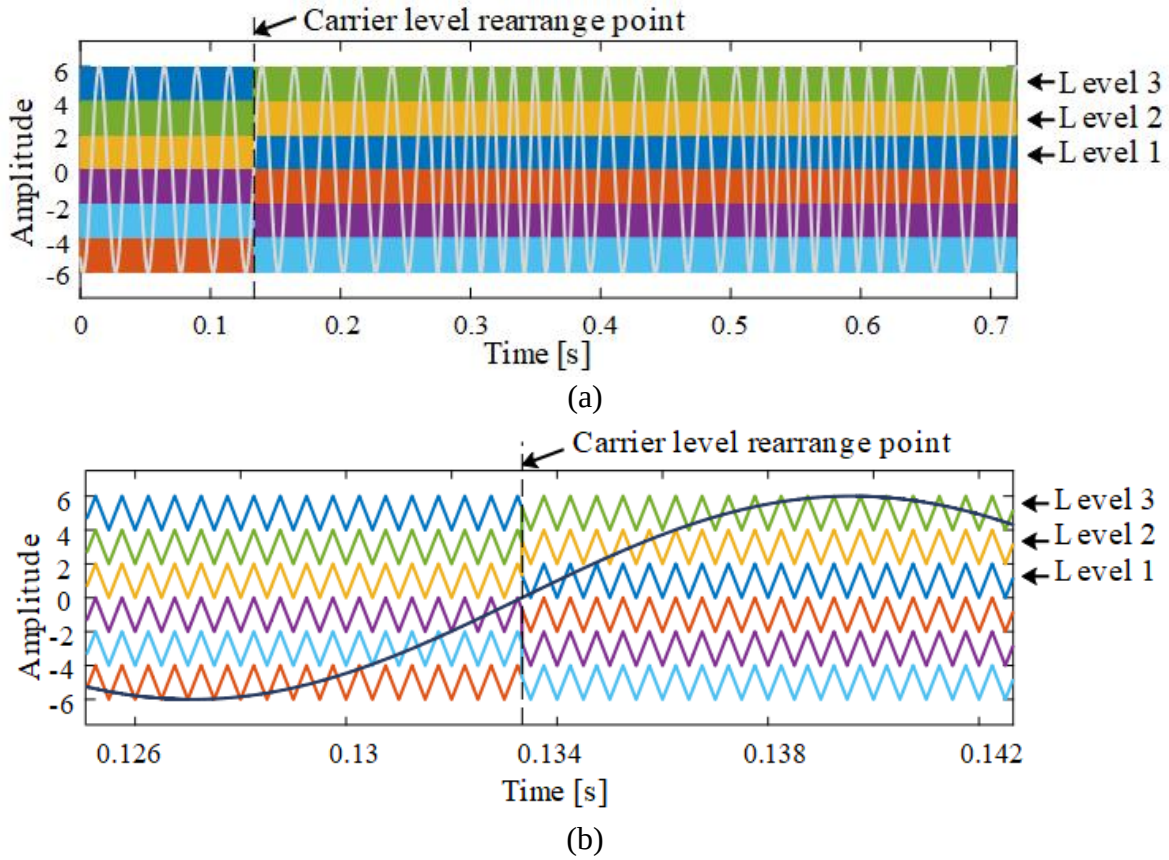

Figure. 5-10. The reset carriers and the reference sinusoidal wave used in the SPWM process, where (a) is the original curves, and (b) is the zoomed curves at the carrier level reset point

Fig. 5-11 presents the SOC curves for the three batteries used in phase *A*. The SOC of the first battery (Fig. 5-11(a)) decreases significantly at 0.4/3s after the transmitted signals successfully restored at receiver as it has the highest SOC value. On the contrary, the third battery has the smallest SOC value, and its rate of decline (Fig. 5-11(c)) becomes slowest at 0.4/3s. The simulation results demonstrate that this system successfully achieves battery balance discharging.

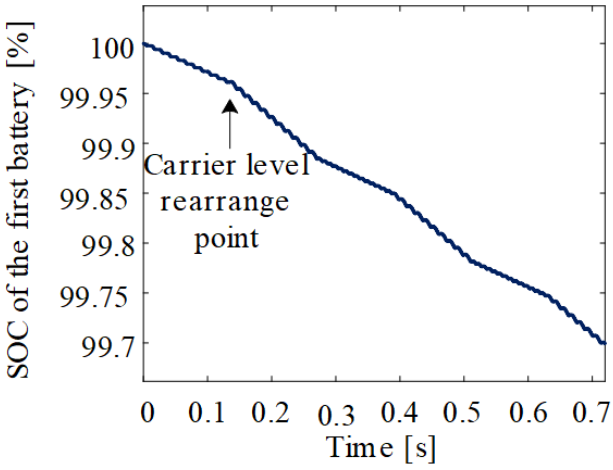

(a)

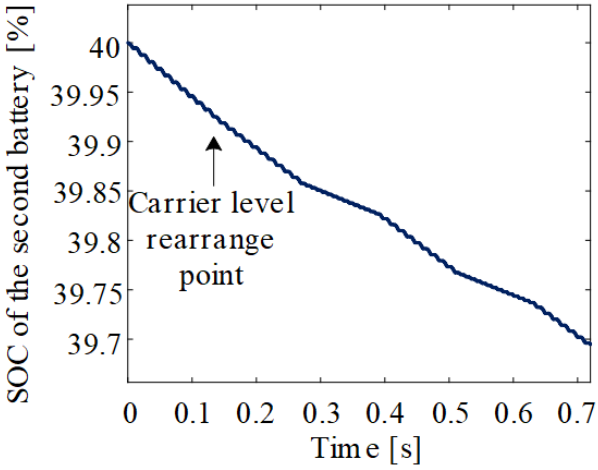

(b)

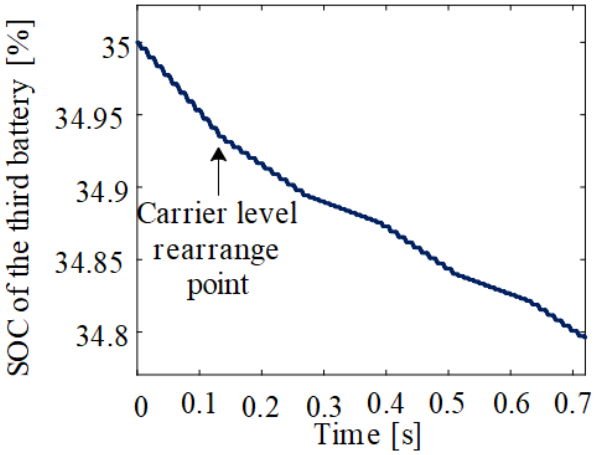

(c)

Figure. 5-11. The SOC curves of the three batteries, where (a), (b), and (c) represent the battery with the initial SOC of 100%, 40%, and 35% respectively

5.4 Summary

In this chapter, a three-phase multilevel inverter-based IPST system for EVs has been proposed. With the IPST technology utilised in the field of EVs, the cost and size of the EV control system can be greatly reduced.

In the proposed system, the SPWM approach is used for power modulation and FSK method is applied for signal transmission. In the designed system, the three batteries' SOC values are transmitted through the phase *A* current waveform in time order. By using envelope detection approach for demodulation, the successfully restored two signals are applied realise the battery balance discharging function. Simulation results indicate that the proposed method can transmit signals with data rate of 240 bps. The designed model only applies Phase *A* current waveform to transmit batteries' SOC signals and thus can further employs Phase *B* and phase *C* current waveforms for the transmission of other signals, such as automotive lighting signals and air conditioning control signals for EVs.

Chapter 6 Integrated Power/Signal Transmission in a Bidirectional Buck/Boost Converter-Based Intelligent Street Lighting System

6.1 Introduction

This chapter proposes an ISL topology based on buck-boost converters. The proposed model employs the IPST technique for two-way communication between the central controller and each streetlight. The sent data is multiplexed with the current waveform and transferred simultaneously with the power conversion since the communication signal is modulated by the buck/boost converter's switching frequency. The following are some of the advantages of the proposed model. Firstly, the traditional buck/boost converter topology is slightly modified to fit the streetlight application, making the model simple to install. Secondly, the proposed approach inherits the advantages of conventional PLC communication in that no additional communication cables are required, while eliminating the need for signal coupling devices for PLC communication. Finally, in contrast to previous research on the same application in [81] and [82], the suggested model employs an additional 'request to send (RTS)/confirm to send (CTS)' method to decrease frame conflicts, allowing for successful remote streetlight control in the ISL system.

The rest of this chapter is exhibited as follows. The system structure of the proposed ISL model is discussed in Section 6.2. The charging and discharging mechanisms of the proposed topology are presented in Section 6.3. Next, Section 6.4 explains the methodology to avoid frame collision. The simulation results and the performance of the proposed system are assessed in Section 6.5. Finally, a brief conclusion is drawn in Section 6.6.

6.2 System Configuration

Fig. 6-1 illustrates the proposed system model. Each streetlight has a large-capacity battery that stores energy from solar panels during the daytime and then uses that energy to power the LEDs at night. Solar panels are installed on the bus station platform's ceiling to collect solar energy

without taking up too much platform area. Furthermore, each streetlight is equipped with a sensor for monitoring road conditions. Additionally, each streetlight has an electronic screen that cycles through commercials, news, and traffic information. Moreover, passengers can utilise the excess electricity provided by the solar panels to charge their electrical equipment [159], [160], [161]. In the event of a large-scale blackout in a city, the battery in each streetlight can also be utilised to charge EVs [162], [163], [164]. If each LED streetlight has a power of 100 W, the distance between two streetlights is 40 m, and the average distance between two platforms is 800 m, then 20 LED streetlights are required between two platforms and the solar panel should at least have 2 kW output power. If each streetlight is powered by a 1.5 m^2, 300 Wp solar panel, approximately 7 to 8 panels are required, covering an area of 10.5 to 12 m^2. Consequently, solar panels can be installed on top of a bus stop.

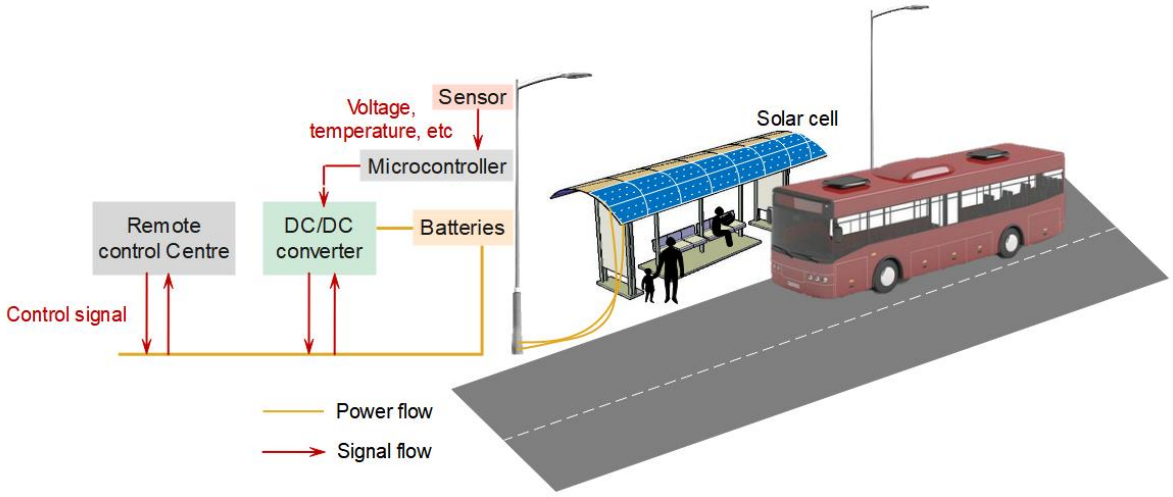

Figure. 6-1. Signal and energy flow structure of the proposed ISL system

Streetlight control signals and LED status data are sent through converters between the control centre and the streetlights for communication purposes. LED status data such as voltage, current, and temperature, are monitored first by appropriate sensors. Then, these data are modulated by the fast-switching switches of a DC/DC converter with the FSK approach by microcontrollers. Next, the data can be retrieved, demodulated, and recovered from the current waveform at the control centre after being transmitted through the DC bus. The same modulation and demodulation approach can be used for the LEDs' operational commands transmission from the control centre. The remote-control centre can quickly update the operating condition of the LED lights and alter the lighting plan based on the battery's remaining power using this two-way communication method.

The proposed buck/boost converter architecture for the ISL application is shown in Fig. 6-2. A battery serves as the DC power source for signal production at the master node of remote-control centre. When battery is charging, the topology will act as a buck converter. Besides, when battery is discharging, the topology will act as a boost converter. Furthermore, each LED branch has a thermistor R_T for LED overcurrent prevention.

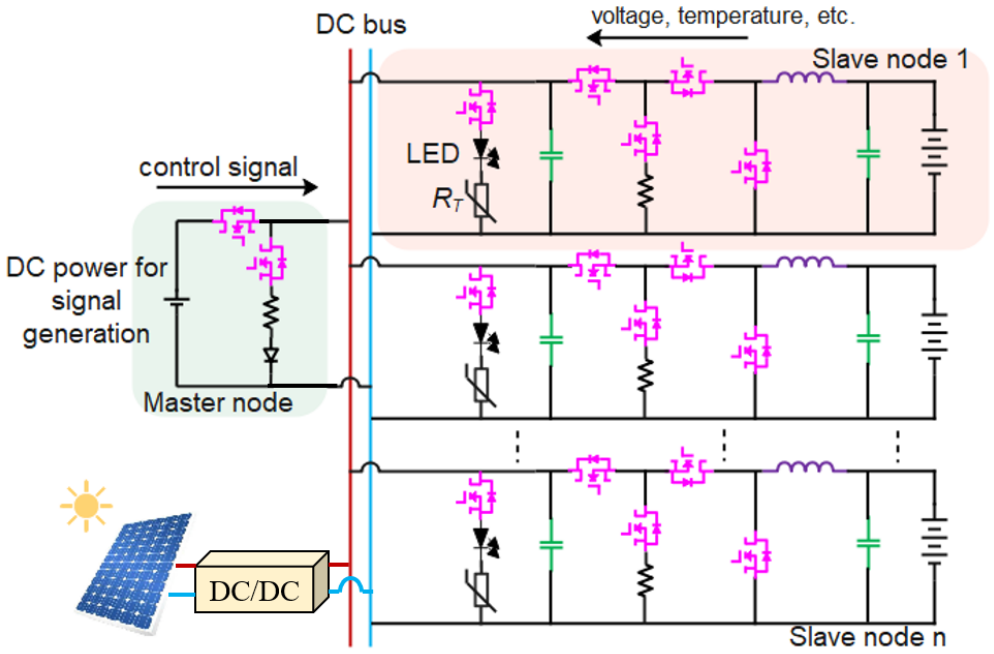

Figure. 6-2. The proposed buck/boost converter topology for the ISL system

6.3 Operation Principle

6.3.1 Charging Mode

When operates in charging mode, the equivalent circuit of the proposed converter is presented in Fig. 6-3. This figure shows one module as an example since different slave modules are charged with the same mechanism. The proposed method employs PWM approach to control switch S_1. The typical waveforms are demonstrated in Fig. 6-4, where v_{gs1}, i_L, i_{S1} and i_{S4} represent the gate signal of switch S_1, the current that flows through inductor L, the current that flows through switch S_1, and the current that flows through switch S_4, respectively.

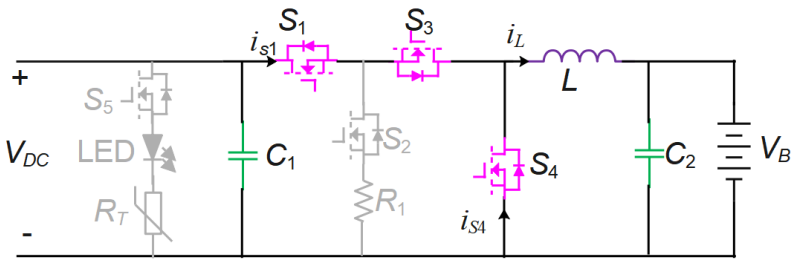

Figure. 6-3. Equivalent circuit of the proposed converter in battery charging mode

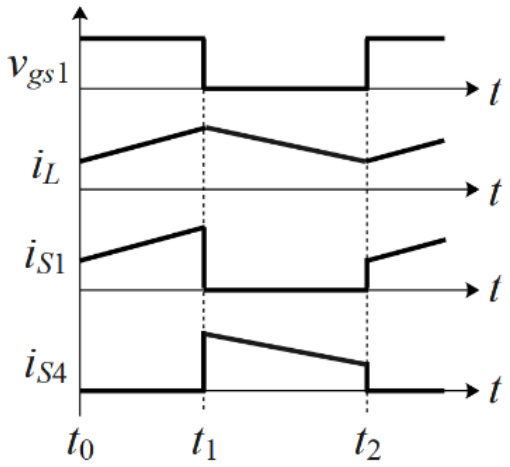

Figure. 6-4. Typical waveforms of the proposed topology in charging mode

The stages of the proposed circuit in continuous conduction mode (CCM) are outlined below, assuming that all components are ideal.

1) *Stage* 1 [t_0−t_1]: Switch S_1 is turned on, the MOSFETs of S_3 and S_4 are off. The power from the DC bus V_{DC} is conducted to inductor L, battery V_B, and capacitors C_1 and C_2. The current flow direction is displayed in Fig. 6-5(a).

2) *Stage* 2 [t_1−t_2]: Switches S_1, S_3 and S_4 are turned off. The energy stored in inductor L is conducted to battery V_B and capacitor C_2. The current flow direction is exhibited in Fig. 6-5(b).

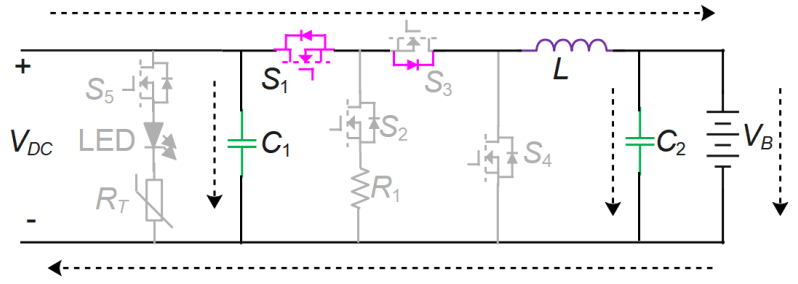

(a)

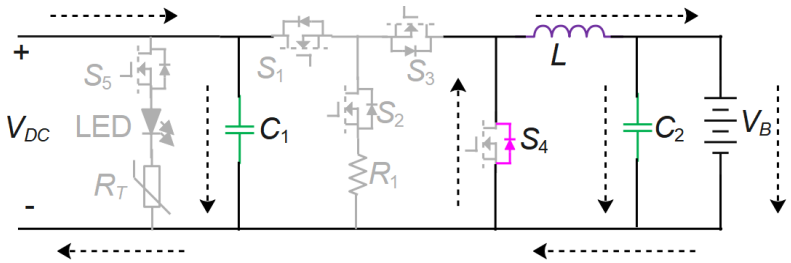

(b)

Figure. 6-5. The current direction (a) [t_0−t_1] and (b) [t_1−t_2] of the proposed converter in charging mode

As the initial value of the inductor current is equal to its final value in a switching period of steady state, the voltage gain G_c can be obtained from

$$G_c = \frac{V_B}{V_{DC}} = D \qquad (6-1)$$

where D is the duty ratio of the switch S_1. The minimum inductor current I_{Lmin} can be derived from

$$I_{Lmin} = I_o - \frac{V_B}{2L} \cdot (1-D) \cdot T_s \qquad (6-2)$$

where I_o is the output current, and T_s is the switching period. As the minimum inductor current is zero at the boundary condition, the value of inductor L can be calculated as

$$L = \frac{(1-D)}{2f_s} \cdot R_B \qquad (6-3)$$

where R_B is the equivalent resistance on the battery side, and f_s is the switching frequency. To guarantee the topology operates in CCM mode, the designed inductor is larger than this boundary value.

6.3.2 Discharging Mode

When the proposed topology operates in discharging mode, its equivalent circuit is exhibited in Fig. 6-6. Switch S_5 is turned on, and the PWM method is utilised to control switches S_3 and S_4 during the battery discharging process. The typical waveforms are demonstrated in Fig. 6-7, where v_{gs3}, v_{gs4}, i_L, i_{S3}, and i_{S4} respectively refer to the gate signal of switch S_3, the gate signal

of switch S_4, the current that flows through inductor L, the current that flows through switch S_3, and the current that flows through switch S_4.

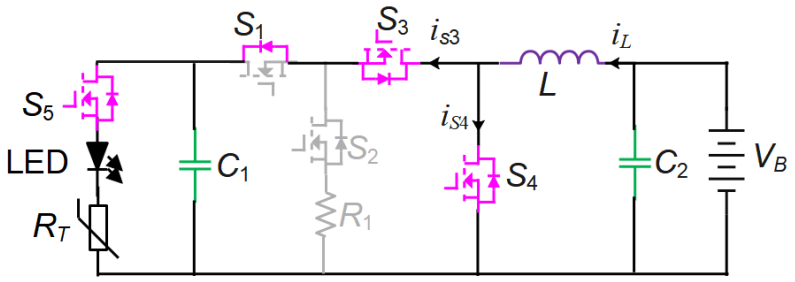

Figure. 6-6. Equivalent circuit of the designed converter in discharging mode

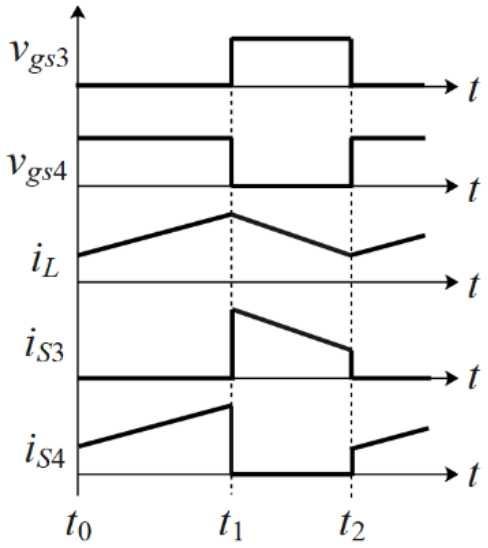

Figure. 6-7. Typical waveforms of the designed converter in discharging mode

The stages of the designed converter during the discharging process in CCM mode are analysed below.

1) *Stage* 1 [t_0−t_1]: Switch S_4 is turned on, and switches S_1 and S_3 are turned off. Inductor L is charged by battery V_B, and the energy stored in capacitor C_1 is used to power the LED. The current flow direction is shown in Fig. 6-8(a).

2) *Stage* 2 [t_1−t_2]: Switch S_4 is turned off, and switch S_3 is turned on. The energy stored in inductor L and battery V_B are discharged to the LED and capacitor C_1. The current flow direction is displayed in Fig. 6-8(b).

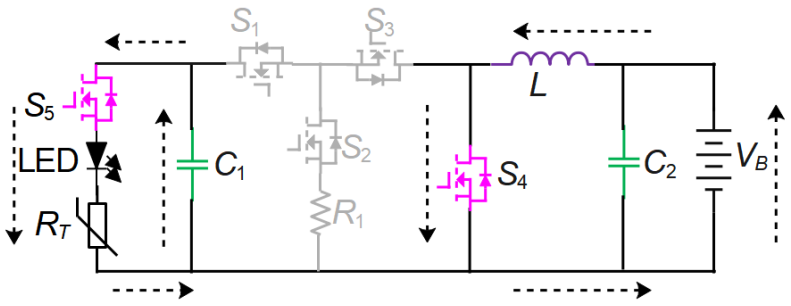

(a)

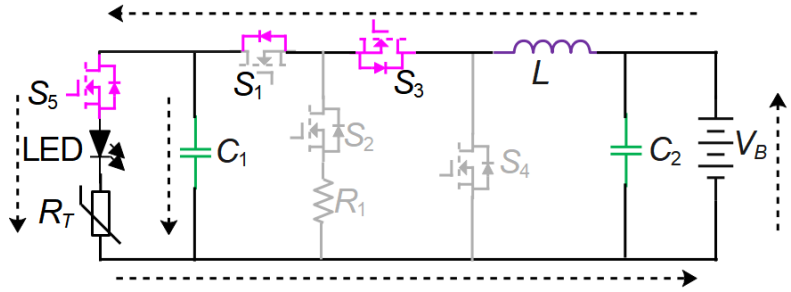

(b)

Figure. 6-8. The current direction (a) [t_0−t_1] and (b) [t_1−t_2] of the designed converter in discharging mode

As the initial value of the inductor current is equal to its final value in a switching period of steady state, the voltage gain G_d can be obtained from

$$G_d = \frac{V_o}{V_B} = \frac{1}{1-D} \qquad (6-4)$$

where V_o is the output voltage. The inductor boundary current I_{LB} is calculated by

$$I_{LB} = \frac{1}{2} \cdot \frac{V_B}{L} \cdot DT_s = \frac{V_B}{2Lf_s} \cdot D \qquad (6-5)$$

Because the output current I_o and the inductor current are the same when switch S_4 is turned off, the output boundary current I_{oB} can be derived from

$$I_{oB} = I_{LB} \cdot (1-D) = \frac{V_o}{2Lf_s} \cdot D(1-D)^2 \qquad (6-6)$$

Therefore, the minimum value of inductor L can be obtained from

$$L_{min} = \frac{RD(1-D)^2}{2f_s} \qquad (6-7)$$

where R is the equivalent resistance on the LED side. An appropriate inductor value for the proposed model can be decided after comparing the boundary value of the inductor in the charging and discharging modes. In other words, the determined inductance is larger than the maximum inductance boundary value calculated in charging and discharging modes.

6.4 Signal Transmission Mechanisms

The developed system can transmit two types of signals. During normal operation, the remote-control centre will send lighting commands to each slave node and the slave nodes will collect and transmit each LED's status data to the control centre in time order. Besides, the emergency signals will be transmitted to the control centre when bulb failure occurs. Since each time only one signal is transmitted with power conversion process, there is no congestion in the proposed system.

6.4.1 Bidirectional Communication

The proposed system uses FSK method for signal modulation and employs envelope detection approach for signal demodulation. Fig. 6-9 depicts the equivalent circuit of the designed converter when the master node sends control signals to a slave node. The circuit structure is like the charging mode topology described in Section 6.3, and both topologies can be considered buck converters. The distinction is that when the master node transmits signals, switch S_6 is used for signal modulation, switch S_1 is used to lead the signal to the slave node, and capacitor C_1 is engaged in the discharging route of inductor L.

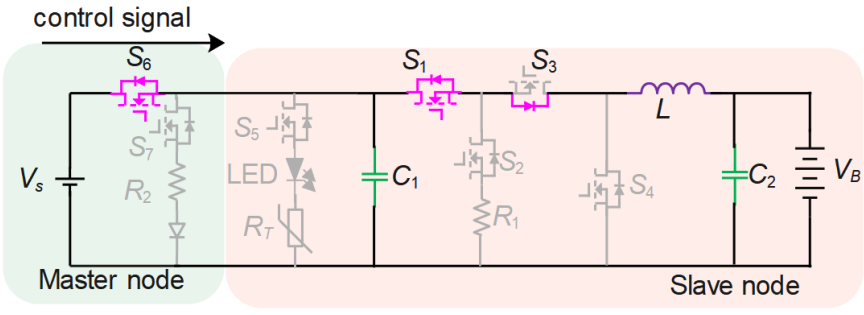

Figure. 6-9. Equivalent topology when the master node transmits signals

When a slave node transmits LED status data to the master node, the equivalent circuit of the proposed topology is shown in Fig. 6-10. This architecture is similar to the one described in

Section 6.3 for discharging mode, which uses switches S_3 and S_4 for signal modulation. In addition, switch S_7 is activated to direct the signal to the master node. The topology used for transmitting LED status data can be considered as a boost converter.

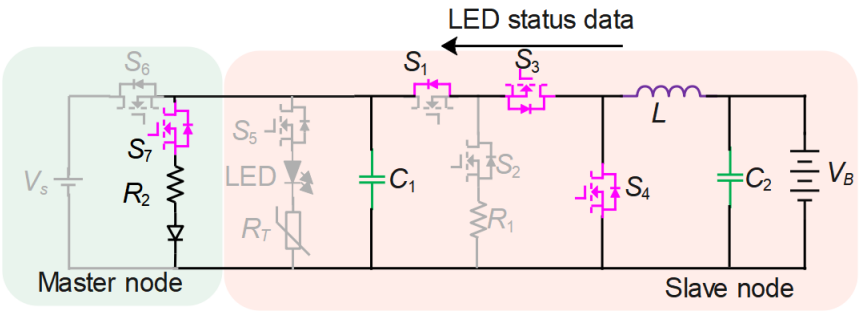

Figure. 6-10. Equivalent topology when the slave node transmits signals

Table 6-1 shows the structure of the data frame. To synchronise the transmitter and receiver, an 8-bit preamble is provided at the start of each frame. Each LED has a unique ID number that is used to identify the information's source/destination address. At the end of each data string, check codes are inserted to examine if the data is damaged or not during transmission. Finally, to indicate frame termination, an 8-bit end code is attached to the end of each frame. Each frame in this example involves data/commands for a single LED, and the data/commands for numerous LEDs are supplied frame by frame according to the node ID sequence.

TABLE 6-1 Structure of a Single Data Frame

Code Type	Preamble	Node ID	Data	Check Code	Ending Character
Length (bits)	8	8	0-64	8	8

6.4.2 Emergency Data Transmission

Despite the system can send LED status data on a regular basis, emergency communication between the staff at the remote-control centre and each LED light is required to deal with crises such as bulb failure. Fig. 6-11 depicts the proposed system's emergency communication approach.

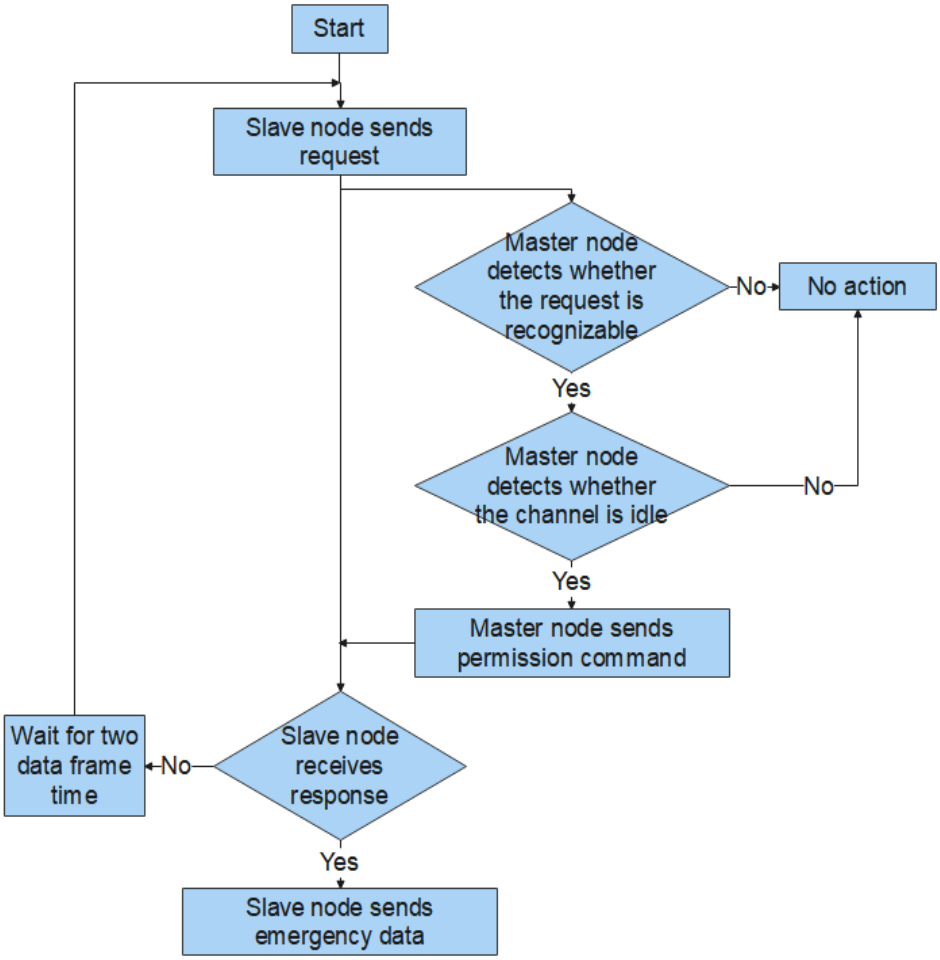

Figure. 6-11. Block diagram of the emergency data transmission approach

Firstly, a slave node transmits a frame of the 'RTS' signal to the master node, informing the master node of the following data transmission action. Secondly, the master node assesses if the communication channel is idle after receiving the 'RTS' signal. Because the proposed converter operates at the carrier frequency of digital '0' under normal conditions, the master node will assume the channel is busy and will not reply if digital '1' is demodulated from the following data frame. Otherwise, the master node will assume the channel is idle and send a 'CTS' signal to the slave node to confirm the request. Finally, the slave node will transmit the emergency data if it receives the 'CTS' signal within two cycles of the data frame. Otherwise, it will wait for a period T_p to resend the 'RTS' signal.

$$T_p = T_s \cdot N, (N \in [0,1,2,\dots,n]) \qquad (6-8)$$

In this equation, T_s is the time spent transmitting a data frame, n is the number of slave nodes, and N is the random integer used to delay the 'RTS' signal's transmission time. The carrier frequencies of 'RTS' and 'CTS' signals are different from that of the data frames. The frame

structure of the ‘RTS’ and ‘CTS’ signals is shown in Table 6-2. Because ‘RTS’ and ‘CTS’ have short frame length, the overall transmission overhead will not be much increased. Furthermore, because the ‘RTS’ signals are modulated by two carriers with the same frequencies when numerous slave nodes transmit requests at the same time, it is possible that the node ID demodulated at the master node does not match the real node address. In this situation, the master node does not respond the request. This approach therefore ensures that when one node transmits data, other nodes will not occupy the channel.

TABLE 6-2 Structure of an RTS/CTS Frame

Code Type	Preamble	Node ID	Check Code	Ending Character
Length (bits)	2	8	2	2

To guarantee that the sent ‘CTS’ signal is received at the slave node, the voltage source value V_s at the master node is designed to be larger than the battery voltage V_B. Fig. 6-12 depicts the equivalent circuit for this circumstance. The master node is delivering a ‘CTS’ signal to slave node 1 in this diagram. Slave node 1 is charging while slave node 2 is discharging. The energy supply at the master node is used to power the LED lights. During the interval when switch S_4 is turned off, switches S_2 and S_3 are switched on to release the charge contained in inductor L.

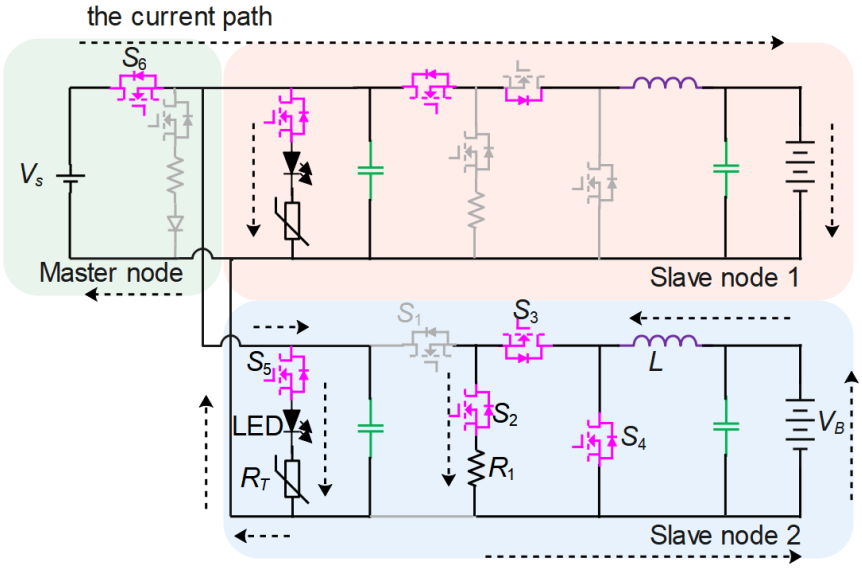

Figure. 6-12. The equivalent circuit when the master node transmits a ‘CTS’ signal to slave node 1

6.5 Results and Analysis

6.5.1 Simulation Results

To evaluate the viability of the proposed system, a simulation model is developed in MATLAB/Simulink. The system characteristics employed in the simulation model are listed in Table 6-3, with switching frequencies of f_1 equal to 30 kHz, f_2 equal to 20 kHz, and f_3 equal to 50 kHz. In the simulation model, the data rate is 2 kbps. Furthermore, the thermistor R_T has a resistance of 10 Ω under normal conditions. Fig. 6-13 and 6-14 show some typical simulation waveforms of a slave node working in charging and discharging modes, respectively. i_{S1}, i_{S3}, and i_{S4} reflect the currents flowing through the switches S_1, S_3, and S_4, respectively. Furthermore, i_L, V_B, and V_O stand for inductor current, battery voltage, and LED output voltage, respectively. The simulation results show that the proposed architecture performs in the CCM mode as anticipated.

TABLE 6-3 Simulation Parameters of the Proposed ISL System

Parameter Name	Value
V_{DC} (DC bus voltage)	20 V
V_B (battery voltage)	12 V
V_O (output voltage of discharging mode)	15 V
V_S (source voltage at the master node)	20 V
L (inductor at slave node)	3 mH
C_1, C_2 (capacitor at slave node)	100 μF
R_T (thermistor)	10 Ω
P_{out1} (output power of a slave node at charging mode)	18 W
P_{out2} (output power of a slave node at discharging mode)	15 W
f_1 (frequency for modulating ‘1’ of a data frame)	30 kHz
f_2 (frequency for modulating ‘0’ or normal switching frequency)	20 kHz
f_3 (frequency for modulating ‘1’ of an RTS/CTS frame)	50 kHz
f_{sample} (sampling frequency of the band-pass filter)	120 kHz

T_U (one-bit data time)	500 μs

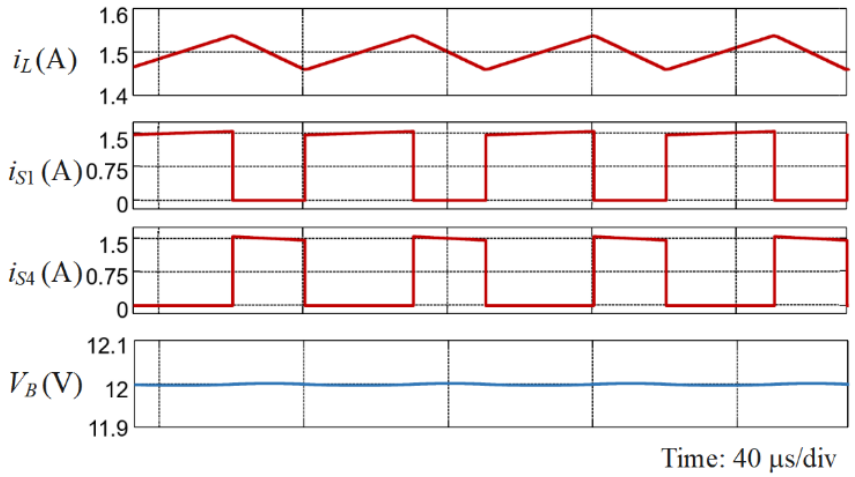

Figure. 6-13. The simulation results of the designed converter operate in charging mode

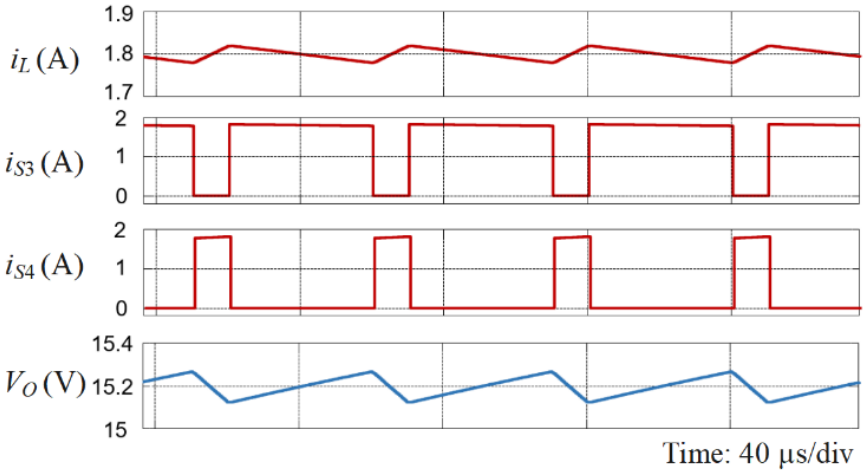

Figure. 6-14. The simulation results of the designed converter operate in discharging mode

The key waveforms of the master node delivering signals to slave nodes and slave nodes sending signals to the master node are shown in Fig. 6-15 and Fig. 6-16, respectively. In the simulation model, three slave nodes are connected to the master node, and these slave nodes send data in order depending on their ID numbers. When one slave node sends data, the other two slave nodes continue to operate normally and power the LED. Fig. 6-15 shows the original signal, demodulated carrier of digital '1', extraction amplitude of the first-order harmonic, and restored signal, which are represented by d_1, d_2, d_3 and d_4 respectively. Data frame from slave node 1, data frame from slave node 2, data frame from slave node 3, demodulated carrier of

digital '1' and restored signal at the master node are depicted as d_5, d_6, d_7, d_8 and d_9 respectively in Fig. 6-16.

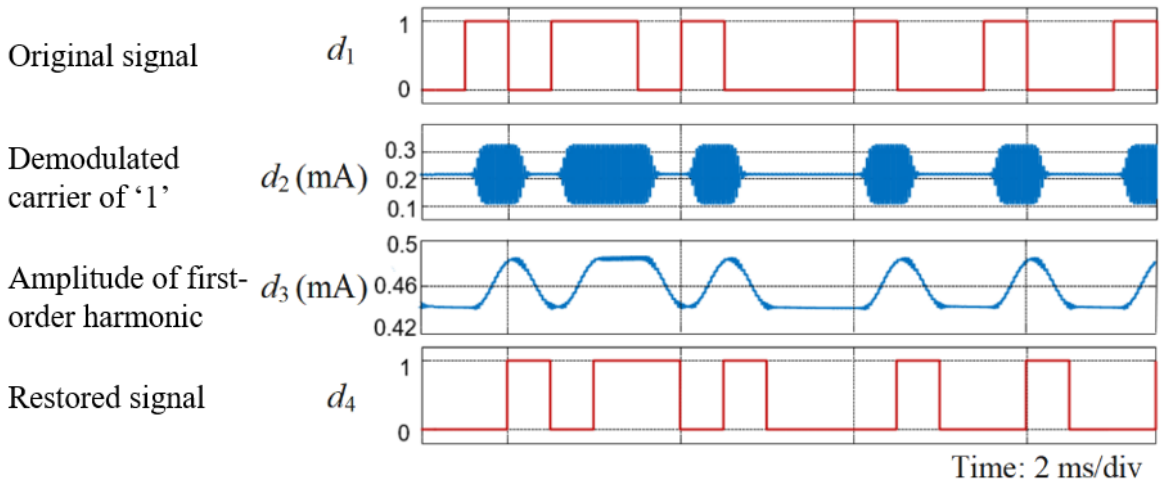

Figure. 6-15. Typical waveforms when the master node sends a signal

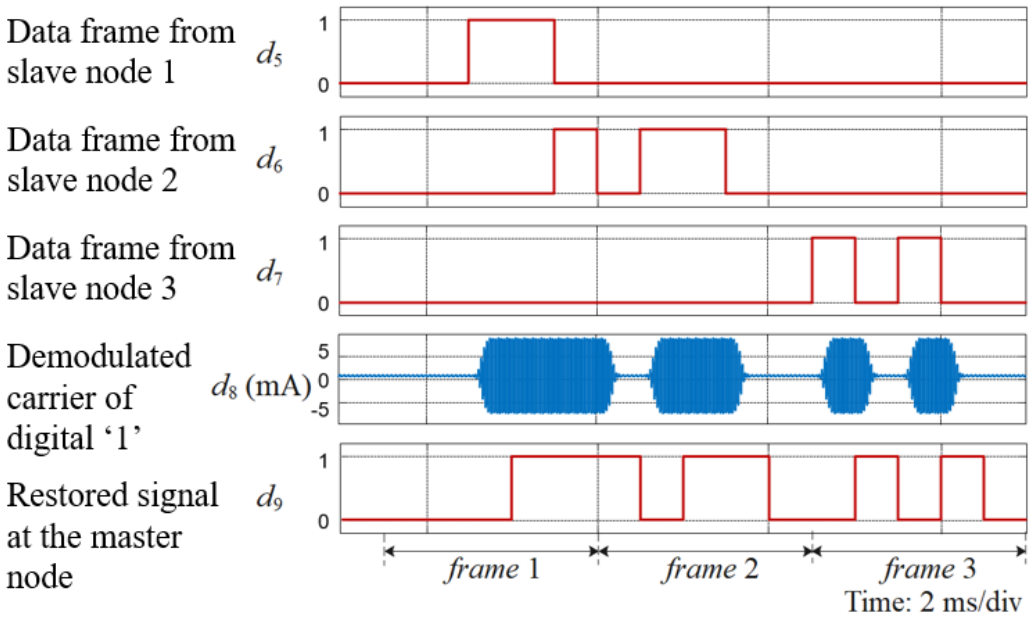

Figure. 6-16. Typical waveforms when the slave nodes transmit signals

When a slave node receives a 'CTS' signal from the master node, the outcome is shown in Fig. 6-17, where d_{10}, d_{11}, d_{12}, and d_{13} represent the original signal, demodulated carrier of digital '1', extraction amplitude of the first-order harmonic, and restored signal, respectively. There is a one-bit delay at the receiver, which is mostly caused by the filtering process and resampling at the original signal rate. The properly recovered signal demonstrates that the IPST approach

can be used in the ISL system. Furthermore, the switching ripple of the converters can be used to convey 'RTS/CTS' signals to reduce data frame collisions.

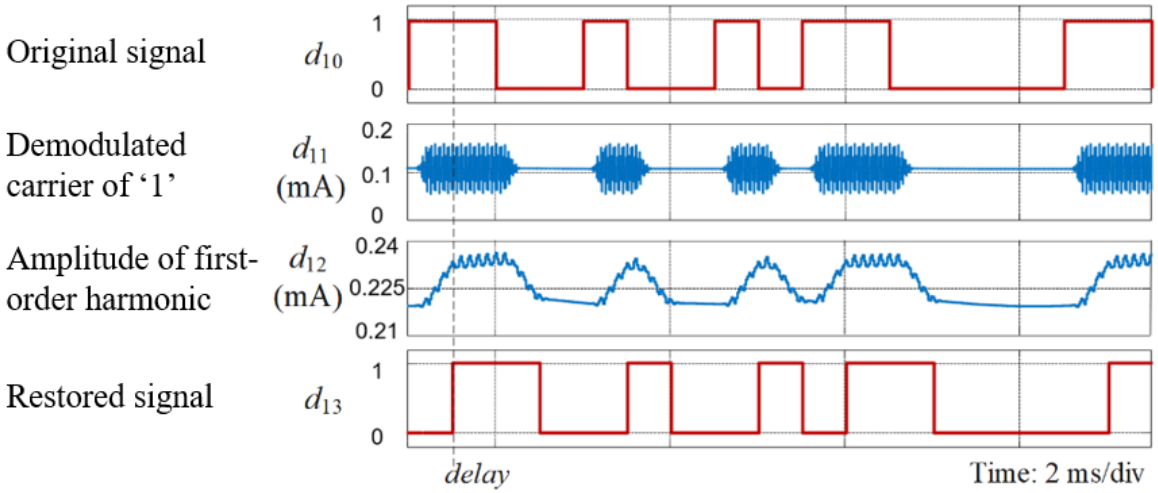

Figure. 6-17. Typical waveforms when the master node transmits a 'CTS' signal

6.5.2 Noise Immunity Analysis

In engineering applications, noise immunity is generally measured by the signal-to-noise ratio (SNR). The higher the signal-to-noise ratio of a device, the less noise it generates. In general, a higher SNR means less noise is mixed into the signal and the BER of the received signal is lower. The noise immunity of the designed model is tested by adding white Gaussian noise to the power line as an environmental interference. The BER is computed by bit-by-bit comparison of sent and received data. By gradually increasing the noise level, the connection between BER and the SNR is obtained. Fig. 6-18 depicts the simulation outcome. The results show that when the SNR increases, the BER drops and thus the proposed IPST approach has acceptable anti-noise capability. When the SNR is more than 10 dB and the data rate is 2 kbit/s, the BER will be less than 10^{-3}.

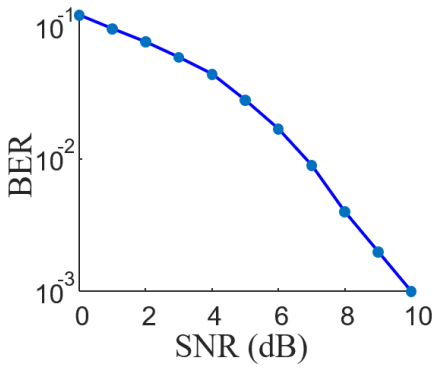

Figure. 6-18. The relationship between BER and SNR of the proposed ISL system

6.6 Summary

A bidirectional buck/boost converter architecture for achieving two-way communication in an ISL system is discussed in this Chapter. In this system, the PWM method is used to modulate the converted energy, and the FSK approach is employed to modulate the transmitted signal. During the daytime, each streetlight's battery is charged, while the charged battery is utilised to power the LEDs at night. The remote-control centre can send LED control signals and receives LED status data with the IPST approach. The cost of system wiring can be decreased by integrating the transmission signals into the current waveform by modulating the switching frequency. Furthermore, the utilised 'RTS/CTS' communication strategy can significantly decrease emergency signal conflict. The practicality of this transmission approach in the ISL system is demonstrated by the simulation model developed in MATLAB/Simulink. In addition, the noise immunity is examined at a data rate of 2 kbit/s. A BER of 10^{-3} can be attained if the SNR is larger than 10 dB.

Chapter 7 Conclusions and Future Works

7.1 Conclusions

Energy transmission and information transmission have in common the transfer of substances from one place to another, but the difference lies in the type of substance being transferred. If the communication signal is transmitted in the form of an electrical energy, it is possible to combine electrical energy and signal together. Based on this hypothesis, this study modulates the signal through the switches of the power electronics converter, thus achieving a complex modulation of power and signal in SESs. By utilising the proposed Integrated power/signal transmission method, the cost on communication cables can be saved and the system wiring can be simplified. The major work and achievements of this study are concluded as below:

Chapter 2 reviews the standards and applications of various communication technologies. Wireless networks have the merits of low maintenance cost, mobility, and ease of installation. However, interference and data security are the main drawbacks of wireless communication. Moreover, wired networks have the benefits of high bandwidth and good data security, but have limited mobility. In addition, Chapter 2 in-depth reviews the relevant studies of IPST transmission strategy. This method can greatly reduce cost and system size by using power lines for data transmission and has a good level of data security because the transmitted data can hardly be hijacked directly from the power lines. Nevertheless, the data transmission rate of this method is low, and the communication signal is subject to interference from other electronic devices connected to the same power line. A valuable topic that extends the IPST technology in AC converters is observed after investigating other studies. Moreover, researchers can acquire a thorough understanding of the merits and drawbacks of various communication approaches from this review.

In Chapter 3, the IPSK/FSK signal modulation approach is proposed to facilitate data rates by making full use of the carrier phase and frequency. Furthermore, the coherent demodulation and envelope detection method are studied. Additionally, the feasibility of these modulation and demodulation approaches is analysed through a simulation model of the Buck converter. The simulation results proves that the IPST approach can simultaneously transmit data and

energy. Furthermore, the IPST method has acceptable noise immunity compared to the PSK and QPSK methods applied in conventional communication systems.

In Chapter 4, a PPP-based TAB converter is exhibited for realising battery balancing and signal transmission functions. The energy flow direction in the three ports is controlled by the leading/lagging condition of the converter switches. With a simulation model implemented in MATLAB/Simulink, the feasibility of the IPST method in the proposed converter is verified. Furthermore, the direction of signal transmission is independent of the direction of power conversion, which means that any of the three ports can operate as either a transmitter or a receiver. The designed three-port topology can be extended to more than three ports in practice. Besides, the proposed PPP-based TAB converter can be employed in the energy management system of the microgrid energy router.

In Chapter 5, a three-phase multilevel inverter-based IPST system for EVs is proposed to reduce the cost and size of the EV control system. With a simulation model developed in MATLAB/Simulink, the results indicate that the proposed method can transmit signals with data rate of 240 bps. The phase *B* and phase *C* current waveforms of the designed model can be further developed for the transmission of other signals, such as automotive lighting signals and air conditioning control signals for EVs in future research.

In Chapter 6, a bidirectional buck/boost converter topology for realising two-way communication in an ISL system is discussed. With the designed simulation model in MATLAB/Simulink, the feasibility of this transmission approach is proved. Moreover, the noise immunity is tested at a data rate of 2 kbit/s. Specifically, the developed simulation model can achieve a BER of 10^{-3} with the SNR larger than 10 dB.

In summary, in terms of the aim about using power electronic converters for signals transmission in SESs, this research integrates both methodology investigation and simulation validation to systematic study of integrated power and signal modulation and demodulation methods. From this perspective, this study has achieved the following milestones:

1) The mechanisms of FSK/PWM, PSK/PWM, and IPSK/FSK approaches are demonstrated, and the data demodulation methods for coherent demodulation and envelope detection from current waveforms are illustrated.

2) The IPST technology is successfully extended to DC/AC converters. Besides, the circuit topologies for EV motor speed control, BMS battery balancing, and remote

streetlight control system are designed, which are significant for reducing the cost and size of communication systems.

3) By adjusting the noise intensity of the transmission environment of the simulation model, the proposed IPSK/FSK method is proven to have decent noise immunity.

7.2 Future Works

According to the above findings and in consideration of the constraints of the existing work, future study can be conducted in the following areas.

i. Further research is required into the relevant literature of BMS. Chapter 4 and 5 employ the IPST-based cascaded full bridge converter and TAB converter for BMS to realise integrated power/signal transmission. However, further analysis is required to compare the proposed structure with other related studies using different topologies, such as a common DC bus for capacitors. Moreover, the cell balancing efficiency of the series structure will be compared with the parallel structure to investigate a more suitable cell balancing topology for IPST function.

ii. Further improve communication speed and stability while ensuring signal integrity. This thesis focuses primarily on the analysis of the feasibility of FSK, PSK and FSK/PSK methods for data transmission in converter-based applications. However, their data speeds are relatively lower than those of wireless communication methods such as 5G and wired communication methods such as fibre optics to ensure data accuracy during power conversion. Therefore, other signal modulation strategies such as frequency hopping (FH), chirp modulation, and orthogonal frequency division multiplexing (OFDM) will be studied to promote the band utilisation rate and achieve higher data rates. Furthermore, the practical effects of these technologies will be evaluated in various applications and the respective merits and drawbacks will be summarised.

iii. Extend the IPST technology to other applications. This thesis employs the IPST method in areas such as motor speed control for EVs and battery balancing for BMS, where it still has many potential applications. Especially with the development of the IoT and microgrids, IPST technology can be applied to DC buildings, energy routers and

underground mines for the instantaneous transmission of power and signals. Moreover, this thesis has designed DC/DC and DC/AC converters for specific applications, and AC/AC and AC/DC converters suitable for IPST technology are still worth investigating.

iv. Experimental validation of the proposed method. Because of the Covid-19 pandemic, the proposed methods have only been theoretically analysed through simulations and have not been experimentally validated. The simulated background noise does not reflect the actual conditions of the application scenario and the choice of power electronic devices will also have an impact on the signal and power transmission efficiency. Therefore, further experiments are required to verify the feasibility of the proposed theory.

Appendices

1. Conference Certificate

IET The Institution of Engineering and Technology

Certificate of Attendance

This is to certify that

Yixuan Zhang

has attended

RPG Dublin Online

on

1 -2 March 2021

CPD
12 hours

Nigel Fine
IET Chief Executive and Secretary

Danielle George
IET President

2. Poster Competition Award

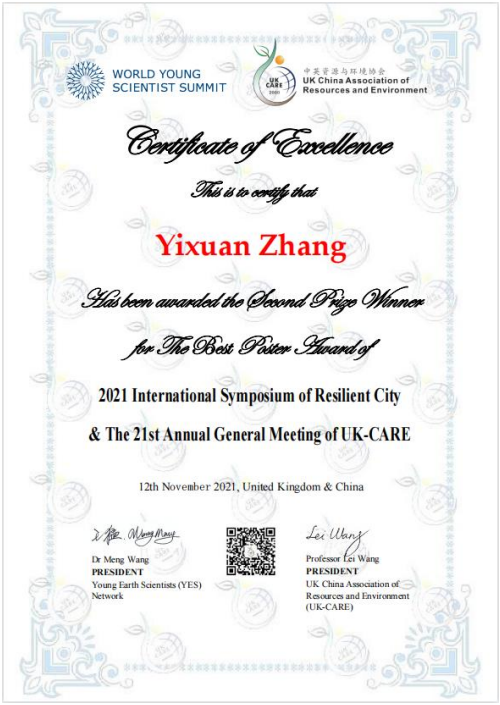

WORLD YOUNG SCIENTIST SUMMIT

UK China Association of Resources and Environment

Certificate of Excellence

This is to certify that

Yixuan Zhang

Has been awarded the Second Prize Winner

for The Best Poster Award of

2021 International Symposium of Resilient City

& The 21st Annual General Meeting of UK-CARE

12th November 2021, United Kingdom & China

Dr Meng Wang
PRESIDENT
Young Earth Scientists (YES) Network

Professor Lei Wang
PRESIDENT
UK China Association of Resources and Environment (UK-CARE)

Abbreviations

SCR	Silicon-controlled rectifier
IC	Integrated circuit
DC	Direct current
AC	Alternating current
IoT	Internet of Things
SES	Smart energy system
PLC	Power line communication
PoE	Power over Ethernet
IP	Internet protocol
VoIP	Voice over Internet protocol
IPST	Integrated power/signal transmission
BMS	Battery management system
EV	Electric vehicle
ISL	Intelligent street lighting
FSK	Frequency shift keying
PSK	Phase shift keying
IPSK/FSK	Integrated phase shift keying/frequency shift keying
BER	Bit error rate
PMSM	Permanent magnet synchronous motor
CAN	Controller area network
PPP	Partial power processing
TAB	Triple active bridge
SOC	State of charge
LED	Light-emitting diode
RTS	Request to send

CTS	Confirm to send
PV	Photovoltaic
5G	Fifth generation
MIMO	Multiple-input multiple-output
OFDM	Orthogonal frequency division multiplexing
EMI	Electromagnetic interference
RF	Radio frequency
WPAN	Wireless personal area network
HAN	Home area network
FH-SS	Hopping-spread spectrum
6LoWPAN	IPv6 over low-power wireless personal area network
IETF	Internet engineering task force
PAN	Personal area network
DSSS	Direct sequence spread spectrum
LoRa	Long range
CSS	Chirp spread spectrum (CSS)
LoRaWAN	Long range wide area network
MAC	Media access controller
SF	Spread factor
NR	New radio
4G	Fourth generation
WISDOM	Wireless system for dynamic operating mega communication
LDPC	Low-density parity checking
SS	Spread spectrum
FH	Frequency hopping
PSE	Power sourcing equipment
PD	Powered device
MCU	Microcontroller unit
AMP	Arbitration on message priority

CSMA/CD	Carrier sense multiple access with collision detection
PWM	Pulse width modulation
FPGA	Field-programmable gate array
DAB	Dual active bridge
DSP	Digital signal processor
DFT	Discrete Fourier transform
ASK	Amplitude shift keying
SDFT	Sliding discrete Fourier transform
DBPSK	Differential binary phase shift keying
QPSK	Quadrature phase shift keying
SNR	Signal-to-noise ratio
TCU	Transmission control unit
PPM	Phase perturbation modulation
ESS	Energy storage system
GSM	Global system for mobile communication
SMS	Short message service
CCM	Continuous conduction mode

References

[1] I. Batarseh and A. Harb, Power Electronics, Springer, 2003.

[2] R. Erickson, Fundamentals of Power Electronics, US: Springer, 2004.

[3] D. G. Holmes and T. A. Lipo, Pulse width modulation for power converters. principles and practice, John Wiley, 2003.

[4] B. K. Bose, "Power electronics-a technology review," *Proceedings of the IEEE,* vol. 80, no. 8, pp. 1303-1334, 1992.

[5] E. M. Rogers, Communication technology, Simon and Schuster, 1986.

[6] I. Glover and P. M. Grant, Digital communications, Pearson Education, 2010.

[7] E. Griffin, A first look at communication theory, McGraw-Hill, 2006.

[8] K. Miller, Communication theories, USA: Macgraw-Hill, 2005.

[9] B. Sklar and F. J. Harris, Digital communications: fundamentals and applications, NJ: Prentice-hall Englewood Cliffs, 1988.

[10] I. Union, "The internet of things. ITU internet reports," International Telecommunication Union, 2005.

[11] X. Li, R. Lu, X. Liang, X. Shen, J. Chen and X. Lin, "Smart community: An internet of things application," *IEEE Communications Magazine,* vol. 49, no. 11, pp. 68-75, 2011.

[12] A. Al-Fuqaha, M. Guizani, M. Mohammadi, M. Aledhari and M. A. 2015., "Internet of things: A survey on enabling technologies, protocols, and applications," *IEEE Communications Surveys & Tutorials,* vol. 17, no. 4, pp. 2347-2376, 2015.

[13] X. Cui, "The internet of things," in *Ethical Ripples of Creativity and Innovation*, Palgrave Macmillan, London, 2016.

[14] I. Dincer and C. Acar, "Smart energy systems for a sustainable future," *Applied energy*, vol. 194, pp. 225-235, 2017.

[15] D. Connolly, H. Lund, B. V. Mathiesen, P. A. Østergaard, B. Möller, S. Nielsen and P. Sorknæs, "Smart energy systems: holistic and integrated energy systems for the era of 100% renewable energy," Aalborg University, Aalborg, 2013.

[16] H. Lund, Renewable energy systems: a smart energy systems approach to the choice and modeling of 100% renewable solutions, Waltham, USA: Academic Press, 2014.

[17] H. Lund, P. A. Østergaard and D. Connolly, "Smart energy and smart energy systems," *Energy,* vol. 137, pp. 556-565, 2017.

[18] K. Tripathi, S. Shrivastava and S. Banarjee, Review in Recent Trends on Energy Delivery System and Its Issues in Smart Grid System, Singapore: Springer, 2020, pp. 117-125.

[19] Q. Sun, X. Ge, L. Liu, X. Xu, Y. Zhang, R. Niu and Y. Zeng, "Review of smart grid comprehensive assessment systems," *Energy Procedia,* vol. 12, pp. 219-229, 2011.

[20] X. Fang, S. Misra, G. Xue and D. Yang, "Smart grid—The new and improved power grid: A survey," *IEEE communications surveys & tutorials,* vol. 14, no. 4, pp. 944-980, 2011.

[21] L. C. Hau, J. V. Lee, Y. D. Chuah and A. C. Lai, "Smart grid-the present and future of smart physical protection: a review," *International Journal of Energy, Information and Communications,* vol. 4, no. 4, pp. 43-54, 2013.

[22] E. Mocanu, P. H. Nguyen, W. L. Kling and M. Gibescu, "Unsupervised energy prediction in a Smart Grid context using reinforcement cross-building transfer learning," *Energy and Buildings,* vol. 116, pp. 646-655, 2016.

[23] M. Ghorbanian, S. H. Dolatabadi, M. Masjedi and P. Siano, "Communication in smart grids: A comprehensive review on the existing and future communi-cation and information infrastructures," *IEEE Systems Journal,* vol. 13, no. 4, pp. 4001-4014, 2019.

[24] Z. Lu, X. Lu, W. Wang and C. Wang, "Review and evaluation of security threats on the communication networks in the smart grid," in *2010-Milcom 2010 Military Communications Conference,* San Jose, CA, USA, 2010.

[25] I. Dincer and C. Acar, "Smart energy systems for a sustainable future," *Applied energy,* vol. 194, pp. 225-235, 2017.

[26] L. E. Jones, Renewable energy integration: practical management of variability, uncertainty, and flexibility in power grids, London Wall, London: Academic Press, 2017.

[27] J. Shi, W. Lee, Y. Liu, Y. Yang and P. Wang, "Forecasting power output of photovoltaic systems based on weather classification and support vector machines," *IEEE Transactions on Industry Applications,* vol. 48, no. 3, pp. 1064-1069, 2012.

[28] G. Strbac, "Demand side management: Benefits and challenges," *Energy Policy,* vol. 36, no. 12, pp. 4419-4426, 2008.

[29] A. Aktas, K. Erhan, S. Ozdemir and E. Ozdemir, "Experimental investigation of a new smart energy management algorithm for a hybrid energy storage system in smart grid applications," *Electr.Power Syst.Res,* vol. 144, pp. 185-196, 2017.

[30] S. Amrouche, D. Rekioua, T. Rekioua and S. Bacha, "Overview of energy storage in renewable energy systems," *Int J Hydrogen Energy,* vol. 41, no. 45, pp. 20914-20927, 2016.

[31] A. Olabi, "Renewable energy and energy storage systems," *Energy,* vol. 136, pp. 1-6, 2017.

[32] B. Scrosati, J. Garche and W. Tillmetz, Advances in battery technologies for electric vehicles, Sawston, Cambridge: Woodhead Publishing, 2015.

[33] A. Fotouhi, D. J. Auger, T. Cleaver, N. Shateri, K. Propp and S. Longo, "Influence of battery capacity on performance of an electric vehicle fleet," in *2016 IEEE International Conference on Renewable Energy Research and Applications (ICRERA)*, Birmingham, UK, 2016.

[34] G. Pistoia, Electric and hybrid vehicles: Power sources, models, sustainability, infrastructure and the market, Jordan Hill, Oxford: Elsevier, 2010.

[35] P. Cazzola, M. Gorner, R. Schuitmaker and E. Maroney, "Global EV outlook 2016," International Energy Agency, France, 2016.

[36] G. Wu, A. Inderbitzin and C. Bening, "Total cost of ownership of electric vehicles compared to conventional vehicles: A probabilistic analysis and projection across market segments," *Energy Policy,* vol. 80, pp. 196-214, 2015.

[37] R. Xiong, L. Li and J. Tian, "Towards a smarter battery management system: A critical review on battery state of health monitoring methods," *Journal of Power Sources,* vol. 405, pp. 18-29, 2018.

[38] D. Pevec, J. Babic and V. Podobnik, "Electric vehicles: A data science perspective review," *Electronics,* vol. 8, no. 10, p. 1190, 2019.

[39] E. S. Chavan and M. C. Butale, "Stabilizing the Thermal Temperature of Lithium Batteries Using Peltier Plate for EV Vehicles," *International Journal of Innovations in Engineering Research and Technology,* vol. 7, no. 08, pp. 85-88, 2020.

[40] J. Zhang, L. Zhang, F. Sun and Z. Wang, "An overview on thermal safety issues of lithium-ion batteries for electric vehicle application," *IEEE Access,* vol. 6, pp. 23848-23863, 2018.

[41] X. Li, L. Zhang, Z. Wang and P. Dong, "Remaining useful life prediction for lithium-ion batteries based on a hybrid model combining the long short-term memory and Elman neural networks," *Journal of Energy Storage,* vol. 21, pp. 510-518, 2019.

[42] X. Hu, K. Zhang, K. Liu, X. Lin, S. Dey and S. Onori, "Advanced Fault Diagnosis for Lithium-Ion Battery Systems: A Review of Fault Mechanisms, Fault Features, and Diagnosis Procedures," *IEEE Industrial Electronics Magazine,* vol. 14, no. 3, pp. 65-91, 2020.

[43] S. T. Plunkett, C. Chen, R. Rojaee, P. Doherty, Y. Oh, Y. Galazutdinova, M. Krishnamurthy and S. Al-Hallaj, "Enhancing thermal safety in lithium-ion battery packs through parallel cell 'current dumping' mitigation," *Applied Energy,* vol. 286, p. 116495, 2021.

[44] H. Ren, Y. Zhao, S. Chen and T. Wang, "Design and implementation of a battery management system with active charge balance based on the SOC and SOH online estimation," *Energy,* vol. 166, pp. 908-917, 2019.

[45] H. Dai, B. Jian, X. Hu, X. Lin, X. Wei and M. Pecht, "Advanced battery management strategies for a sustainable energy future: Multilayer design concepts and research trends," *Renewable and Sustainable Energy Reviews,* vol. 138, p. 110480, 2021.

[46] Amin, K. Ismail, A. Nugroho and S. Kaleg, "Passive balancing battery management system using MOSFET internal resistance as balancing resistor," in *2017 International Conference on Sustainable Energy Engineering and Application (ICSEEA)*, Jakarta, Indonesia, 2017.

[47] E. Din, C. Schaef, K. Moffat and J. T. Stauth, "A Scalable Active Battery Management System With Embedded Real-Time Electrochemical Impedance Spectroscopy," *IEEE Transactions on Power Electronics,* vol. 32, no. 7, pp. 5688-5698, 2017.

[48] Z. B. Omariba, L. Zhang and D. Sun, "Review of Battery Cell Balancing Methodologies for Optimizing Battery Pack Performance in Electric Vehicles," *IEEE Access,* vol. 7, pp. 129335-129352, 2019.

[49] S. Dalvi and S. Thale, "Design of DSP Controlled Passive Cell Balancing Network based Battery Management System for EV Application," in *2020 IEEE India Council International Subsections Conference (INDISCON)*, Visakhapatnam, India, 2020.

[50] D. Thiruvonasundari and K. Deepa, "Optimized Passive Cell Balancing for Fast Charging in Electric Vehicle," *IETE Journal of Research,* pp. 1-9, 2021.

[51] V. C. Valchev, P. V. Yankov and D. D. Stefanov, "Improvement on LiFePO4 cell balancing algorithm," *TEM Journal,* vol. 7, no. 1, p. 19, 2018.

[52] A. F. Moghaddam and A. V. D. Bossche, "An active cell equalization technique for lithium ion batteries based on inductor balancing," in *2018 9th International Conference on Mechanical and Aerospace Engineering (ICMAE)*, Budapest, Hungary, 2018.

[53] N. Ganesha, G. Yadav and C. Gowrishankara, "Analysis and Implementation of Inductor Based Active Battery Cell Balancing Topology," in *2020 IEEE International Conference on Power Electronics, Drives and Energy Systems (PEDES)*, Jaipur, India, 2020.

[54] Y. Wang, H. Yin, S. Han, A. Alsabbagh and C. Ma, "A novel switched capacitor circuit for battery cell balancing speed improvement," in *2017 IEEE 26th International Symposium on Industrial Electronics (ISIE)*, Edinburgh, UK, 2017.

[55] Y. Ye and K. W. E. Cheng, "Analysis and Design of Zero-Current Switching Switched-Capacitor Cell Balancing Circuit for Series-Connected Battery/Supercapacitor," *IEEE Transactions on Vehicular Technology,* vol. 67, no. 2, pp. 948-955, 2018.

[56] A. Samanta and S. Chowdhuri, "Active Cell Balancing of Lithium-ion Battery Pack Using Dual DC-DC Converter and Auxiliary Lead-acid Battery," *Journal of Energy Storage,* vol. 33, p. 102109, 2021.

[57] M. Shousha, A. Prodić, V. Marten and J. Milios, "Design and Implementation of Assisting Converter-Based Integrated Battery Management System for Electromobility Applications," *IEEE Journal of Emerging and Selected Topics in Power Electronics,* vol. 6, no. 2, pp. 825-842, 2018.

[58] Y. Shang, S. Zhao, Y. Fu, B. Han, P. Hu and C. C. Mi, “A Lithium-Ion Battery Balancing Circuit Based on Synchronous Rectification,” *IEEE Transactions on Power Electronics,* vol. 35, no. 2, pp. 1637-1648, 2020.

[59] L. Tian, M. Hong, Z. He and M. Gao, “Active Battery Balancing Circuit Based on Optimized Flyback Convertor for Large Lithium-ion Battery Packs,” in *2018 IEEE 4th International Conference on Control Science and Systems Engineering (ICCSSE)*, Wuhan, China, 2018.

[60] P. d. Toit, C. Kruger, G. P. Hancke and T. D. Ramotsoela, “Smart Street Lights Using Power Line Communication,” in *2017 IEEE AFRICON*, Cape Town, South Africa, 2017.

[61] SEA, “Efficient Public Lighting Guide,” 2012. [Online]. Available: http://www.cityenergy.org.za/uploads/resource_17.pdf. [Accessed 7 3 2021].

[62] T. Novak, K. Pollhammer, H. Zeilinger and S. Schaat, “Intelligent Streetlight Management in a Smart City,” in *Proceedings of the 2014 IEEE Emerging Technology and Factory Automation (ETFA)*, Barcelona, Spain, 2014.

[63] Z. Gu, K. Yang, X. Wang and Q. Meng, “Design of DC Charging Pile Based on Intelligent LED Lamp Rod,” in *International Conference on Mechatronics and Intelligent Robotics*, Springer, Cham, 2018.

[64] A. Adriansyah, A. W. Dani and G. I. Nugraha, “Automation Control and Monitoring of Public Street Lighting System Based on Internet of Things,” in *2017 International Conference on Electrical Engineering and Computer Science (ICECOS)*, Palembang, Indonesia, 2017.

[65] M. M. Mohsin, I. S. Jadhav and V. D. Chaudhari, “High Efficiency Intelligent Street Lighting System Using a Zigbee Network and GSM,” *International Journal for Research in Applied Science and Engineering Technology*, vol. 5, no. 2, p. 510–516, 2017.

[66] Z. X. Hui, K. P. Hua, Z. Xu and L. Yang, “Intelligent Street Lamp Energy Saving System Based on ZigBee,” in *2015 Fifth International Conference on Instrumentation and Measurement, Computer, Communication and Control (IMCCC)*, Qinhuangdao, China, 2015.

[67] L. Lian and L. Li, “Wireless Dimming System for LED Street Lamp Based on ZigBee and GPRS,” in *2012 3rd International Conference on System Science, Engineering Design and Manufacturing Informatization*, Chengdu, China, 2012.

[68] K. Y. Rajput, G. Khatav, M. Pujari and P. Yadav, “Intelligent Street Lighting System Using GSM,” *International Journal of Engineering Science Invention*, vol. 2, no. 3, pp. 60-69, 2013.

[69] J. Liu, C. Feng, X. Suo and A. Yun, “Street Lamp Control System Based on Power Carrier Wave,” in *2008 International Symposium on Intelligent Information Technology Application Workshops*, Shanghai, China, 2008.

[70] S. Deo, S. Prakash and A. Patil, “Zigbee-based Intelligent Street Lighting System,” in *2014 2nd International Conference on Devices, Circuits and Systems (ICDCS)*, Coimbatore, India, 2014.

[71] E. Bingöl, Ö. Gül and S. Şener, “A Review of Intelligent Street Lighting System for Smart Cities,” in *2nd International Symposium on Multidisciplinary Studies and Innovative Technologies*, 2019.

[72] G. Gagliardi, M. Lupia, G. Cario, F. Tedesco, F. Cicchello Gaccio, F. Lo Scudo and A. Casavola, “Advanced Adaptive Street Lighting Systems for Smart Cities,” *Smart Cities*, vol. 3, no. 4, pp. 1495-1512, 2020.

[73] C. L. Fan and Y. Guo, “The Application of a ZigBee Based Wireless Sensor Network in the LED Street Lamp Control System,” in *2011 International Conference on Image Analysis and Signal Processing*, Wuhan, China, 2011.

[74] D. Jin, C. Hannon, Z. Li, P. Cortes, S. Ramaraju, P. Burgess, N. Buch and M. Shahidehpour, “Smart Street Lighting System: A Platform for Innovative Smart City Applications and a New Frontier for Cyber-security,” *The Electricity Journal*, vol. 29, no. 10, p. 28–35, 2016.

[75] R. Caponetto, G. Dongola, L. Fortuna, N. Riscica and D. Zufacchi, “Power Consumption Reduction in a Remote Controlled Street Lighting System,” in *2008 International Symposium on Power Electronics, Electrical Drives, Automation and Motion*, Ischia, Italy, 2008.

[76] S. R. Parekar and M. M. Dongre, “An Intelligent System for Monitoring and Controlling of Street Light Using GSM Technology,” in *2015 International Conference on Information Processing (ICIP)*, Pune, India, 2015.

[77] H. P. Khandagale, R. Zambare, P. Pawar, P. Jadhav, P. Patil and S. Mule, “Street Light Controller with GSM Technology,” *International Journal of Engineering Applied Sciences and Technology*, vol. 4, no. 10, p. 268–271, 2020.

[78] E. Zhu, X. Liu and Y. Aliaosha, “Development and Application of Low Voltage Power Line Communication Test System,” in *2011 International Conference on Advanced Power System Automation and Protection*, Beijing, China, 2011.

[79] X. Xu, A. Zhan and X. Li, “Design and Implementation of Street Light Control System Based on Power Line Carrier Communication,” *Procedia Computer Science,* vol. 155, p. 734–739, 2019.

[80] J. Liu, C. Feng, X. Suo and A. Yun, “Street Lamp Control System Based on Power Carrier Wave,” in *2008 International Symposium on Intelligent Information Technology Application Workshops*, Shanghai, China, 2008.

[81] C. Li, J. Wu and X. He, “Realization of a general LED lighting system based on a novel Power Line Communication technology,” in *2010 Twenty-Fifth Annual IEEE Applied Power Electronics Conference and Exposition (APEC)*, Palm Springs, CA, USA, 2010.

[82] N. Bertoni, S. Bocchi, M. Mangia, F. Pareschi, R. Rovatti and G. Setti, “Ripple-based Power-line Communication in Switching DC-DC Converters Exploiting Switching Frequency Modulation,” in *2015 IEEE International Symposium on Circuits and Systems (ISCAS)*, Lisbon, Portugal, 2015.

[83] J. Chen, J. Wu, R. Wang, R. Zhang and X. He, “Coded PWM Based Switching Ripple Communication Applied in Visible Light Communication,” *IEEE Transactions on Power Electronics,* vol. 36, no. 8, pp. 9659-9667, 2021.

[84] C. Ranhotitogamage, S. C. Mukhopadhyay, S. N. Garratt and W. M. Campbell, “Measurement and monitoring of performance parameters of distributed solar panels using wireless sensors network,” in *2011 IEEE International Instrumentation and Measurement Technology Conference*, Hangzhou, China, 2011.

[85] I. Pavić, M. Beus, V. Bobanac and H. Pandžić, “Decentralized master-slave communication and control architecture of a battery swapping station,” in *2018 IEEE International Conference on Environment and Electrical Engineering and 2018 IEEE Industrial and Commercial Power Systems Europe*, Palermo, Italy, 2018.

[86] W. Huagang, T. R. Meng and L. S. Wen, “Measurement and analysis of electromagnetic emissions for broadband power line (BPL) communication,” in *2017 IEEE 5th International Symposium on Electromagnetic Compatibility*, Beijing, China, 2017.

[87] International Electrotechnical Commission, *Industrial communication networks - Fieldbus specifications - Part 2: Physical layer specification and service definition*, IEC, 2014.

[88] H. C. Ferreira, H. M. Grové, O. Hooijen and A. J. Han Vinck, Power line communication, Wiley Encyclopedia of Electrical and Electronics Engineering, 2001.

[89] A. Cataliotti, A. Daidone and G. Tine, “Power line communication in medium voltage systems: Characterization of MV cables,” *IEEE Transactions on Power Delivery,* vol. 23, no. 4, pp. 1896-1902, 2008.

[90] G. Bumiller, L. Lampe and H. Hrasnica, “Power line communication networks for large-scale control and automation systems,” *IEEE Communications Magazine,* vol. 48, no. 4, pp. 106-113, 2010.

[91] A. Ndjiongue and H. Ferreira, “Power line communications (PLC) technology: More than 20 years of intense research,” *Transactions on Emerging Telecommunications Technologies*, vol. 30, no. 7, p. e3575, 2019.

[92] P. Baier, K. Dostert and M. Pandit, “A novel spread-spectrum receiver synchronization scheme using a SAW-tapped delay line,” *IEEE Trans.Communication*, vol. 30, no. 5, pp. 1037-1047, 1982.

[93] K. M. Dostert, “A novel frequency hopping spread spectrum scheme for reliable power line communications,” in *IEEE Second International Symposium on Spread Spectrum Techniques and Applications*, Yokohama, Japan, 1992.

[94] K. Fazel, “Performance of CDMA/OFDM for mobile communication system,” in *Proceedings of 2nd IEEE International Conference on Universal Personal Communications*, Ottawa, ON, Canada, 1993.

[95] M. Bhardwaj, A. Gangwar and D. Soni, “A review on OFDM: Concept, scope & its applications,” *IOSR Journal of Mechanical and Civil Engineering (IOSRJMCE)*, vol. 1, no. 1, pp. 7-11, 2012.

[96] H. Harada and Y. KAMIO, “A feasibility study of the 16QAM-OFDM transmission scheme for multimedia mobile access communication systems,” *IEICE Transactions on Communication,* vol. 84, no. 8, pp. 2207-2218, 2001.

[97] E. R. Wade and H. H. Asada, “Design of a broadcasting modem for a DC PLC scheme,” *IEEE/ASME Transactions on Mechatronics,* vol. 11, no. 5, pp. 533-540, 2006.

[98] E. Roman, R. Alonso, P. Ibanez, S. Elorduizapatarietxe and D. Goitia, “Intelligent PV module for grid-connected PV systems,” *IEEE Transactions on Industrial Electronics,* vol. 53, no. 4, pp. 1066-1073, 2006.

[99] H. Nosato, Y. Kasai, E. Takahashi and M. Murakawa, “A very low-cost low-frequency PLC system based on DS-CDMA for DC power lines,” in *2012 IEEE International Symposium on Power Line Communications and Its Applications*, Beijing, China, 2012.

[100] IEC, “International Electrotechnical Commission,” in *Industrial communication networks - Fieldbus specifications - Part 2: Physical layer specification and service definition,* 2014.

[101] M. Felser, “The fieldbus standards: History and structures,” in *Technology Leadership Day,* 2002.

[102] C. Diedrich and T. Bangemann, “Profibus PA: Instrumentation Technology for the Process Industry,” in *Oldenbourg Industrieverlag,* 2007.

[103] R. V. White, “Electrical isolation requirements in power-over-ethernet (PoE) power sourcing equipment (PSE),” in *Twenty-First Annual IEEE Applied Power Electronics Conference and Exposition,* Dallas, TX, USA, 2006.

[104] M. Eisen, “Introduction to PoE and the IEEE802. 3af and 802.3 at standards,” in *presentation slideware,* 2010.

[105] G. Mendelson, “All you need to know about power over ethernet (PoE) and the IEEE 802.3 af standard,” 6 2004. [Online]. Available: http://www.argo-contar.com/download/Passive/PoE_and_IEEE802_3af_literature.pdf. [Accessed 26 11 2021].

[106] D. Abramson, “IEEE P802. 3bt Mutual Identification,” in *IEEE802. 3bt Interim Meeting,* 2014.

[107] P. Sharma, S. Pardeshi, R. K. Arora and M. Singh, “A review of the development in the field of fiber optic communication systems,” *International Journal of Emerging Technology and Advanced Engineering,* vol. 3, no. 5, pp. 113-119, 2013.

[108] P. J. Winzer, D. T. Neilson and A. R. Chraplyvy, "Fiber-optic transmission and networking: the previous 20 and the next 20 years," *Optics express,* vol. 26, no. 18, pp. 24190-24239, 2018.

[109] S. Kwan, "Principles of optical fibers," Partial Fulfillment of Course Requirement for MatE, San Jose State University, 2002.

[110] M. Bozdal, M. Samie, S. Aslam and I. Jennions, "Evaluation of can bus security challenges," *Sensors,* vol. 20, no. 8, p. 2364, 2020.

[111] G. Spencer, F. Mateus, P. Torres, R. Dionísio and R. Martins, "Design of CAN Bus Communication Interfaces for Forestry Machines," *Computers,* vol. 10, no. 11, p. 144, 2021.

[112] Y. Peng, Z. Shujuan and G. Xin, "Design of motor drive module on CAN bus," in *Proceedings of the Second International Conference on Intelligent NEtworks and Intelligent Systems*, Tianjin, China, 2009.

[113] X. Yue, A. Zhu, J. Song, G. Cao, D. An and Z. Guo, "The Design and Implementation of Human Motion Capture System Based on CAN Bus," in *Proceedings of the 2020 17th International Conference on Ubiquitous Robots (UR),* Kyoto, Japan, 2020.

[114] J. Jousse, N. Ginot, C. Batard and E. Lemaire, "Power line communication management of battery energy storage in a small-scale autonomous photovoltaic system," *IEEE Transactions on Smart Grid,* vol. 8, no. 5, pp. 2129-2137, 2017.

[115] J. Wu, C. Li and X. He, "A novel power line communication technique based on power electronics circuit topology," in *2010 Twenty-Fifth Annual IEEE Applied Power Electronics Conference and Exposition (APEC),* Palm Springs, CA, USA, 2010.

[116] J. Wu, S. Zong and X. He, "Power/signal time division multiplexing technique based on power electronic circuits," in *2011 Twenty-Sixth Annual IEEE Applied Power Electronics Conference and Exposition (APEC),* Fort Worth, TX, USA, 2011.

[117] S. Zhao, J. Xu and O. Trescases, "Burst-Mode Resonant LLC Converter for an LED Luminaire With Integrated Visible Light Communication for Smart Buildings," *IEEE Transactions on Power Electronics,* vol. 29, no. 8, pp. 4392-4402, 2014.

[118] S. Saggini, W. Stefanutti, P. Mattavelli, G. Garcea and M. Ghioni, "Power line communication in dc-dc converters using switching frequency modulation," in *Twenty-First Annual IEEE Applied Power Electronics Conference and Exposition,* Dallas, TX, USA, 2006.

[119] W. Stefanutti, P. Mattavelli, S. Saggini and L. Panseri, “Communication on power lines using frequency and duty-cycle modulation in digitally controlled dc-dc converters,” in *IECON 2006 - 32nd Annual Conference on IEEE Industrial Electronics*, Paris, France, 2006.

[120] W. Stefanutti, S. Saggini, P. Mattavelli and M. Ghioni, “Power line communication in digitally controlled DC–DC converters using switching frequency modulation,” *IEEE Transactions on Industrial Electronics,* vol. 55, no. 4, pp. 1509-1518, 2008.

[121] R. Zhang, X. Liu, H. Pu, P. Sun, Z. Sun and D. Xu, “Bidirectional DCDC Based Power/Signal Integrated Transmission in Energy Router,” in *2021 4th International Conference on Energy, Electrical and Power Engineering (CEEPE)*, Chongqing, China, 2021.

[122] D. Yu, K. Li, S. Yu, H. Trinh, P. Zhang, A. M. Oo and Y. Hu, “A Novel Power and Signal Composite Modulation Approach to Powerline Data Communication for SRM in Distributed Power Grids,” *IEEE Transactions on Power Electronics,* vol. 36, no. 9, pp. 10436-10446, 2021.

[123] H. Choi and J. Jung, “Enhanced Power Line Communication Strategy for DC Microgrids Using Switching Frequency Modulation of Power Converters,” *IEEE Transactions on Power Electronics,* vol. 32, no. 6, pp. 4140-4144, 2017.

[124] J. Wu, C. Zhao, Z. Lin, J. Du, Y. Hu and X. He, “Wireless Power and Data Transfer via a Common Inductive Link Using Frequency Division Multiplexing,” *IEEE Transactions on Industrial Electronics,* vol. 62, no. 12, pp. 7810-7820, 2015.

[125] J. Rodriguez Mendez, D. González Lamar, D. Garcia Aller, P. Fernandez Miaja and F. J. Sebastián Zúñiga, “Reproducing multi-carrier modulation schemes for visible light communication with the ripple modulation technique,” *IEEE Transactions on Industrial Electronics,* vol. 67, no. 3, pp. 1532-1543, 2019.

[126] J. Wu, J. Du, Z. Lin, Y. Hu, C. Zhao and X. He, “Power Conversion and Signal Transmission Integration Method Based on Dual Modulation of DC–DC Converters,” *IEEE Transactions on Industrial Electronics,* vol. 62, no. 2, pp. 1291-1300, 2015.

[127] J. Du, J. Wu, R. Wang, Z. Lin and X. He, “DC Power-Line Communication Based on Power/Signal Dual Modulation in Phase Shift Full-Bridge Converters,” *IEEE Transactions on Power Electronics,* vol. 32, no. 1, pp. 693-702, 2017.

[128] R. Wang, Z. Lin, J. Du, J. Wu and X. He, “Direct Sequence Spread Spectrum-Based PWM Strategy for Harmonic Reduction and Communication,” *IEEE Transactions on Power Electronics,* vol. 32, no. 6, pp. 4455-4465, 2017.

[129] R. Wang, “Research on Key Technologies of Power/Data Integrated Energy Router,” Zhejiang University, Zhejiang, China, 2019.

[130] O. I. Rumyantsev, J. A. Lecoq, O. Hernandez, Y. Zhang, J. Savall, R. Chrapkiewicz, J. Li, H. Zeng, S. Ganguli and M. J. Schnitzer, “Fundamental bounds on the fidelity of sensory cortical coding,” *Nature,* vol. 580, no. 7801, pp. 100-105, 2020.

[131] Z. Wang, “Research on Photovoltaic Power Optimized System and Power Line Communication,” Zhejiang University, Zhejiang, China, 2018.

[132] C. H. T. Santos and V. Pereira, “Envelope estimation using geometric properties of a discrete real signal,” *Digital Signal Processing,* vol. 120, p. 103229, 2022.

[133] S. Ren, G. Xia, Y. Xue, W. Zhao, X. Rao and X. Wang, “Research on Performance of Optical DPSK Modulation Format in All Optical Network,” in *2018 10th International Conference on Communication Software and Networks (ICCSN),* Chengdu, China, 2018.

[134] M. Hervás, J. L. Pijoan, R. M. Alsina-Pagès, M. Salvador and D. Badia, “Single-carrier frequency domain equalisation proposal for very long haul HF radio links,” *Electronics letters,* vol. 50, no. 17, pp. 1252-1254, 2014.

[135] J. R. R. Zientarski, M. L. d. S. Martins, J. R. Pinheiro and H. L. Hey, “Evaluation of Power Processing in Series-Connected Partial-Power Converters,” *IEEE Journal of Emerging and Selected Topics in Power Electronics,* vol. 7, no. 1, pp. 343-352, 2019.

[136] J. Anzola, I. Aizpuru, A. A. Romero, A. A. Loiti, R. Lopez-Erauskin and C. Bernal, “Review of Architectures Based on Partial Power Processing for DC-DC Applications,” *IEEE Access,* vol. 8, pp. 103405-103418, 2020.

[137] V. M. Iyer, S. Gulur, G. Gohil and S. Bhattacharya, “An Approach Towards Extreme Fast Charging Station Power Delivery for Electric Vehicles with Partial Power Processing,” *IEEE Transactions on Industrial Electronics,* vol. 67, no. 10, pp. 8076-8087, 2020.

[138] K. A. K. Niazi, Y. Yang, T. Kerekes and D. Sera, “A Simple Mismatch Mitigating Partial Power Processing Converter for Solar PV Modules,” *Energies,* vol. 14, no. 8, p. 2308, 2021.

[139] J. Qi and D. D.-C. Lu, “A flyback converter based partial power processing structure for BESS with voltage/current regulation and battery balancing functionalities,” in *2017 IEEE International Telecommunications Energy Conference (INTELEC)*, Broadbeach, QLD, Australia, 2017.

[140] M. Pape and M. Kazerani, “An Offshore Wind Farm With DC Collection System Featuring Differential Power Processing,” *IEEE Transactions on Energy Conversion*, vol. 35, no. 1, pp. 222-236, 2020.

[141] S. Mishra, S. Tamballa, M. Pallantala, S. Raju and N. Mohan, “Cascaded Dual-Active Bridge Cell Based Partial Power Converter for Battery Emulation,” in *20th Workshop on Control and Modeling for Power Electronics (COMPEL)*, Toronto, ON, Canada, 2019.

[142] S. Honarmand, A. Rajaei, M. Shahparasti, A. Luna and E. Pouresmaeil, “A modified partial power structure for quasi Z-source converter to improve voltage gain and power rating,” *Energies,* vol. 12, no. 11, p. 2139, 2019.

[143] G. Chen, Y. Liu and W. Cui, “Partial Power Processing Multi-Port DC-DC Converters,” in *IECON 2020 The 46th Annual Conference of the IEEE Industrial Electronics Society*, Singapore, 2020.

[144] T. Ohta, P. -Y. Huang and Y. Kado, “Bidirectional Isolated Ripple Cancel Triple Active Bridge DC-DC Converter,” in *2020 22nd European Conference on Power Electronics and Applications (EPE'20 ECCE Europe)*, Lyon, France, 2020.

[145] C. M. Orallo, I. Carugati, G. Nikolic, D. Cvetkovic and M. Cakic, “Single bin sliding discrete Fourier transform,” in *Fourier Transforms: High-tech Applications and Current Trends, Anonymous*, InTech, 2017, pp. 748-751.

[146] D. Tian, Z. Zhu and C. Chen, “A Selective Harmonic Optimization Method for STATCOM in Steady State Based on the Sliding DFT,” in *2015 IEEE International Conference on Systems, Man, and Cybernetics*, Hong Kong, China, 2015.

[147] S. M. Lukic, J. Cao, R. C. Bansal, F. Rodriguez and A. Emadi, “Energy storage systems for automotive applications,” *IEEE Transactions on Industrial Electronics*, vol. 55, no. 6, pp. 2258-2267, 2008.

[148] L. Casals, B. García and M. Benítez, “Aging model for re-used electric vehicle batteries in second life stationary applications,” *Project Management and Engineering Research*, pp. 139-151, 2017.

[149] M. Palacin and A. d. Guibert, “Why do batteries fail?,” *Science,* vol. 351, no. 6273, p. 1253292, 2016.

[150] K. Bayindir, M. Gözüküçük and A. Teke, “A comprehensive overview of hybrid electric vehicle: Powertrain configurations, powertrain control techniques and electronic control units,,” *Energy conversion and Management,* vol. 52, no. 2, pp. 1305-1313, 2011.

[151] X. Zhu, H. Zhang, J. Xi, J. Wang and Z. Fang, “Optimal speed synchronization control for clutchless AMT systems in electric vehicles with preview actions,” in *2014 American Control Conference,* Portland, OR, USA, 2014.

[152] F. Zhou, S. Li and X. Hou, “Development method of simulation and test system for vehicle body CAN bus based on CANoe,” in *2008 7th World Congress on Intelligent Control and Automation*, Chongqing, China, 2008.

[153] M. Zheng, B. Qi and H. Wu, “A Li-ion battery management system based on CAN-bus for electric vehicle,” in *2008 3rd IEEE Conference on Industrial Electronics and Applications,* Singapore, 2008.

[154] L. M. Tolbert, F. Z. Peng and T. G. Habetler, “Multilevel inverters for electric vehicle applications,” *Power Electronics in Transportation,* pp. 79-84, 1998.

[155] Z. Du, B. Ozpineci, L. M. Tolbert and J. N. Chiasson, “DC–AC cascaded H-bridge multilevel boost inverter with no inductors for electric/hybrid electric vehicle applications,” *IEEE Transactions on Industry Applications,* vol. 45, no. 3, pp. 963-970, 2009.

[156] J. Qi and D. D.-C. Lu, “Review of battery cell balancing techniques,” in *2014 Australasian Universities Power Engineering Conference (AUPEC),* Perth, WA, Australia, 2014.

[157] M. A. Hannan, M. S. Mollik, A. Q. Al-Shetwi, S. A. Rahman, M. Mansor, R. A. Begum, K. M. Muttaqi and Z. Y. Dong, “Vehicle to grid connected technologies and charging strategies: Operation, control, issues and recommendations,” *Journal of Cleaner Production,* vol. 339, p. 130587, 2022.

[158] C. Blake and C. Bull, IGBT or MOSFET: Choose wisely, International Rectifier, 2001.

[159] G. Chu, H. Wen, L. Jiang, Y. Hu and X. Li, “Bidirectional Flyback Based Isolated-port Submodule Differential Power Processing Optimizer for Photovoltaic Applications,” *Solar Energy,* vol. 158, p. 929–940, 2017.

[160] Y. Hu, B. Gao, X. Song, G. Y. Tian, K. Li and X. He, "Photovoltaic Fault Detection Using a Parameter Based Model," *Solar Energy,* vol. 96, p. 96–102, 2013.

[161] Y. Hu, W. Cao, S. J. Finney, W. Xiao, F. Zhang and S. F. McLoone, "New Modular Structure DC–DC Converter Without Electrolytic Capacitors for Renewable Energy Applications," *IEEE Transactions on Sustainable Energy,* vol. 5, no. 4, p. 1184–1192, 2014.

[162] Y. Hu, X. Song, W. Cao and B. Ji, "New SR Drive With Integrated Charging Capacity for Plug-in Hybrid Electric Vehicles (PHEVs)," *IEEE Transactions on Industrial Electronics,* vol. 61, no. 10, p. 5722–5731, 2014.

[163] Y. Hu, C. Gan, W. Cao, C. Li and S. J. Finney, "Split Converter-fed SRM Drive for Flexible Charging in EV/HEV Applications," *IEEE Transactions on Industrial Electronics,* vol. 62, no. 10, p. 6085–6095, 2015.

[164] Y. Hu, C. Gan, Q. Sun, P. Li, J. Wu and H. Wen, "Modular Tri-port High-power Converter for SRM Based Plug-in Hybrid Electrical Trucks," *IEEE Transactions on Power Electronics,* vol. 33, no. 4, p. 3247–3257, 2017.

END